THE UNIVERSITY OF MICHIGAN

INDUSTRY PROGRAM OF THE COLLEGE OF ENGINEERING

AN INVESTIGATION OF THE ANISOTROPY OF TENSILE AND COMPRESSIVE PROPERTIES OF COMMERCIALLY PURE ALUMINUM PRESTRAINED UNDER SIMPLE DIRECT STRESS

Alimullah Khan

A dissertation submitted in partial fulfillment
of the requirements for the degree of
Doctor of Science in the
University of Michigan
Department of Mechanical Engineering
1963

January, 1964

IP-656

Doctoral Committee:

Professor Joseph Datsko, Chairman
Professor Robert M. Haythornthwaite
Assistant Professor Alexander Henkin
Professor Robert C. Juvinall
Professor Clarence A. Siebert

ACKNOWLEDGMENTS

The author wishes to acknowledge his appreciation and indebtedness to everybody who aided in this investigation, particularly:

Professor Joseph Datsko, Chairman of the Doctoral Committee, except for whose encouragement, guidance, advice and help in all possible ways, it would have taken a great deal longer to complete this investigation than it has.

Professors Robert M. Haythornthwaite, Robert C. Juvinall, Clarence A. Siebert and Alexander Henkin, members of the Doctoral Committee for their advice and assistance.

The Agency for International Development and the Government of East Pakistan, for financial support to meet his expenses here, in Pakistan and for transportation and travel.

Professor Gordon J. Van Wylen, Chairman, Mechanical Engineering Department and the General Electric Company for financial support for the research.

The staff of the Mechanical Engineering Machine Tools Laboratory for their assistance in preparing specimens of very exacting quality.

The Civil Engineering and Engineering Mechanics Departments for allowing the author to use their laboratory facilities.

The members of the staff of the Industry Program of the College of Engineering, the University of Michigan, for their assistance in preparation and reproduction of this dissertation.

The friends who helped to keep the morale high during the long period of experimental work.

Last, but by no means the least, the author's wife, Mrs. Quazi Jahan Ara Khan, who shouldered all the family responsibilities for more than two years, which made the endeavor possible.

TABLE OF CONTENTS

TABLE OF CONTENTS CONT'D

LIST OF TABLES

LIST OF FIGURES

LIST OF FIGURES CONT'D

LIST OF FIGURES CONT'D

LIST OF FIGURES CONT'D

LIST OF FIGURES CONT'D

LIST OF FIGURES CONT'D

LIST OF FIGURES CONT'D

CHAPTER I

INTRODUCTION

One of the many demands the contemporary engineers have to meet is to design and manufacture structures and components under conditions of service which needs utmost ingenuity and extensive knowledge of the properties of materials. In recent years these demands have grown more exacting; particularly in the space field where weight is so critical. To meet them a number of exotic materials have been developed and highly sophisticated analysis are called for.

To make the best use of the available materials and the methods of analysis, the most important prerequisite is the detailed knowledge of the behavior of materials, in general, and also for particular materials. Unfortunately, our knowledge of the properties of materials as functions of processing history is not yet adequately known.

The mathematical theory of plasticity has been very well developed during the past century within the limits of the assumptions on which it is based. For the purpose of mathematical tractability, the materials are idealized; they are usually assumed to be isotropic in the annealed state, and either rigid-ideal-plastic or elastic-ideal-plastic in their plastic properties. Theoretical investigations have also been made for ideally strain hardening materials, although to a much restricted scale. On the other hand, investigations on the behavior of anisotropic materials are very few indeed.

The limitations of the present day theories of plasticity is not so much the lack of availability of technical literature as the limits of application of the theories, particularly so far as mechanical engineering practice is concerned. The theories have been developed primarily to satisfy the needs of structural engineering; to predict the behavior of structural members where a few percent of plastic strain causes the structure to become useless or the geometry changes so much that the stress distribution changes substantially from that at the initiation of yield. In the analyses which takes strain hardening into consideration, stress and strain are assumed to be linearly related. For real materials, this can be approximately true for small strains only. Hence these analyses are also limited to rather small strains.

But very large strains are quite common in mechanical engineering practice. Processes like extrusion, drawing, etc, involve large strains. As another very important application, materials are cold worked to enhance their strength. Cold working also improves the machinability of soft annealed materials like low carbon steels, aluminum, copper, etc.

The situation becomes much more complicated when cold worked material is used to fabricate machine components, particularly when fabrication involves cold straining in a direction different from that the material had undergone during previous cold work. This kind of application is common in sheet metal work. It is necessary to know the property of the material in the cold worked condition to be able to ensure that a certain fabrication procedure is possible

without undue waste in terms of scrap and machine capacity. It is also necessary to be able to predict the properties of the material after fabrication to ensure proper functioning of the component in usage.

Since Bauschinger noticed in 1881 that when a material is loaded beyond its elastic limit, unloaded and reloaded in the opposite direction, the subsequent elastic limit is lower than that of the original material, it has been known that plastic deformation causes an otherwise isotropic material to become anisotropic. It can also be reasoned that since plastic deformation is primarily distortional, it is likely that a material, after plastic straining, should acquire mechanical properties which are different in different directions.

The purpose of mechanical engineering design is to take advantage of the properties of materials to produce sound machines and machine components at minimum cost. This, of course, presupposes that the properties of all engineering materials are known in all possible detail. Unfortunately, this is not quite so. Design stresses are usually based, from safety considerations, on the lowest strength expected of the material. But, at least in certain applications, where weight of the components concerned is critical, advantage can and should be taken of the variation of the strength of a material. Or, if it is known that a material is weaker in a particular direction, precautions can be taken to ensure safe functioning of the components made of it.

Although it is well known that cold working produces anisotropy of mechanical properties, systematic data regarding the directionality of these properties of cold worked materials is very scarce, and our

knowledge about them is very incomplete and inadequate.

In view of these facts it was deemed profitable to systematically explore, document and compare the directionality of some of the mechanical properties of cold worked material.

The material chosen for this investigation was commercially pure aluminum. The reasons for selecting this particular material is discussed in Chapter IV.

The material was prestrained to various degrees in tension and in compression and the following investigations of properties were made.

(a) Determination of the stress-strain relations. The relationship between stresses and strains in the plastic range were investigated for three orthotropic directions, both in tension and in compression. Torsion tests were not included since the material was anisotropic, and if subjected to plastic torsion, the principal strains would not stay in coincidence with the orthotropic directions and an analysis would be rather untractable.

(b) Construction of yield surfaces. Yield surfaces were constructed from yield data obtained from tension, compression and plane strain tests and measurement of Poisson's ratios.

(c) Residual ductility was determined from measured fracture cross-section for tension tests in all the orthotropic directions and correlated to prestrains.

A few definitions may be examined here for use later on. Engineering stress is defined as the load divided by the initial cross-section and engineering strain as deformation divided by the

initial length. So long as the deformation and change in geometry is small, engineering stress and strain can be used to describe material behavior. But for large strains and consequent change in geometry, engineering stress and strain looses its significance and meaning. The logical thing to do then is to use natural stress and strain. Natural stress is defined as load divided by instantaneous area, and natural strain as the summation of instantaneous strains based on instantaneous length, rather than the original length. Assuming constancy of volume, this can also be expressed in terms of instantaneous cross-section. These concepts had been suggested and used as long ago as 1907 by Ludwik. Since the present investigation deals primarily with large strains, all stresses and strains mentioned hereafter are natural stresses and strains and mentioned simply as stress and strain for the sake of brevity, unless specifically mentioned otherwise.

In the case of tension tests, after the test specimen starts necking, the stress distribution at the neck is rather complex, and Bridgmans semi-empirical correction has been applied to correct for the triaxiality of stresses. Hence, whenever applicable, stress mentioned in case of tension tests always means corrected true stress.

Since aluminum does not show a sharp yield point, an artificial yield point had to be defined. The usual definition of yield stress as the stress at 0.2% plastic strain was not satisfactory in all cases, and a modification was necessary. This has been discussed in detail in Chapter V.

Residual ductility has been defined as the true strain at fracture of a specimen fabricated from prestrained material. In literature, ductility has often been defined as reduction in area in percent. Although the two definitions are equivalent, the later definition as the theoretical upper limit of 100%, whereas the first definition does not have any such upper numerical limit. Also, since all the strains have been measured as true strains, this is logical to measure the ductility also in the same terms. Perhaps the most important reason for measuring ductility in terms of natural strain is the fact that natural strains are additive. When a certain amount of ductility has been used up by working a material, the residual ductility can be found by direct subtraction of the used up ductility from the expected ductility. This is not possible when percent elongation or reduction of area is used as a measure of ductility.

In this investigation the term "direction" means one of the three axes of orthotropy denoted by the symbols X, Y and Z. The designation of these directions have been explained in Chapter IV. All of the testing has been done with reference to these three directions only.

Two kinds of tests can be made in a particular direction, a tension test and a compression test. They are considered to be opposite in "sense" with respect to each other. When a subsequent test is such that the strains produced by the test is a continuation of the previous strain in a certain direction, the sense of the subsequent test is said to be the same as that of previous strain.

Originally the term "Bauschinger effect" was used to indicate the reduction in the elastic limit on reversal of loading after plastic yielding by the first loading. However, this term has been used subsequently in a much wider sense. In the present investigation the Bauschinger effect is defined as the difference between the flow stresses for testing in tension and in compression in a certain direction.

In engineering practice the percent elongation at fracture has been widely used as a material property. Unfortunately, this quantity varies with many geometrical factors like gage length, size, taper, etc., and hence can hardly be called a fundamental property of the material. Hence, no attempt was made to collect data on percent elongation.

Fracture strength or stress defined as fracture load divided by the fracture cross-section is widely reported as a property of ferrous materials. In the present investigation and also in previous tests it has been found that aluminum test specimens do not break into two until the cross-section becomes very small and the load comes down to few pounds only. Also, fracture actually starts within the neck and just before the specimen breaks into two pieces, the load is supported by only a fraction of the apparent cross-section. Obviously, in such a case the fracture stress means very little and was not calculated.

CHAPTER II

THEORETICAL CONSIDERATIONS

This chapter deals with the outlines of some of the theories of plasticity concerning the yield and flow of metals.

No attempt has been made to describe the theories with rigorous mathematics, or to lay down all the assumptions involved. The theories are described only in so far as it is required to build a physical concept of the mechanism of yield and flow of metals. Some of them will be dealt with in more detail in the chapter "Review of Literature." Empirical stress-strain relations for uniaxial loading are also discussed.

General Remarks

The theory of plasticity assumes the existence of a yield surface which is defined as a surface in stress space such that any stress condition within the space enclosed by the surface produces elastic deformation only; and when the stress is removed, the strains also vanish. Plastic flow can occur only when the stress state is on the yield surface.

In general, four mechanical models of materials are used in plasticity analysis: (1) Rigid-ideal plastic; (2) Elastic-ideal plastic, (3) Elastic-strain hardening and (4) rigid-strain hardening. Although there is no material which is perfectly rigid under any condition of stress, if the plastic strains are large compared to the

elastic strains, the rigid-plastic approximation may be very good. On the other hand, when elastic and plastic strains are of the same order of magnitude, it is more logical to assume the material to be elastic-ideally plastic rather than rigid-plastic.

When a material is considered as ideally plastic, it is assumed that plastic straining does not change the properties of the material, and that the strain rates at yielding are of arbitrary magnitude. The yield surface remains stationary in stress space for this type of material. For a previously cold worked material subjected to small plastic strains as encountered in structural applications, these assumptions may represent actual behavior to a close approximation.

However, for larger strains, the assumption of a stationary yield surface is not realized in practice. Nearly all metals have their recrystallization temperature above the ambient temperature, and become stronger with increasing strain. Hence, the yield surface does not remain stationary. The material is then called strain hard-enable. In the theory of plasticity it is assumed that for uniaxial loading increments of stress and strain are linearly related. This can be approximately true for strains of a few percent in magnitude for certain metals.

As a material becomes stronger with increasing strain, the yield surface is no longer stationary in stress space, and has to move or change in shape or size to accommodate the increase in strength.

Yield Conditions

The two most widely used yield conditions for homogeneous isotropic materials are as follows:

(a) Tresca Criterion. This theory postulates that yielding occurs when the maximum shear stress in the material concerned reaches a certain maximum value. This can be expressed mathematically by the equation:

$$\{(S_2 - S_3)^2 - 4k^2\}\{(S_3 - S_1)^2 - 4k^2\}\{(S_1 - S_2)^2 - 4k^2\} = 0 \qquad \text{(II-1)}$$

where S_1, S_2, and S_3 are the stress deviators referred to principal axes and k is the yield strength of the material in shear. The surface in stress space is a regular hexagonal prism of infinite length, its axis being equally inclined to the three principal stress axes and each side having a width $\frac{2\sqrt{6}}{3}$ k. The trace of the prism in a plane containing two stress axes is a hexagon as shown in Figure II-1.

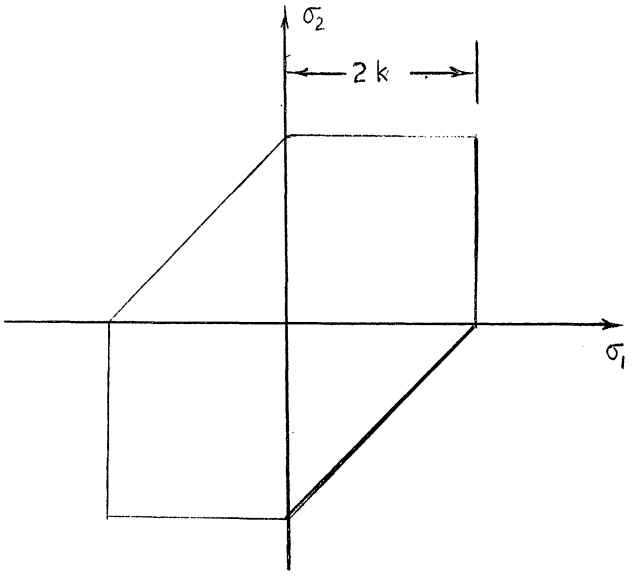

Figure II-1. Tresca Criterion for Yield in σ_1-σ_2 Plane.

(b) Von Mises Criterion. In this theory it is assumed that the material yields when the shear strain energy reaches a maximum value. The same condition is reached when octahedral shear stress reaches a maximum value. Mathematically it can be expressed as:

$$S_1^2 + S_2^2 + S_3^2 - 2k^2 = 0 \qquad \text{(II-2)}$$

The surface in stress space is a right circular cylinder of infinite length and radius $\sqrt{2}k$. The axis of the cylinder being inclined equally to the three stress axes. The trace of the cylinder on a plane containing two stress axes is an ellipse as shown in Figure II-2.

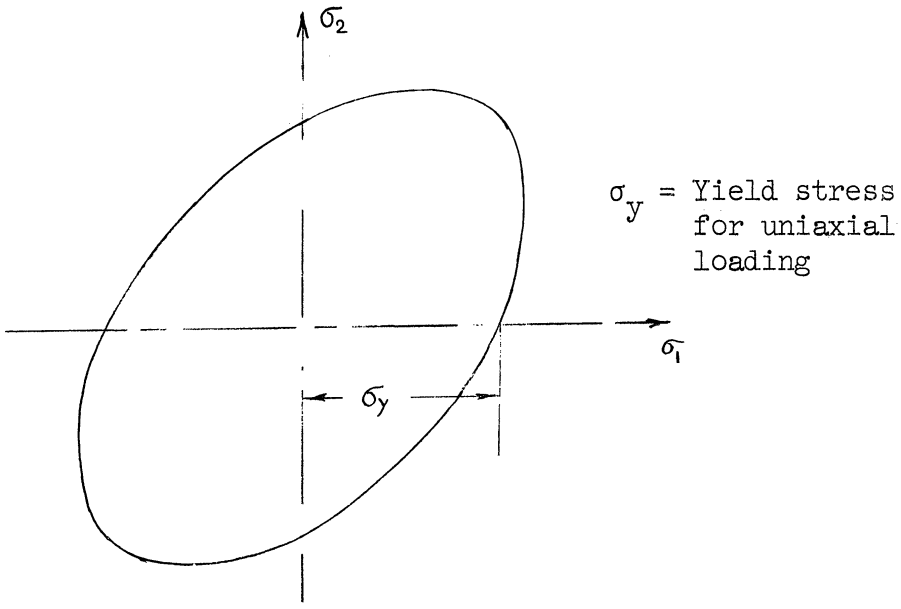

Figure II-2. Von Mises Criterion for Yield in $\sigma_1 - \sigma_2$ Plane.

Other Theories of Yield Criteria

Several other criteria have been suggested at different times to describe the yield phenomenon. Well known among them are maximum

principle stress, maximum strain and maximum strain energy criteria.

Recently Haythornthwaite[1] has suggested a maximum reduced stress criterion for yielding. This is intended primarily for use as bounding yield condition when the available amount of experimental data is limited. This postulates that yielding occurs when the largest stress deviator reaches a certain maximum magnitude.

Strain Hardening[2,3]

When a strain hardenable material is subjected to a state of stress not included within the yield surface, plastic strains result and the strength of the material changes in such a way that the yield surface translates, expands, or distorts until the stress is contained on the yield surface. There are several theories which attempt to predict the motion of the yield surface. Unfortunately none of them seem to represent the actual process in general, although they produce good qualitative approximations in certain cases. Several common theories are explained below.

(a) Isotropic Hardening. This theory postulates that the shape of the yield surface remains the same, and all the dimensions are increased by a constant factor. In other words, if $F - f(\sigma_{ij}) = 0$ represents the original yield surface, the final yield surface can be represented by $F - kf(\sigma_{ij}) = 0$ where k is a constant. Unfortunately this theory cannot accommodate the well known Bauschinger effect. Also it has been shown mathematically by Drucker[4] that isotropic strain hardening is not physically permissible, although it is convenient to use. Tension-torsion tests by Marin and Wiseman[5] corroborates the statement.

(b) Kinematic Hardening. This rule, as developed by Prager,[6,7] assumes that the yield surface is rigid and does not rotate, but translates in a direction normal to the surface at the loading point. This is a mechanical model which accounts for the Bauschinger effect, but for large strains it becomes increasingly less valid since the yield surface is known to become larger with increasing plastic deformation. Methematically, if the initial yield surface is represented by $f(\sigma_{ij}) = k^2 = \text{const}$, the yield surface after plastic deformation is given by

$$f(\sigma_{ij} - \alpha_{ij}) = k^2 \qquad \text{(II-3)}$$

where α_{ij} represents the translation of the yield surface.

(c) Piecewise Linear Theory of Hardening. P. G. Hodge[8,9] developed a more general theory which can take into account any combination of isotropic hardening and Bauschinger effect. This theory assumes that the yield surface is made up of a finite number of linear loading functions of the stress, and that the plastic stress-strain curve can be approximated by a single straight line. Elastic strains are neglected. The loading functions are assumed to be able to translate parallel to themselves and independent of each other, but not so much so that one of them may vanish. This was found valid when the load point stayed in contact with one side of the yield surface, but not in general cases.

A theory based on an infinite number of loading surfaces was discussed by Sanders.[45] The fundamental feature of this theory is the treatment of a curved yield surface as the limiting case of plane loading surfaces when the number of such surfaces tend to infinity.

(d) Slip Theory of Hardening. Batdorf and Budiansky[10,11] developed a theory of plasticity based on slip in crystals. The primary deformation of the yield surface according to this theory is to change the shape of the surface near the loading point by producing or rotating planes to include the subsequent loading point.

In conclusion it may be stated that experimental evidence[12] indicates the actual behavior of a material under an arbitrary state of stresses above the elastic limit to be exceedingly complicated; and even if a completely accurate theory could be devised, it would probably be too cumbersome to be of any use.[5] Therefore, it is still necessary to investigate the yield behavior of cold worked materials for engineering design purposes.

Stress-Strain Relations

For materials like mild steel that exhibit a sharp yield point, it is possible to approximate the plastic stress-strain relations for small strains under uniaxial load by a linear function. Unfortunately this is not true for most materials, particulary at large strains. Various empirical relations have been suggested by investigators.

The first attempts to find a relationship for the plastic extension of metals was at the beginning of this century. As noted by Hill[1], as early as 1909 Ludwik suggested a power relation for annealed material given by

$$\sigma = a + b\epsilon^m$$

where a, b and m are experimental constants. In the opinion of Hill, if ϵ does not exceed 0.2, then, for low values of ϵ, this relation

would produce an underestimated, and at high values of ϵ, an overestimated value of σ, since in his opinion, the exponential law does not provide for sufficiently rapid variation in stress. In 1948-49 Voce and Palm suggested a more complicated relation given by

$$\sigma = a + (b-c)\,(1-e^{-c\epsilon}) \qquad \text{(II-4)}$$

where a, b, and c are experimental constants. They report it gives better results for certain metals. Unfortunately, this is a rather awkward relation for convenient use. However, Zaitsev[13] has shown that Ludwik's power law can be used as a good approximation if the stresses are corrected for triaxiality after necking starts in a tensile test. For the material used in the present investigation a plot of the stress-strain curve on logarithmic co-ordinates was a straight line to a close approximation in the range of strain of our interest. This suggests that within that range the stress-strain relation can be expressed as:[14,15,16]

$$\sigma = \sigma_o\, \epsilon^m \qquad \text{(II-5)}$$

where σ_o and m are experimental constants.

When a material is strained to a true strain of say, ϵ_p, in a certain geometrical direction of the material, unloaded, and then loaded again, then except for a small anelastic effect near the new elastic limit, the stress-strain curve follows the extrapolation of the original curve, since the second loading is just a continuation of the first one. Hence, if we wish to express the stress-strain relation of a material that has been cold worked to a true strain

of ϵ_p, it is obviously best to refer it to the annealed condition and hence, if we denote the subsequent current strain by ϵ, the relation is given by:

$$\sigma = \sigma_o(\epsilon_p + \epsilon)^m \qquad \text{(II-6)}$$

where the constants σ_o and m are the same as in Equation (II-5). This is valid only for straining the material in the same direction and sense as the prestrain.

Unfortunately such a simple relation cannot be deduced when the direction or the sense of straining is different from that of the prestrain, and any such relation has to be found experimentally.

From Equation (II-5) we have

$$\log \sigma = \log \sigma_o + m \log \epsilon$$

Hence, if the stress-strain curve is plotted on logarithmic co-ordinates, the intercept of the curve at $\epsilon = 1$ gives the value σ_o, and m is the slope of the curve which is constant. To find the slope of the curve for pre-strained material strained in the same direction as the prestrain, we have, from Equation (II-6),

$$\ln \sigma = \ln \sigma_o + m \ln (\epsilon_p + \epsilon) \qquad \text{(II-7)}$$

Let $y = \ln \sigma$

$x = \ln \epsilon$

Then $\epsilon = e^x$

From Equation (II-7)

$$y = \ln \sigma_o + m \ln (\epsilon_p + e^x)$$

or

$$dy = m \frac{1}{\epsilon_p + e^x} e^x \, dx$$

or

$$\frac{dy}{dx} = \frac{d(\log \sigma)}{d(\log \epsilon)} = m \frac{\epsilon}{\epsilon_p + \epsilon} \qquad \text{(II-8)}$$

Hence, it is apparent that the stress strain curve for previously cold worked material on logarithmic co-ordinates will have an increasing slope. In practice, it is possible to draw an approximate straight line for small strains. From Equations (II-7) and (II-8) it is also apparent that the slope of such an approximate line will be smaller with increasing value of ϵ_p, but its intercept at $\epsilon = 1$ will be higher. Similar general comments can be made for straining in directions other than that of prestraining, but the relation shown in Equation (II-8) is not expected to hold true.

Anistropic Yield and Flow

A yield criterion of material with orthotropic anisotropy in strength has been suggested by Hill.[17]

Similar relations from different assumptions have been stated by L. R. Jackson et al.[18] and by J. E. Dorn[10] and applied to the plastic flow of anisotropic sheet metals. Since these will be discussed in Chapter III, "Review of Literature," they are not presented here.

Physical Theory

In the theory of plasticity, the material is treated as a continuum, although in reality it is not. All metals consist of atoms

arranged geometrically according to the structure of their crystals. A polycrystalline material, as used in the present investigation, is composed of a large number of crystals with grain boundaries between them. The grain boundaries are areas of misfit and the atoms there are not properly lined up with the geometrical patterns of the grains they separate.

Although in the present investigation the material is treated as a continuum, a few comments about the physical nature of strain hardening should be made here.

Undeformed annealed metallic crystals contain about 10^6 to 10^8 dislocations per sq. cm. arranged in a random spatial network. On the application of a stress, some of the network elements can act as Frank-Read sources (dislocation generators), since their end points are more or less fixed. Also, often other structures in the crystals act as sources.

The mutual elastic interaction of dislocations increases with the dislocation density. In a highly cold worked material the density may be 10^{11} to 10^{12} dislocations per sq. cm. This is considered to be the basis of work hardening.(20)

Another effect is the mutual encounter of nearly parallel dislocations moving on different intersecting slip planes, resulting in a sessile dislocation which forms a barrier to other dislocations. A Frank-Read source on a slip plane where a barrier occurs can emit only a limited number of dislocation loops even under increasing shear stress because the loops cannot move further from the source than the

barrier permits and will pile up against it. Long range elastic stresses are associated with such dislocation pileups. Large stresses also occur on other slip planes in the neighborhood of a pileup and these limit the dislocation mobility on other slip systems[21] and hence plastic deformation is resisted.

Another important factor in strain hardening is the mutual intersection of non-parallel dislocations. This usually results in the formation of jogs and subsequent formation of point defects. A dislocation loop expanding through a forest of obstacles is likely to have an irregular shape.[22] Under certain conditions the jogs may be rendered immobile due to interaction with other obstacles. The loop then leaves behind vacancies or interstitials. With larger plastic deformation local tangles gradually develop into a network of subgrain boundaries.

Some very interesting electron micrographs have been presented by Snowden[23] showing dislocation patterns of cold worked aluminum crystals. More references to similar work have been made in Chapter III.

CHAPTER III

REVIEW OF LITERATURE

General Remarks

Recent literature on anisotropic behavior of materials has been reviewed in this chapter. Existing literature in this field can be roughly subdivided in three broad groups as follows:

(1) Those which present a theory of anisotropic strength and flow of material and try to check the theory by experiment;

(2) Those which try to present a physical model of anisotropic behavior;

(3) Those which investigate the actual behavior of materials.

The present investigation will, by and large, fall in the third group. However, to draw significant conclusions, it is necessary to keep in mind and also to refer to the findings of the first group of studies, and hence, short reviews of some works which are properly placed in the first group has been included here. The first few reviews are from this group. Reviews of articles from the third group follows those of the first.

Concise discussions of some of the articles of the third group that have direct bearing on the present investigation are presented. Space restrictions have forced others only to be mentioned.

From the second group, a few references have only been mentioned.

It has long been recognized that plastic strain is essentially a distortional[24,25] rather than a volumetric change. Plastic strain is therefore intrinsically directional. In cold working a material its mechanical properties change in response to this directional strain. Therefore, it cannot be postulated that an initially isotropic material will remain so after plastic strain. If the principal axes of stress remain unaltered and coincident with the axes of orthotropy while the strains develop, the principal axes of strain should also remain coincident with those of the stress, but the response of the material to stresses in those directions will not necessarily be the same; in fact they will be different in general, and this gives rise to anisotropy of mechanical properties.[26,27] Although the relations between stresses and strains for an annealed and presumably isotropic metal can be expressed as a function independent of direction, the stress-strain curves of a slightly coldworked metal have been found to vary considerably with the direction of testing.[28]

Three types of anisotropy have been listed by Klinger and Sachs[28,29,30]:

(a) Crystallographic anisotropy which results from preferred orientation or texture in the crystal structure of the metal. This develops gradually in an initially apparently isotropic material with the increase in cold work.[31-35]

(b) The second kind of anisotropy is due to mechanical fibring and elongation of inclusions, impurities and secondary phases due to processing. The probable effect of this kind of anisotropy is the variation of fracture characteristics.[25,32]

(c) The third kind of anisotropy has been called anelastic anisotropy which is supposedly due to residual stresses set up due to cold working.[29]

Anistropy in mechanical strength which causes earing during drawing is generally objectionable; but it has been said that the difference in properties in directions perpendicular and parallel to the sheet can be an asset in good drawability and be beneficial to press performance.[36]

Most of the experimental investigations concerning anisotropy of mechanical properties has been concerned with the behavior of rolled sheet or drawn tubes and rods.

Theoretical investigations were made on the basis of certain basic assumptions. Anisotropic behavior of materials were predicted according to these theories. The predicted behaviors were then compared with the behaviors of actual materials to assess the validity of the theories.

A number of investigators have used aluminum alloys for their tests and all of them used the old designations to identify them. In the following review the designations used by them has been retained. The table below is included as a ready reference showing the old and the new aluminum alloy designations.

TABLE III-I

DESIGNATION OF ALUMINUM ALLOYS

Old Number	New Number
2S*	1100
11S	2011
14S	2014
17S	2017
24S	2024
3S	3003
32S	4032
52S	5052
61S	6061
75S	7075

*The 'S' designates a wrought material.

Theoretical Investigations

Yield criterion of an anisotropic material. Hill[37] postulated that the yield criterion for an anisotropic material should be of the form

$$2f(\sigma_{ij}) \equiv F(\sigma_y-\sigma_z)^2 + G(\sigma_z-\sigma_x)^2 + H(\sigma_x-\sigma_y)^2 + 2L\tau_{yz}^2 + 2M\tau_{zx}^2 + 2N\tau_{xy}^2 = 1 \qquad \text{(III-1)}$$

where σ and τ's are the direct and shear stresses referred to the axes of orthotropy and F, G, H, L, M and N are parameters characteristic of the current state of anisotropy. It was assumed that no Bauschinger effect was present. It was shown that if U, V, and W denotes the yield stresses in the principal directions of anisotropy and R, S and

T the yield stresses in shear with respect to the principal axes, then,

$$2F = \frac{1}{V^2} + \frac{1}{W^2} - \frac{1}{U^2}$$

$$2G = \frac{1}{W^2} + \frac{1}{U^2} - \frac{1}{V^2}$$

$$2H = \frac{1}{U^2} + \frac{1}{V^2} - \frac{1}{W^2}$$

$$2L = \frac{1}{R^2}$$

$$2M = \frac{1}{S^2} \qquad \text{(III-2)}$$

and $$2N = \frac{1}{T^2}$$

For an isotropic material U = V = W and R = S = T and $U = \sqrt{3}R$.

Hence

$$F = G = H = \frac{1}{2U^2}$$

$$L = M = N = \frac{1}{2R^2} = \frac{3}{2}\frac{1}{U^2} \qquad \text{(III-3)}$$

and Equation (III-1) reduced to Von Mises criterion for yielding for isotropic materials.

The strain increment relations are given by

$$d\epsilon_x = d\lambda\,[H(\sigma_x - \sigma_y) + G(\sigma_x - \sigma_z)]$$

$$d\epsilon_y = d\lambda\,[F(\sigma_y - \sigma_z) + H(\sigma_y - \sigma_x)]$$

$$d\epsilon_z = d\lambda\,[G(\sigma_z - \sigma_x) + F(\sigma_z - \sigma_y)]$$

$$d\gamma_{yz} = d\lambda L\tau_{yz}$$

$$d\gamma_{zx} = d\lambda M\tau_{zx}$$

and $$d\gamma_{xy} = d\lambda N\tau_{xy} \qquad \text{(III-4)}$$

where ϵ and γ's are shear strains referred to the axes of orthotropy and λ a rate constant.

Jackson, et al.[18] described anisotropy in terms of several parameters describing deviation from isotropy and plastic Poisson's ratios. They assumed that strain increments can be expressed as:

$$d\epsilon_x = \frac{\overline{d\epsilon}}{\overline{\sigma}} (a\sigma_x - b\mu_{yx}\sigma_y - c\mu_{zx}\sigma_z)$$

$$d\epsilon_y = \frac{\overline{d\epsilon}}{\overline{\sigma}} (-a\mu_{xy}\sigma_x + b\sigma_y - c\mu_{zy}\sigma_z)$$

and $$d\epsilon_z = \frac{\overline{d\epsilon}}{\overline{\sigma}} (-a\mu_{xz}\sigma_x - b\mu_{yz}\sigma_y + c\mu_z) \qquad \text{(III-5)}$$

where $\overline{\sigma}$ = "Effective stress"

$$= \left\{ \frac{3}{2(K_{yz} + K_{xz} + K_{yz} K_{xz})} [K_{yz} K_{xz} (\sigma_x - \sigma_y)^2 + K_{xz} (\sigma_z - \sigma_x)^2 + K_{yz}(\sigma_y - \sigma_z)^2] \right\}^{\frac{1}{2}}$$

$\overline{d\epsilon}$ = "Effective strain"

$$= \frac{\sigma_x d\epsilon_x + \sigma_y d\epsilon_y + \sigma_z d\epsilon_z}{\overline{\sigma}}$$

$$K_{yz} = \frac{\epsilon_y}{\epsilon_z}, \qquad \text{when} \quad \sigma_y = \sigma_z = 0$$

$$K_{xz} = \frac{\epsilon_x}{\epsilon_z}, \qquad \text{when} \quad \sigma_x = \sigma_z = 0$$

$$\mu_{xy} = -\frac{d\epsilon_y}{a\sigma_x}, \qquad \text{when} \quad \sigma_y = \sigma_z = 0$$

$$\mu_{xz} = -\frac{d\epsilon_z}{a\sigma_x}, \qquad \text{when} \quad \sigma_y = \sigma_z = 0$$

$$\mu_{yz} = -\frac{d\epsilon_z}{b\sigma_y} \quad , \qquad \text{when} \quad \sigma_x = \sigma_z = 0$$

etc.

a, b and c are measures of deviation of the material from isotropy and a + b + c = 3. x, y and z are axes of orthotropic symmetry.

In an isotropic material,

$$a = b = c = 1 \quad \text{and} \quad \mu_{xy} = \mu_{yz} = \ldots = \mu$$

They used rimmed annealed sheet steel, aluminum killed annealed and temper rolled sheet steel and "Cor-ten"* sheet steel for their tests. Straining was done by direct tensile tests and circular and elliptical bulging by hydraulic pressure. True effective stresses were plotted against true effective strains assuming isotropic symmetry and again assuming orthotropic symmetry. In the first case tensile and bulge tests showed wide divergence. In the second case about half the tests showed good agreement.

Assuming that the components of strain rates are linear functions of stresses, Dorn[14] formulated six plastic strain rate equations as follows:

$$\dot{\epsilon}_{xx} = \dot{A}_{11}\tau_{xx} + \dot{A}_{12}\tau_{yy} + \dot{A}_{13}\tau_{zz} + \dot{A}_{14}\tau_{xy} + \dot{A}_{15}\tau_{yz} + \dot{A}_{16}\tau_{zx}$$

$$\dot{\epsilon}_{xy} = \dot{A}_{41}\tau_{xx} + \dot{A}_{42}\tau_{yy} + \dot{A}_{43}\tau_{zz} + \dot{A}_{44}\tau_{xy} + \dot{A}_{45}\tau_{yz} + \dot{A}_{46}\tau_{zx}$$

etc. (III-6)

*Composition: 0.10 max. C, 0.1 - 0.3 Mn, 0.1 - 0.2 P, 0.5 - 1.0 Si, 0.3 - 0.5 Cu, 0.5 - 1.5 Cr., balance Fe.
Small amount of Ni may be added.

This is noted that in a general case $\dot{A}_{kl} \neq \dot{A}_{lk}$ and hence the 36 coefficients may be different from one another. However, for planer plastic flow, as in sheet metals and assuming symmetry about y-z plane,* the equations reduce to:

$$\dot{\epsilon}_{xx} = \dot{A}_{11}\tau_{xx} + \dot{A}_{12}\tau_{yy}$$

$$\dot{\epsilon}_{yy} = \dot{A}_{21}\tau_{xx} + \dot{A}_{22}\tau_{yy}$$

and

$$\dot{\epsilon}_{xy} = \dot{A}_{44}\tau_{xy} \qquad \text{(III-7)}$$

if x and y are orthotropic axes and $\tau_{zz} = 0$.

Assuming constant anisotropy, relations similar to that of Jackson, et al.[18] were found.

This theory was experimentally verified by Hazlett et al.[38] It was shown that Equation (III-7) can be expressed as:

$$d\epsilon_{xx} = \frac{\overline{d\phi}}{\bar{\sigma}} \{\alpha_{11}\sigma_{xx} + \alpha_{12}\sigma_{yy}\}$$

$$d\epsilon_{yy} = \frac{\overline{d\phi}}{\bar{\sigma}} \{\alpha_{21}\sigma_{xx} + \alpha_{22}\sigma_{yy}\}$$

and

$$d\epsilon_{xy} = \frac{\overline{d\phi}}{\bar{\sigma}} \{\alpha_{44}\sigma_{xy}\} \qquad \text{(III-8)}$$

where $d\epsilon_{xx}$ = Strain increment on a fiber instantaneously in the cross rolling direction.

$d\epsilon_{yy}$ = Strain increment on a fiber instantaneously in the rolling direction.

$d\epsilon_{xy}$ = Shear strain increment between fibers instantaneously in the cross-rolling and rolling directions respectively.

*x and y are the transverse and the rolling directions respectively, and the z direction is normal to the x and y directions.

σ_{xx} = Normal stress in the cross rolling direction on a plane whose normal is in the cross rolling direction.

σ_{yy} = Normal stress in the rolling direction of a plane whose normal is in the rolling direction.

σ_{xy} = Shear stress in Y direction on a plane whose normal is in the X-direction.

α_{ij} = Coefficients of anisotropy (i = 1 to 6, j = 1 to 6)

$$\bar{\sigma} = \sqrt{\sigma_{xx}(\alpha_{11}\sigma_{xx} + \alpha_{12}\sigma_{yy}) + \sigma_{yy}(\alpha_{21}\sigma_{xx} + \alpha_{22}\sigma_{yy}) + \alpha_{44}\sigma_{xy}^2}$$

and

$$\overline{d\phi} = \sqrt{\left(\frac{\alpha_{22}(d\epsilon_{xx})^2 - (\alpha_{12} + \alpha_{21})d\epsilon_{xx}d\epsilon_{yy} + \alpha_{11}(d\epsilon_{yy})^2}{\alpha_{11}\alpha_{22} - \alpha_{12}\alpha_{21}} + \frac{(d\epsilon_{xy})^2}{\alpha_{44}}\right)}$$

Observations on the deformation of mild steel plates were in excellent agreement with the theory. However, the ratios α_{21}/α_{22} and α_{21}/α_{11} were -0.48 for this material, while for an isotropic material it would be -0.5 which means that the material was rather close to isotropy to begin with and hence the agreement may not be significant. For 3S-0 aluminum alloy for which the coefficients were

$$\alpha_{11} = 1.0; \quad \alpha_{12} = -0.383; \quad \alpha_{21} = -0.34 \quad \text{and} \quad \alpha_{22} = 0.957$$

agreement between theory and observation was not very good. The theory was applied to data reported by Stang et al.[39] for 24S-T3 alloy. The coefficients were $\alpha_{11} = 1$, $\alpha_{12} = -0.436$, $\alpha_{21} = -0.375$ and $\alpha_{22} = 0.939$. Again, the theoretical and experimental values were not in precise agreement. Deviations were noted with 61S-T6 alloy also.

A rather different theory was proposed by Fisher.[40] This is based on the concept of slip in metal crystals. Slip bands are thought of as regions of relative motion between two plastically undisturbed portions of a crystal. During the slip process the slip bands are unable to support a shearing stress in the direction of slip. After slip has occurred, however, the bands very rapidly regain their ability to withstand shearing stresses. During slip the elastic strain energy near the slip band is relieved and a smaller amount of strain energy is concentrated near the perimeter of the slip band, unless the band terminates at a free surface of the metal.

The plastic stress-strain relationships were derived assuming this slip mechanism of plastic flow. The essential features of this theory are as follows:

(1) The definition of an effective stress proportional to the square root of the strain energy per unit volume released by slip in the neighborhood of a slip band.

(2) The definition of an effective strain such that the integral of effective stress with respect to effective strain gives the work done in deforming a unit volume of material.

(3) The assumption that the effective strain (or the work done per unit deformed volume) is a satisfactory measure of deformation.

(4) A demonstration that there exists a functional relationship between the effective strain and the effective stress required to maintain a constant strain rate at a constant temperature.

(5) A demonstration that the plastic strain increments are proportional to the difference between (a) the elastic strains before slip and (b) the elastic strains in the slip region after slip.

Principal axes of stresses and strains were assumed to coincide with the axes of orthotropic symmetry. It was also assumed that after slip, the stresses in the slipped region are linear functions of applied principal stresses σ_1, σ_2 and σ_3

$$\begin{aligned}
\sigma_1' &= \alpha_{11}\sigma_1 + \alpha_{12}\sigma_2 + \alpha_{13}\sigma_3 \\
\sigma_2' &= \alpha_{21}\sigma_1 + \alpha_{22}\sigma_2 + \alpha_{23}\sigma_3 \\
\sigma_3' &= \alpha_{31}\sigma_1 + \alpha_{32}\sigma_2 + \alpha_{33}\sigma_3 \\
\tau_{23}' &= \alpha_{41}\sigma_1 + \alpha_{42}\sigma_2 + \alpha_{43}\sigma_3 \\
\tau_{31}' &= \alpha_{51}\sigma_1 + \alpha_{52}\sigma_2 + \alpha_{53}\sigma_3 \\
\text{and} \quad \tau_{12}' &= \alpha_{61}\sigma_1 + \alpha_{62}\sigma_2 + \alpha_{63}\sigma_3 \qquad \text{(III-9)}
\end{aligned}$$

From these assumptions, it was shown that the effective stress can be defined as:

$$\bar{\sigma} = \frac{1}{\sqrt{2}} \sqrt{[(\sigma_1-\sigma_2)^2 + (1+m)(\sigma_2-\sigma_3)^2 + (\sigma_3 - \sigma_1)^2]}$$

And the effective strain increment can be defined as:

$$\begin{aligned}
\overline{d\epsilon} &= \frac{1}{\bar{\sigma}} (\sigma_1 d\epsilon_1 + \sigma_2 d\epsilon_2 + \sigma_3 d\epsilon_3) \\
&= \sqrt{2}\, \frac{\beta d\epsilon_1^2 + d\epsilon_2^2 + d\epsilon_3^2}{\sqrt{[(\beta d\epsilon_1 - d\epsilon_2)^2 + (1+m)(d\epsilon_2 - d\epsilon_3)^2 + (d\epsilon_3 - \beta d\epsilon_1)^2]}}
\end{aligned}$$

where

$$m = \frac{4(\alpha_{22} - \alpha_{11})(1 - \alpha_{11} - 2\alpha_{22})}{(1 + 3\alpha_{11})(1 - \alpha_{11})}$$

and

$$\beta = \frac{1 + \alpha_{11} - 2\alpha_{22}}{1 - \alpha_{11}}$$

Tests on an aluminum bar, 10 feet long and 6 inches in diameter showed that the predictions of this theory deviated from the experimental value by about 4% compared to about 9% deviation for distortion energy theory.

Batdorf and Budiansky[10,11] proposed a theory of plasticity based on slip in the crystals of polycrystalline aggregates. The basic assumptions are as follows:

(1) A metal that is isotropic in the gross mechanical sense can be sufficiently approximated theoretically by an aggregate of randomly oriented crystals regarded identical with each other except for orientation.

(2) The grain is the smallest structural unit.

(3) Local variation of stress within a grain can be neglected.

(4) The grains deform by slip.

The theory was successfully applied in the case of biaxial, loading, but its application to tension followed by partial unloading and then to torsion was found unsatisfactory.

One consequence of the postulates of this theory is the possibility of production of a corner on a otherwise smooth yield surface. Naghdi, et al.[41] tested anisotropic tubes of 24S-T4

aluminum alloy subjected to variable ratios of tension and torsion. Their findings suggest existence of such yield corners. Linearity of the increment of the plastic strain in the increment of stress could not be ascertained.

Ashkenazi[42] formulated anisotropy of yield strength of materials assuming that the yield strength can be treated as a fourth order tensor, and developed mathematical relations which would permit the determination of the whole field of resistance in the material if its strength in several basic directions are experimentally determined.

Experimental Investigations

Perhaps the earliest experimental investigation in the anisotropy of yield properties of cold strained material was by Professor Bauschinger[43] of Munich. He showed that when a material is loaded beyond its elastic limit, unloaded and reloaded in the opposite sense, the second elastic limit is found to be lower than that of the virgin material. Also, he concluded that the higher the stress in the first loading, the lower is the elastic limit for subsequent loading in opposite sense. This effect is known as the Bauschinger effect and was first recognized in 1881. Subsequently it was found that not only was the elastic limit lowered, but the material was weakened for subsequent loading in the opposite direction after prestraining, and the stress strain curve for the subsequent test was below that of the virgin material.

Schwartzbart, et al.[44] studied the Bauschinger effect in copper and brass prestrained in tension and tested in compression. Their findings are as follows:

(a) The Bauschinger effect develops at very small prestrains, less than $\epsilon_p = 0.005$, and remains essentially constant up to a prestrain of $\epsilon_p = 0.65$.

(b) The Bauschinger effect disappears after a strain in the subsequent compression test exceeded $\epsilon = 0.01$.

(c) Tensile prestrain weakens the material in subsequent compression. The degree of weakening increases with prestrain up to about $\epsilon_p = 0.30$, above which the effect is constant.

(d) The shape of the stress-strain curve in compression after tensile prestrain is a function of the prestrain. For prestrains below $\epsilon_p = 0.15$, the form of the curve is similar to that for an annealed specimen. Above this prestrain, the curve exhibits a region of low slope immediately after initial yielding. The slope of this initial part, in turn, decreased with increasing prestrain until it becomes practically horizontal at a prestrain of $\epsilon_p = 0.24$. This behavior is similar to the "yield point effect" in mild steel. Once the initial region of low slope was exceeded the slope of the compression curve was essentially parallel to the virgin compression curve.

They introduced a correction factor for compression to take into account the texture produced by cold work in such a way that ratio of flow stress in tension and in compression is a constant at any strain level. The validity of such correction seems questionable.

Naghdi, et al.[26] investigated the change of the yield surface of 24S-T4 aluminum alloy tubes under a program of tension and torsion where the tensile stresses were always less than the yield stress. They reported the following observations:

(a) The initial as well as subsequent yield surfaces in tension-torsion plane are convex;

(b) The initial yield surface is essentially symmetric about the tension axis;

(c) While the yield stress in tension is unaltered, the yield surfaces in the neighborhood of the torsion axis display a pronounced Bauschinger effect which gradually vanishes as the curve approaches the tension axis;

(d) The effect of work hardening rapidly diminishes as the tension axis is approached but is accompanied by a gradual linearization of the subsequent yield surfaces in the first quadrant, producing a region of high curvature about the torsion axis.

This is reminiscent of corners predicted by the slip theory of plasticity.[10] This may also be viewed in terms of incremental theory based on an infinite set of plane loading surfaces.[45]

(e) The initial yield surface is almost identical with von Mises type yield surface.

Cunningham, et al.[46] reported variation in the distortion energy ellipse for different stages of straining. Biaxial tension

tests with variable stress ratio for 14S-T4 aluminum alloy was made by Marin and Hu[47] which showed that neither distortion energy, nor maximum shear criterions were adequate. Similar tests on 14S-T6 aluminum alloy and cold drawn mild steel[48] and 24ST aluminum alloy[49] showed similar results.

Based on Hill's theory of plasticity[37] for anisotropic materials, Hu[50] derived plastic stress-strain increment relations for strain hardening materials. He also discussed the influence of anisotropy on the plastic behavior of metals in a state of plane stress or plane strain. It was found that the pressure carrying capacity of a thick walled cylinder under internal pressure can be increased by decreasing the axial strength. For conventional biaxial stresses, the method of interpretation of test results were found valid for biaxial tension tests of anisotropic materials, but not valid for tension-torsion tests.

Bridgman[51] investigated the variation of yield and flow stresses in the longitudinal and the transverse directions of steels cold worked to large strains under high superimposed hydraulic pressure. His investigations can be divided into the following sections:

(a) Simple Tension After Prestraining in Tension. Specimens were pulled in tension under different hydrostatic pressures and then pulled again under atmospheric pressure. It was possible to pull to a much higher strain under pressure than was possible under atmospheric pressure, and in spite of that fact there was residual ductility left for straining at atmospheric pressure. The stress-strain points on

the second pulling at atmospheric pressure fall on a single line irrespective of the pressure or the strain of the first pulling.

The stress-strain curve for pulling under pressure lies higher than the stress-strain curve for atmospheric pressure; the difference being greater with higher pressure.

(b) Simple Tension After Prestraining in Compression. The material was strained in compression to a true strain of about 1.25 under hydrostatic pressure. Tension specimens cut in logitudinal and transverse directions were tested. It was found that the strength of the material increased in both directions compared to the virgin material, but hardening was not equal in two directions. The transverse direction was found to be much stronger in tension than the longitudinal direction. The strain hardening rate was lower and so also the residual ductility.

(c) Simple Tension After Prestraining in Two Dimensional Compression. The material was prestrained in compression in such a way that the strain in one transverse direction was zero. The prestrain was about 0.4.

The material was found anisotropic after prestraining, although the strength was higher in all directions compared to the virgin metal. The tensile strength was lowest in the direction of compressive prestrain, but the residual ductility at fracture was highest. The mechanical properties in the other two directions did not show any such consistency.

(d) Compression After Tension Under Pressure. Compression tests were made on specimens taken from the necked region and tested

in the same direction. For small prestrains, reduction in the compressive strength was noticed.

(e) Simple Compression After Prestraining in Compression. The material was found anisotropic after prestraining to different strains. Strengths in the transverse directions were found lower than in the longitudinal direction, although higher than that of the virgin material.

(f) Simple Compression After Prestraining in Two Dimensional Compression. Cr-V steel and stainless steel were used for this test. Strain in one direction was held at zero. Subsequent compression in the direction of zero strain showed slightly lesser strength than the original compressive stress in the direction of compression. Moreover slight strain-softening was noticed during the subsequent test.

Mehringer and McGregor[52] investigated the variation of stress-strain properties of cold rolled low carbon steel. They rolled steel bars to different reductions in thickness, machined tensile specimens cut out at different angles with the direction of rolling and plotted true stress-strain diagrams. However, they did not consider the triaxiality of stresses[53,54,55] at the neck, and true stress was defined simply as load divided by instantaneous area at the neck, and hence the stresses obtained after necking were too high.

The material used was isotropic in the annealed state so far as the strength was concerned, but was anisotropic in strains which was manifested by the ellipticity of the test specimens at strains beyond necking. They observed that the cross sections remained circular during uniform strains, and became elliptical only after

necking started. They also investigated the effect of cold working by tensile pull on true stress-strain curves. Mehringer and McGregor made the observations as below:

The "modulus of strain hardening" $m = \partial\sigma/\partial\epsilon$ is not greatly affected up to a reduction of 10%. It decreases for higher reductions, and the greatest decrease is for the 90° inclination to the rolling direction.

Increased reductions by rolling also reduce the true uniform strain at the maximum load, and the true fracture strains.

No appreciable increase in the true fracture stress takes place until about 30% reduction is reached, except for the specimens at 90° to the rolling direction.

True stress at maximum load is increased by large reductions by rolling.

The net effect of stretching up to 15% on the true stress-true strain properties is equivalent to the same reduction by cold rolling on specimens cut out at 0° to the rolling (and stretching) direction. However, for specimens cut at 90° to the rolling direction, 10% reduction by rolling is equivalent to a 15% reduction by stretching.

Up to 10% reduction by rolling, the true stress at maximum load remains constant for all directions. After that, it increases rapidly. True stress at fracture remains practically constant till about 35% reduction for

specimens at 0° and 45° to the rolling direction and then increases slightly. For specimens at 90°, it remains constant to about 15% and then increases a little more rapidly than those at 0° and 45°.

The modulus m decreases with increasing reduction by rolling, although the scatter is rather large.

Vickers hardness values increases rapidly with small reductions in rolling. The rate of increase of hardness decreases until a reduction of about 45% is reached. Thereafter, it increases uniformly. All true stress-true strain diagrams were plotted in Cartesian co-ordinates.

Klinger and Sachs[28] investigated the anisotropic behavior of 24ST and 24SRT aluminum alloy sheet. During fabrication, 24ST sheet is a stretched, and/or rolled by about 1% while 24SRT is rolled by 5 to 6% to increase its strength. They found that the tensile strength is higher than the compressive strength when tested parallel to the grain. When tested perpendicular to the grain, the strengths are of intermediate value, the compressive strength being higher than the tensile strength. If no cold work is applied, the strengths are almost identical in both directions. Table III-II shows some of the data obtained by them.

It was also found that after prestraining by rolling, the transverse stress-strain curve in tension is similar to the longitudinal stress-strain curve in compression. Apparently, rolling acts, in this respect, similar to stretching by tension.

For any given plastic strain, the stress decreases first approximately linearly with the angle between rolling direction and testing direction to about 50°, and then decreases at a much slower rate, to 90°. The total difference increases rapidly with decreasing strain, the transverse strength being about 76% of longitudinal strength in tension. Anisotropy in compression is considerably smaller than in tension.

Cold rolled 24ST aluminum plates were found to have definite degree of preferred orientation. For annealed material, the yield strength varied only slightly, but the plastic Poisson's ratio showed large deviation from isotropy.

TABLE III-II

STRENGTH OF 24ST AND 24SRT ALUMINUM ALLOYS

		0.2% Offset Yield Stress in ksi		Flow Stress in ksi at 1% Total Strain	
		Tension	Compression	Tension	Compression
24ST	Parallel to Grain	51.5	42.0	53.0	48.0
	Perp. to Grain	43.5	47.5	48.5	51.0
24SRT	Parallel to Grain	63.0	53.0	64.5	58.0
	Perp. to Grain	55.5	58.5	59.5	61.0

Ebert[56] investigated the transverse and longitudinal properties of steel bars, cold drawn through carbide dies of 8° half angle. Most specimens were roller straightened and others were left unstraightened.

He found that the steels respond to the strengthening effect of cold work as regards the tensile and yield strengths in the same relative manner in both the transverse and longitudinal directions.

The shape of the trend curves for the yield and tensile strengths as functions of the amount of cold work are not as consistent for the transverse tests as they are for longitudinal tests, the major difference being the absence of the last rapid increase in strength. He observed two apparent anomalies. First, the leveling off of the "strength trend curve" for 1040 steel at reductions above 25%, and perhaps even a slight decrease with increasing cold work. Second, the slight decrease in the tensile strength of 1060 steel at a very small amount of cold work.

The tensile strength and yield strength values are somewhat lower for the transverse specimens compared to those for the longitudinal ones. This difference was quite small when stress relieved[4] values were compared.

Two steels, 1040 and 4615 showed high initial directionality in ductility which increased with further cold working.

Ebert concluded from his tests that cold working by drawing produces little directionality in the tensile strength, marked directionality in the yield stress, which can be removed by stress relieving and a limited directionality in the ductility.

Rosalsky[57] used 3/4 inch 2S-0 aluminum plate to investigate the effect of prestraining by different stress states on yield and fracture properties. Tensile prestrains were produced by tension and by cross compression, and compressive prestrains by direct

compression and by bulging. The material was tested in tension in different directions. No stress-strain curves were plotted.

His conclusions were that the fracture properties of 2S-O aluminum depend not only upon the nature and magnitude of the prestrain, but also upon the stress state under which a given prestrain is effected. For tensile prestrains of the same magnitude (after a critical amount of prestrain) a stress state of biaxial compression resulted in a higher retained ductility than did a stress state of simple tension. However, for tensile prestrains of the same magnitude, a stress state of simple tension resulted in the same retained tensile ductility as did a stress state of cross compression.

For compressive prestrains of the same magnitude, a stress state of simple compression resulted in a higher tensile fracture stress in subsequent testing, than such prestrain obtained by biaxial tension.

The shapes of the curves obtained for the tensile fracture stress versus prestrain differed considerably when the stress state for prestraining was varied.

No significant changes in the tensile yield strength versus prestrain curves were obtained by variations in the prestraining stress state. For the tests, the material was annealed at 650° for 30 minutes. From the yield data it seems unlikely that annealing was complete.

Burns and Heyer[58] investigated the anisotropy of strength and plastic properties of low carbon sheet steel. They used flat specimens in an attempt to measure variations in plastic strains.

Since the slip line fields for flat and for round specimens are very different from each other, the correlations found may be doubtful. It has been recommended by Rittenhouse and Picklesimer[38] that only round specimens should be used for such studies.

Stowell and Pride[27] deduced a large number of semi-empirical relations between Poisson's ratios in the plastic range and presented stress-strain curves both in tension and in compression. Tests were carried out on aluminum blocks and stainless steel sheets. Correlation appears to be good.

Gerard and Wildhorn[59] reported a set of test data for the variation of Poisson's ratio in the yield region of the stress-strain curve for the aluminum alloys 14S-T6, 24S-T4 and 75S-T6.

Miller[60] reported experimental stress-strain data for tension and compression of different thicknesses of 75S-T6 aluminum alloy sheets which showed small anisotropy of strength at small plastic strains, but the stress-strain diagrams almost coinciding for elastic strains and large plastic strains.

Anisotropic behavior of Zircaloy-2,[61] which is an important material for reactor applications, was investigated by Mehan. He analyzed the stress-strain characteristics under combined stresses according to Hill's theory for anisotropic flow, although it has not been shown whether Hill's postulates are satisfied. Some of the data seem to be good.

A very extensive investigation on the effects of fabrication on the anisotropic behavior of Zircaloy was made by Rittenhouse and Picklesimer.[62,63]

A few investigations on the dislocation patterns produced by cold working are mentioned below.

N. F. Mott[64] investigated the phenomenon of piling up of dislocations against a barrier, theoretically as well as experimentally. Wilsdorf and Schmitz[65] presented electron micrographs of glide dislocations and dislocation tangles in 99.99% pure aluminum single crystals oriented for single slip for deformations up to 1%. Tomlinson[66] deformed magnesium, cobalt, copper, nickel, aluminum, brass and iron 0.8 to 25% by rolling and by tension and prepared electron micrographs of dislocation tangles and subgrain boundaries. Segall and Partridge[67] investigated the dislocation arrangements in deformed aluminum polycrystals.

CHAPTER IV

EXPERIMENTAL PROGRAM

From the preceding chapters, viz. Theoretical Considerations and Review of Literature, it is seen that although a large amount of work has been done on the anisotropic behavior of metals under different conditions of plastic straining our knowledge about the same is far from complete.

Most of the investigations about the anisotropic behavior of prestrained materials have been limited to small prestrains only. However, as noted in the Introduction, there are a variety of processes like extrusion, drawing, etc. which are common in mechanical engineering practice and involve very large plastic strains. Experimental data regarding directional variation of mechanical properties developed by such large strains is very scarce. In an attempt to explore this field the following experimental program was drawn up.

This chapter on experimental program has been divided into three sections and discussed as below:

A. Selection of Material;

B. Program Outline;

C. Experimental Procedure.

A. Selection of Material

Reasons for Selecting Aluminum

As mentioned in Chapter I, commercially pure aluminum was selected as the material for the present investigation. The reasons

for this selection are as follows:

(a) Being a single phase solid solution, it would be possible to extend the conclusions arrived at to a wide variety of materials;

(b) It is a very widely used engineering material, is readily available and is inexpensive;

(c) Blocks big enough to yield tensile specimens can be prestrained without too great difficulty.

(d) Being a fcc solid solution, it has a large number of slip planes and was expected to exhibit reasonable isotropy in the annealed condition.

Fabrication Procedure

One bar of 1100-F aluminum, 4 inches in diameter and 12 feet long was purchased as supplied by retailers. The chemical composition of the material is given in Table IV-I.

The fabrication procedure used to manufacture this bar is as follows:

The metal is cast as a 14" x 14" square ingot, hot rolled to 6-3/8" x 6-3/8" bloom stock, cooled to room temperature and scalped to 6" x 6" square billet. The billet is hot rolled to finish size, cooled to room temperature, and finally roll straightened.

It has been stated that the cold work in processing is limited to the small amount involved in roll straightening. As such, it was assumed that the grains would be randomly oriented. Unfortunately, it did not corroborate to later experimental findings. The material was

TABLE IV-I

COMPOSITION OF 1100-0 ALUMINUM

	Required		
Element	Minimum	Maximum	Actual
Aluminum	99.00	----	99.07
Iron	-----	----	.57
Silicon	-----	----	.12
Iron + Silicon	-----	1.00	.69
Copper	-----	0.20	.18
Manganese	-----	0.05	.008
Zinc	-----	0.10	.00
Others			
Each	-----	0.05	.03
Total	-----	0.15	.06

found to be anisotropic at least as far as the strains are concerned even in the annealed state.

B. Program Outline

For the purpose of investigation of the directional variation of the mechanical properties, it was decided to proceed as detailed below:

(a) The material was to be machined to produce prestrain specimens for tensile and for compressive prestrains.

After machining, the prestrain specimens were to be annealed and then strained to different prestrain states in tension and in compression at the lowest practicable strain rate.

(b) The axes of orthotropy were to be found by measurement of diameters of the prestrained material.

(c) Blanks were to be cut from the prestrained material with reference to the three orthotropic directions to make specimens for the tests mentioned below in (d).

(d) Three kinds of tests were to be made, viz.,

(i) Tension tests;

(ii) Compression tests;

(iii) Plane Strain tests.

For tension and for compression tests, an average of two tests were to be taken for each case. Test specimens were to be machined out of the blanks cut from the prestrain specimens.

(e) True stress-true strain diagrams were to be plotted from the data obtained from the tension and compression tests and flow constants determined. The curves were to be drawn in different combinations to assess the differences between the curves.

(f) Yield surfaces were to be constructed with the help of the yield data obtained from the three kinds of tests and measured values of plastic Poisson's ratios.

(g) Fracture cross-sections were to be measured and residual ductilities in tension were to be calculated and plotted against prestrains.

C. Experimental Procedure

This section is devoted to descriptions of the processing of the material, equipment used, specimens, and methods of testing.

Processing of Material

The material was purchased as a 4 inch diameter bar in the 1100-F condition. An outline of prior processing has been mentioned in a preceding section of this chapter. It was anticipated from this processing history that the material should be in an almost annealed condition with very small amount of cold work in it and also that it should be isotropic; at least there should be an axial symmetry of properties. Unfortunately, that was not the case. A hardness traverse of a cross-section showed variations from 57 R_H to 67 R_H from the center to the periphery, which is equivalent to true strains from 0.05 to 0.15 according to previous investigations by the author. Also it was found that when an annealed specimen was strained along an axis parallel to the axis of the bar, transverse strains were not uniform, but a circular section became approximately elliptical. The directions for largest and smallest strains remained always constant irrespective of the location of the specimen in the bar. Also, when a specimen taken at right angles to the bar axis was strained, one of the principal axes was always found parallel to the bar axis. Hence, it was deduced

that the material was not isotropic, but was orthotropic in nature, one of the axes of orthotropy being parallel to the axis of the bar.

Designation of Prestrain

Now, since it was recognized that the material was anisotropic, it was necessary to designate the three principal directions of orthotropy by some means. The axial direction was called the 'Z' direction, the direction of largest transverse strain when the material was stressed uniaxially along the Z direction was designated as the 'X' direction and that of smallest transverse strain was called the 'Y' direction. They are shown in Figure IV-1. On all specimens tested, at least two of these directions were marked on the specimens at all stages of fabrication.

The material was always prestrained in the 'Z' direction. The material was tested in the annealed condition, 10 conditions of varying degrees of compressive prestrain, and 4 conditions of tensile prestrain. The coding system and their repsective prestrains are given in Table IV-II.

It was possible to prestrain in compression to a true strain of 1.953, but in tension only to 0.245. The limiting factor in compressive prestrain was the tallest specimen of 4 inch diameter that could be compressed without causing buckling. A specimen 4 inches in diameter and 7 inches long was successfully compressed, but an 8 inch long specimen buckled and had to be discarded. On the other hand, in tensile prestrain the limiting factor was the end of uniform elongation and incipient necking. Figures IV-2 and IV-3 show the approximate

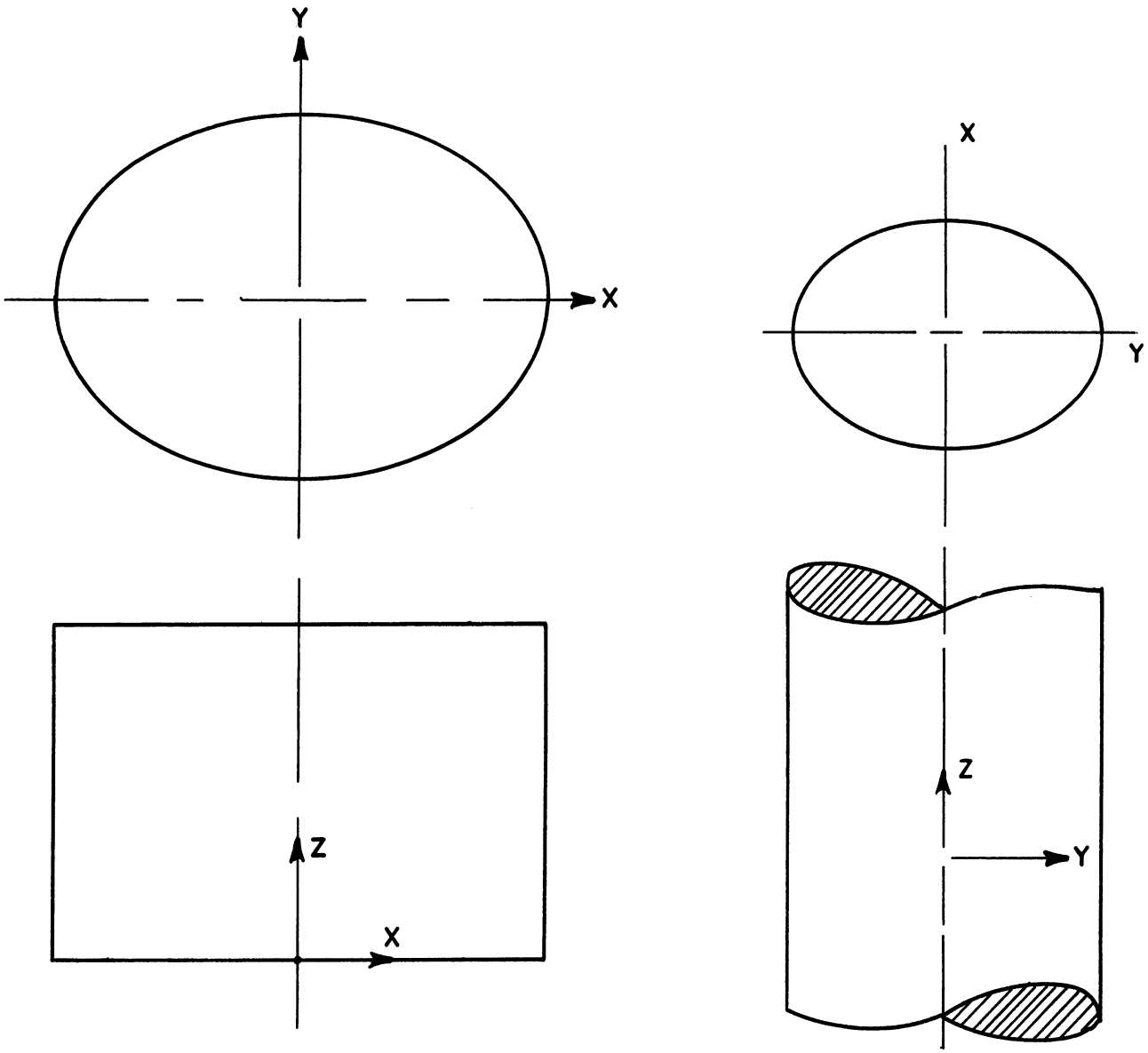

Figure IV-1. Axes of Orthotropy.

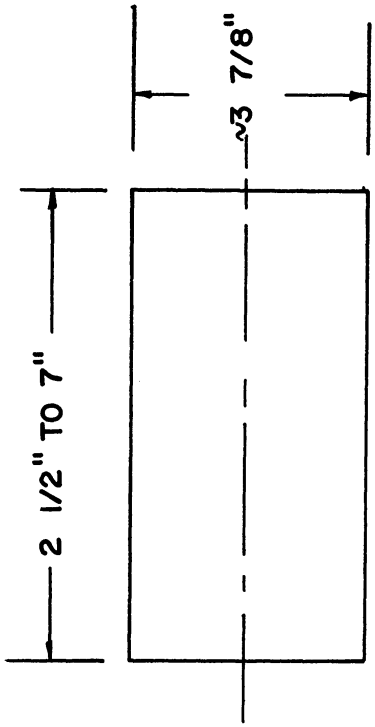

Figure IV-2. Specimen for Compressive Prestraining.

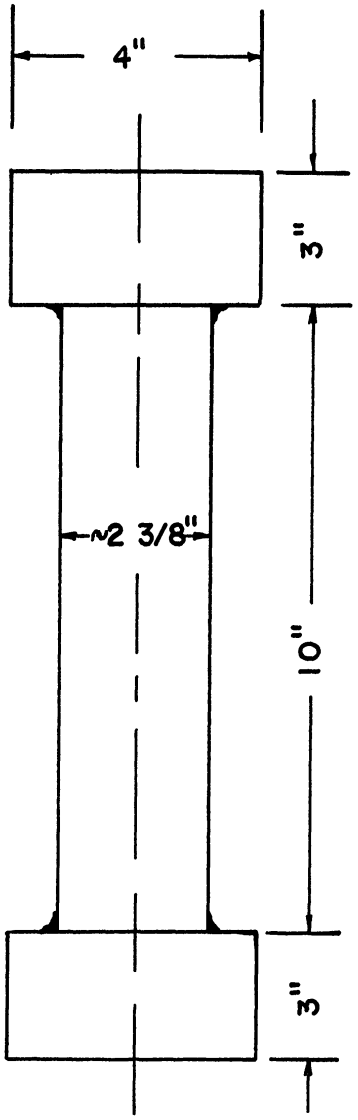

Figure IV-3. Specimen for Tensile Prestraining.

TABLE IV-II

PRESTRAIN DESIGNATIONS*

A	Zero prestrain	
C2	Compressive prestrain	0.106
C3	Compressive prestrain	0.1494
C4	Compressive prestrain	0.204
C5	Compressive prestrain	0.244
C6	Compressive prestrain	0.300
C7	Compressive prestrain	0.455
C8	Compressive prestrain	0.673
C9	Compressive prestrain	1.953
C10	Compressive prestrain	1.010
C11	Compressive prestrain	1.490
T11	Tensile prestrain	0.1098
T15	Tensile prestrain	0.152
T20	Tensile prestrain	0.206
T25	Tensile prestrain	0.245

*Designation of tests are described in a later section of this chapter.

dimensions of the specimens before prestraining. The length of the compression specimens were such that after prestraining the length was reduced to approximately 2 inches except for specimens C9 and C11, for which the final lengths were 0.633 inch and 1.576 inches respectively.

Annealing

The specimens for prestraining were machined, and then annealed. It was first expected that one hour at 900°F would suffice to bring the material to its softest condition, but in practice it was found that annealing was not complete in one hour; presumably since the surface was machined bright and very little radiant heat was absorbed by the specimens. Therefore the annealing time had to be increased to three hours for the compressive prestrain specimens and to two hours and thirty minutes for the tensile prestrain specimens. They were allowed to

cool in the furnace which took about 20 hours to reach 100°F from the annealing temperature of 900°F. After annealing the Rockwell H hardness was found to be about 30-32 which is about the softest condition that this material can be brought to.

A slightly different procedure had to be followed for testing at zero prestrain. Since it would be very difficult to machine test specimens from annealed material, the specimens were made first and then annealed for 35 minutes at heat and cooled in the furnace.

Prestraining

The compressive prestraining was done in a 400,000 lb. Tinius Olsen mechanical type testing machine between two hardened and ground steel plates. Some of the specimens had to be remachined to reduce the diameter before prestraining could be completed.

A commercial preparation of MoS_2 was used to lubricate the ends of the blocks in order to reduce the friction and avoid barrelling. This lubricant worked admirably well; so much so that after 10% reduction in length the variation of diameter from the ends to the middle of a block was never more than a few thousandths of an inch. In case of the longer specimens, the lengths were reduced by 0.200 inch by each loading, unloaded and reloaded. The ends were lubricated after every reduction of length of 0.600 inch. For shorter specimens ends were lubricated more frequently.

Tensile prestraining was done in a 120,000 lb. Riehle mechanical type testing machine. To prestrain such large specimens

special adapters had to be made which are shown in Figure IV-4. There was hardly any variation in diameter at all over the middle 6 inches of the strained specimen. This section was used for testing.

Figure IV-5 shows one tensile prestrain specimen mounted on the testing machine for prestraining.

Strain Rate

It is well known that stresses are functions not only of strains, but also of strain rates. However, stresses are of little concern while prestraining since the variable concerned is strain and not stress. Still, to eliminate any possibility of introducing strain rate as a variable, the rate was kept as low as practical. Compressive prestraining was done with a machine head speed of about 0.050 inch per minute, which is equivalent to about 0.00042 "/" per second at the last stages of compression. It is considered slow enough to give practically static condition of straining.[68] In case of the C9 specimen, where the final length was less than 2 inches, a slower head speed was used. For tensile prestraining the strain rate was about 0.0001 "/" per second. No increase in temperature was detectable to touch during the straining operation.

After prestraining, smaller test specimens were cut out of the blocks and tested. Three kinds of tests were made, viz.,

(i) Tension test

(ii) Compression test

(iii) Plane strain test

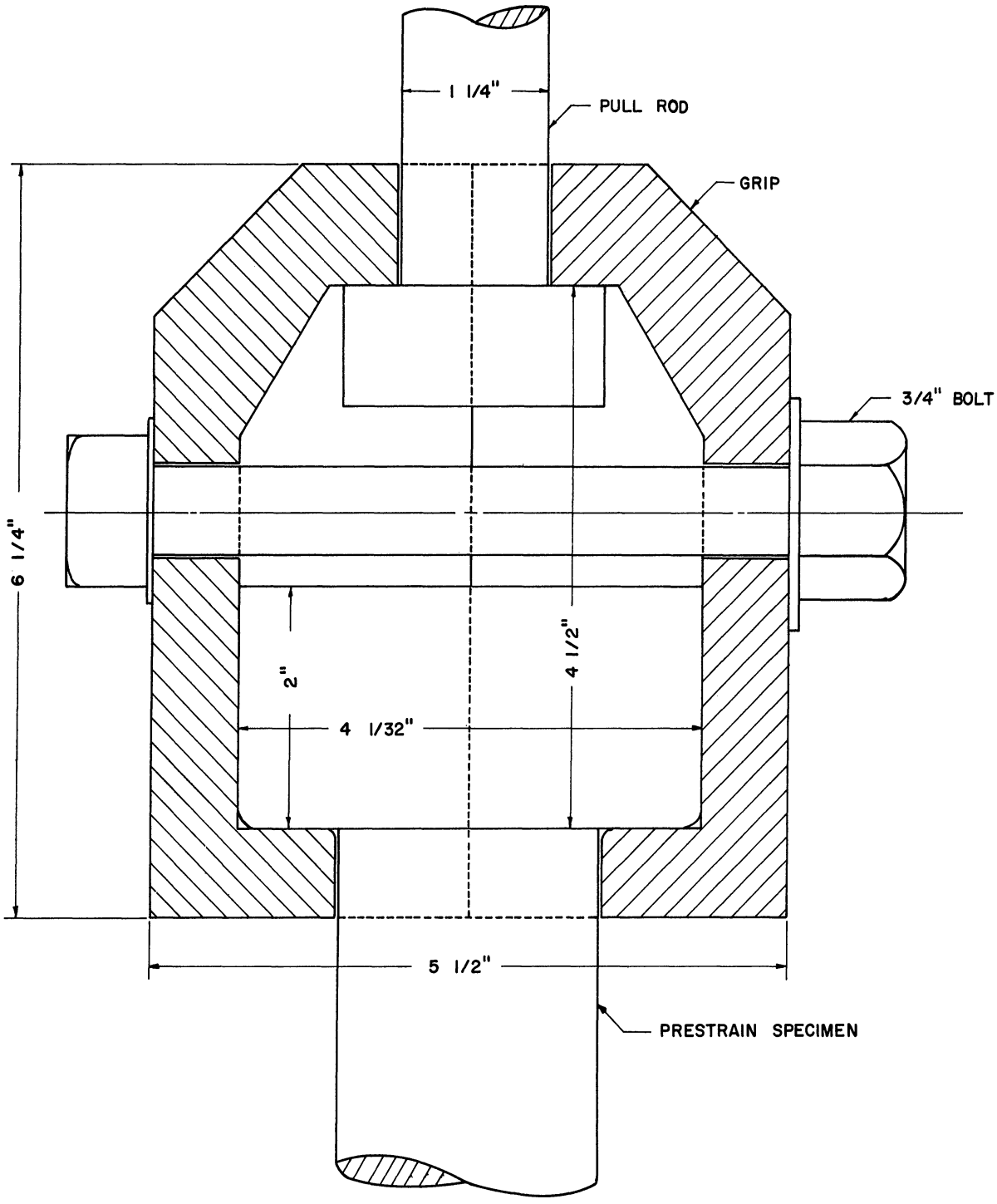

Figure IV-4. Large Grips for Tensile Prestraining.

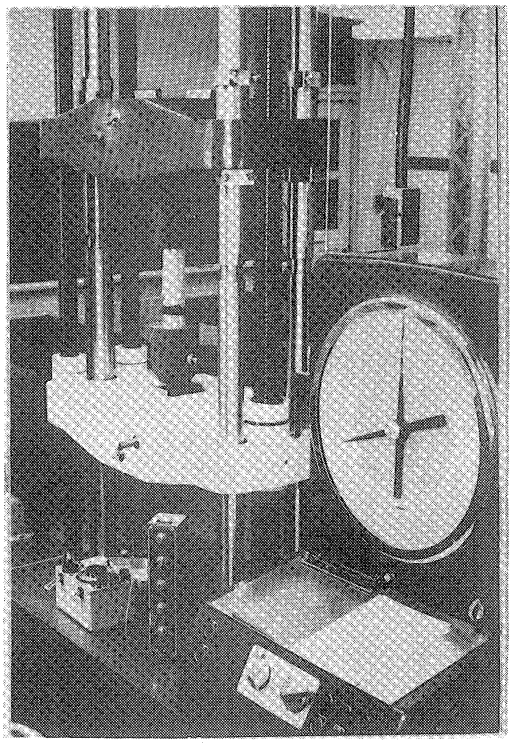

Figure IV-5.

Set-up for Prestraining in Tension.

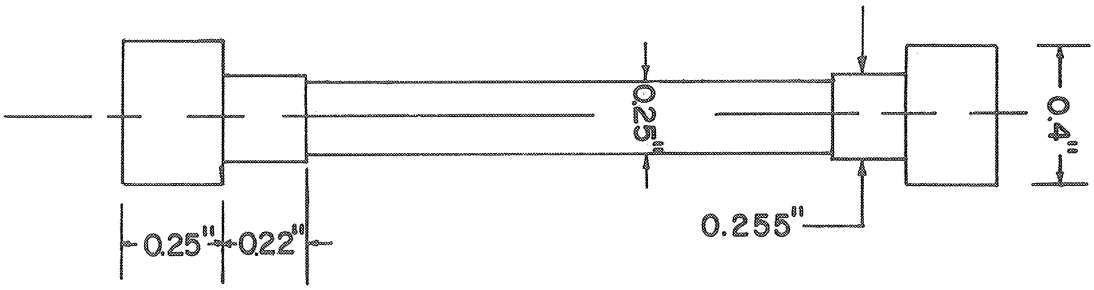

Figure IV-6. Tension Specimen.

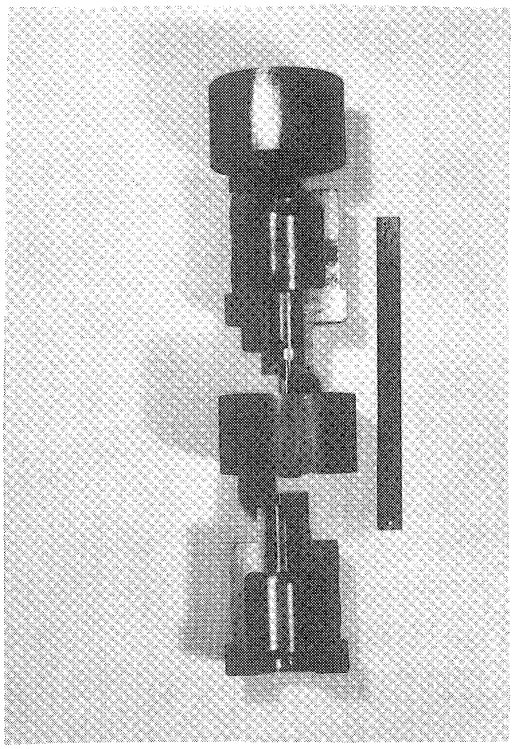

Figure IV-7.

Small Grips for Tension Test.

Two identical specimens of the same orientation were used for each of the tension and compression tests.

Tension Test Specimens

A sketch of a tension test specimen is shown in Figure IV-6. Lengths of the specimens varied according to the size of the block from which the specimens were taken. It was convenient to have the specimens as long as possible to facilitate measurements, and hence no attempt was made to standardize the lengths. The tolerance on the diameter was $\pm$ .005 inch and no attempt was made to make it any closer. However, the variation in diameter of a single specimen was kept within 0.0002 inch. Special grips had to be made for testing the specimens. They are shown in Figure IV-7. Three-quarter inch gage length was used. A small step was machined on the specimens to prevent the specimen from necking within the grips.

Compression Test Specimens

Originally it was intended to make the compression test specimens of the same diameter as the tension test specimens, but it was found impracticable to test specimens of so small a diameter and hence the diameter had to be increased. Some compression specimens of about 0.400 inch diameter were tested. Then it was found that with increasing prestrain, certain compression specimens behaved very much like an ideal elastic-plastic material and if the length was substantially larger than the diameter, localized plastic deformation would start and render the specimen useless. Hence, it was

attempted to make the compression specimens as large in diameter as possible from 1/2 inch square blanks. As such, the diameters varied from .400 inch to .435 inch and lengths from .400 inch to .450 inch.

With specimens of so small lengths it was found difficult to measure the small plastic strains accurately. To circumvent this difficulty, two types of specimens were used. The longer ones were used to measure small strains and shorter ones were used for large strains. They are shown in Figure IV-8.

Plane Strain Specimens

Plane strain specimens are shown in Figure IV-9. To obtain a condition of plane strain, the width was made large compared to the length and thickness. The flanges of large section effectively eliminated any contraction of the width. Theoretically, the length should have been large compared to the thickness, but it was found impracticable to make very thin specimens without introducing substantial strain during manufacture.

Designation of Tests

Every test had to be given a code designation for reference. The first letter and numeral denotes the prestrain state. The next letter is T, C or S indicating tension, compression or plane strain test respectively. In case of tension or compression tests, the next letter is X, Y or Z denoting the axis of the specimen with respect to the axes of orthotropy. In case of plane strain specimens, after the letter S, there are two letters from among X, Y and Z. The first letter indicates the direction of zero strain, and the second

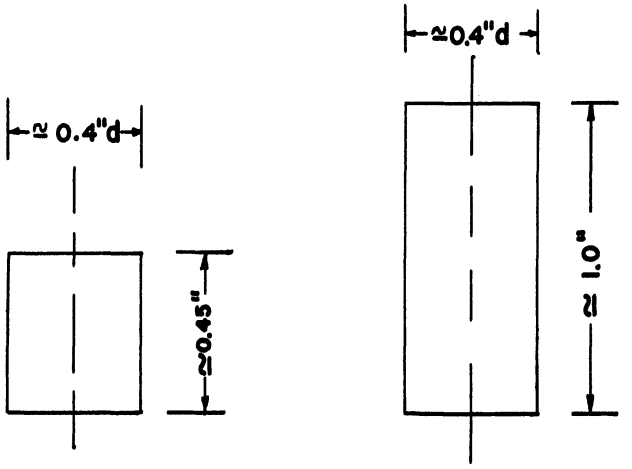

(a) Short Compression Specimen.

(b) Long Compression Specimen.

Figure IV-8. Compression Specimens.

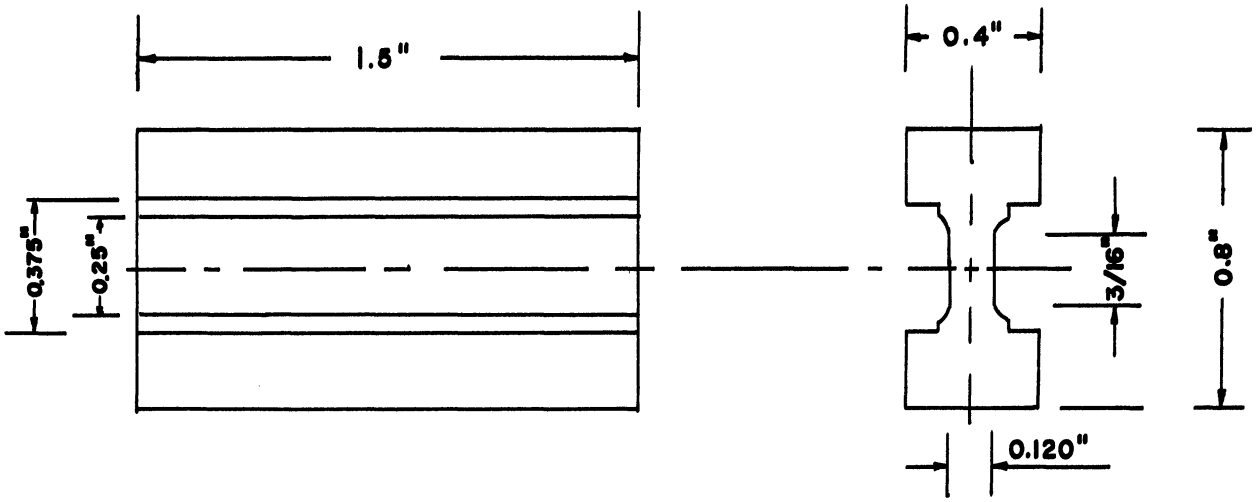

Figure IV-9. Plane Strain Specimen.

letter shows the direction in which the specimen has been pulled. When more than one specimen of a kind is tested, they are numbered, and the number is placed at the end of the designation code. As an example, C8TY2 refers to a tension specimen whose axis is parallel to the Y direction and the prestrain state of the block from which it has been machined is C8.

Fabrication

After prestraining, the major and minor axes were marked. The blocks were first sliced with a band saw to produce blanks from which test specimens were to be machined. To prevent any overheating with consequent change in strength state of the material, the blocks were cooled in ice prior to slicing and were frequently cooled during cutting too.

Tension and compression test specimens were machined on a lathe with a copious supply of kerosine to produce a good surface finish and also to keep the specimens cool. It was essential to keep the thickness of the material disturbed during cutting operation to a minimum. For this purpose, the tools were ground and honed to a sharp edge. The tool signature was 10, 30, 8, 8, 20, 0, 0 in accordance with the ASA standards. During the finishing cuts, the feed was 0.0012 inch per rev. and the speed was about 60 fpm.

The plane strain specimens were prepared by milling with sharp end cutting cutters. Copious amount of kerosine was used as a coolant.

Testing Procedure

All of the testing was done on a 60,000 lb. hydraulic drive testing machine.

(a) Tension Tests. A clip-on electromechanical strain gage and recorder was used for most of the tension tests. A load-extension diagram was obtained until the maximum load was attained, at which time the gage was taken off and instantaneous cross sections at the neck was recorded along with instantaneous loads.

Measuring the instantaneous cross section posed certain problems. The material being anisotropic in transverse strain, a circular section did not remain circular, but became elliptical. Hence, it became necessary to record both maximum and minimum diameters, and the area was calculated assuming that the cross section remained elliptical, which is true to a close approximation.

Measurements were made with a pointed micrometer until the surface became too rough to make accurate measurements possible. However, the specimens were strained until fracture and the cross section at fracture was noted.

(b) Compression Tests. As mentioned before, there were two kinds of compression specimens. The longer ones were for small strains and the shorter ones were for large strains.

For small strains an electromechanical clip-on strain gage with Baldwin-Southwork stress-strain recorder was used to obtain a load-deflection curve from which the stress strain diagram was calculated up to a strain of about 0.02. Shorter specimens were compressed between two ground flats and the ends were lubricated

between each compression to reduce friction. After every compression the load was noted, the specimen taken out and measured with a micrometer.

(c) Plane Strain Tests. In the case of the plane strain tests, only the yield stress is required. The stress-strain diagram was not plotted, and only the yield load was noted from the load-deflection diagram.

To test these specimens special adapters were designed and made. The deformation of the specimens was picked up by an electromechanical clip-on gage. Figure IV-10 shows the adapters used and Figure IV-11 shows the adapter and an electromechanical clip-on gage mounted on the testing machine together with a servomotor. Two electromechanical clip-on gages are shown in Figure IV-12.

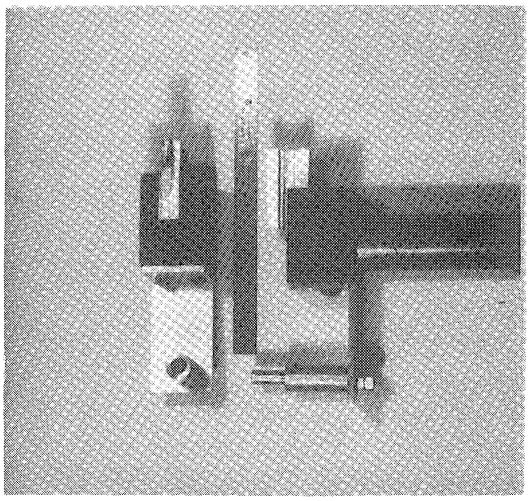

Figure IV-10.

Adapter for Plane Strain Test.

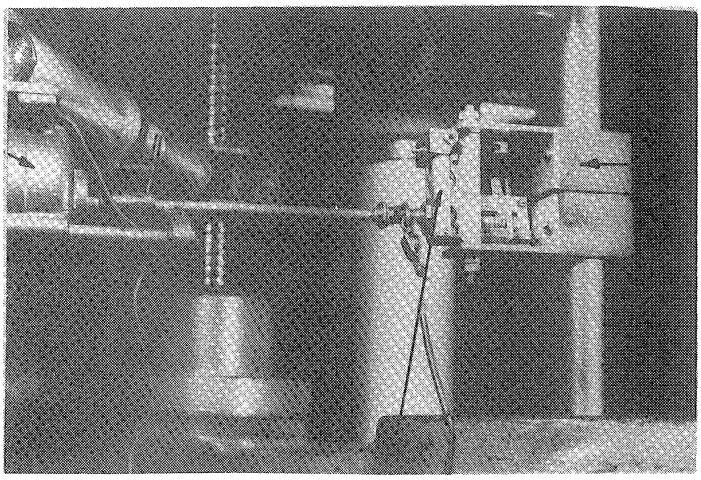

Adapter

Figure IV-11.

Set-up for Plane Strain Test.

Electromechanical Clip-on Gage

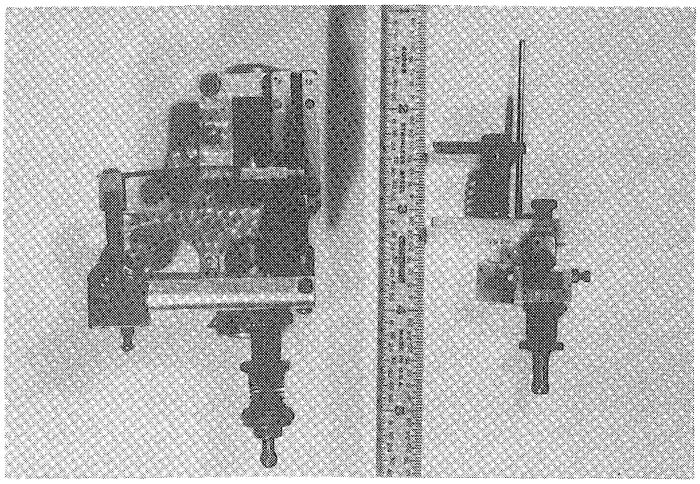

Figure IV-12.

Electromechanical Clip-on Gage.

CHAPTER V

DISCUSSION OF RESULTS

Introduction

The results of the present investigation as obtained by tests outlined in Chapter IV are presented and discussed in this chapter. They are also compared with the findings of previous investigators where possible. The few references made in this chapter are primarily for the purpose of analyzing the data obtained and comparing with the present work.

The stress-strain relations for different tests are presented in the form of tables and also as curves on logarithmic co-ordinates for comparison. Yield and ductility data are also given both as tables and diagrams.

Definitions

Before starting the discussion of the results obtained in the present investigation, it would be of advantage to restate the meaning of some terms used in this chapter.

The term "flow stress" has been used in the literature to mean different things in different places. Whenever this term is used hereafter, it means the stress level as a function of strain under a given condition of straining.

The term "strain" always means the natural strain measured from the beginning of a particular test, irrespective of the prestrain or prior history of the material. By "stress" is meant the true stress,

corrected by the use of the Bridgman correction factor whenever applicable. Stress and strain are denoted by σ and ϵ respectively.

Material

Since the material was found to be orthotropic as regards strains, it was expected to be orthotropic in flow properties, too. Hence, it was necessary to test it in the annealed condition as well as in the prestrained conditions in all the three directions. Since two specimens of each kind were tested in tension and compression, for each prestrain state, six tension specimens, six long compression specimens and six short compression specimens were tested. It was not found feasible to repeat plane strain tests since it took more material to make these specimens than was available.

Prestrain

Compressive prestrain is expressed as

$$\epsilon_p = \ln \frac{\ell_o}{\ell_f}$$

where ℓ_o and ℓ_f are original and final lengths of the block respectively. Elastic strain is neglected. Tensile prestrain is expressed as

$$\epsilon_p = \ln \frac{\ell_f}{\ell_o}$$

where ℓ_o and ℓ_f are gage lengths before and after straining. Diametral strains are also expressed in a similar way. In compression, the ratio of the two transverse strains were found to be 1.47 and that in tension 1.59. In accordance with the above definition, prestrains are always

numerically positive. This has been done to avoid carrying along the positive and negative signs.

Strain Recording

In most of the tension and compression tests an electromechanical strain gage was used. For a few tension tests SR-4 electric resistance strain gages were used as a check. Figure V-1 shows a comparison of data obtained by the two methods for testing two C9TY specimens. The largest strains recorded by the electromechanical and by the SR-4 electrical strain gages were 0.017 and 0.015 respectively, the maximum load having occurred at those strains. It is apparent from the diagram that the agreement is reasonably good with very little scatter.

Tension Test and Correction for Triaxiality of Stress in the Neck

Specimens with low prestrain when tested in tension in the Z direction showed substantial uniform strain before necking started, as is expected in such cases. During the uniform straining the cross-section did not remain circular, but became elliptical, which is in contradiction to the observations of Mehringer and McGregor[52] in testing low carbon steels.

With larger prestrains and while testing in the X and Y directions, the uniform elongation was small and necking started early. In addition, the section became elliptical. The stress distribution becomes complex after the initiation of necking, and hence reasonably accurate true stress-true strain diagrams can be plotted

for small strains only unless a correction for the triaxiality of stresses at the neck is resorted to. Three semi-empirical approaches for such corrections are available. The correction factor arrived at by Siebel[69] and by Davidenkov and Spiridonova[54] are identical, although derived in different ways. The relationship for the correction factor derived by Bridgman[53] is rather different from the other as shown later.

In all the approaches, the material is assumed to be isotropic, and hence a circular section is assumed to remain circular. To apply the correction, it is necessary to measure the radius of curvature of the specimen at the neck on a plane containing the axis of the specimen, and also the radius at the neck. The correction factors are given as follows:

$$\text{Bridgman's Correction factor } K_b = \frac{1}{\left(1 + \frac{2R}{a}\right) \ln \left(1 + \frac{a}{2R}\right)}$$

$$\text{Siebel's Correction factor } K_s = \frac{1}{1 + \frac{a}{4R}}$$

where a = minimum radius; and

R = radius of curvature at the neck.

In the present investigation, the material being anisotropic, the necked down section became elliptical and hence the radii of curvature were different in different directions. Hence, even if it were possible to measure the radii, it would not have been possible to use these corrections without modification.

However, there have been attempts to relate the ratio a/R with the current strain state, so as to eliminate the necessity for the measurement of the radii, which is a rather cumbersome process.

Kula and Larson,[70] and Nunes[71] investigated the relationship between the ratio a/R and strain, and suggest that to a good approximation the ratio a/R can be replaced by the strain after necking starts. Since the necking begins at the maximum load, the following substitution can be made:

$$\frac{a}{R} = (\epsilon - \epsilon_m)$$

where ϵ = current strain; and

ϵ_m = strain at maximum load.

Assuming this substitution is valid for the material under consideration, it now becomes possible to apply corrections to the test data, using either Bridgman's or Siebel's correction factor. The choice seems to be rather immaterial since for $\epsilon - \epsilon_m = 1.0$, the Siebel's correction factor is only about 3% less than the Bridgman's correction factor, and the difference is much smaller for lesser values of $\epsilon - \epsilon_m$. Considering the uncertainties of the assumptions involved in the derivation of these factors, in the substitution for a/R values and the experimental errors involved, there seems to be hardly any reason to prefer one to the other. This could be important if data are collected to larger strains, but the largest strain recorded in the present investigation was about 1.0. For many specimens, the largest strain was only 0.6. The largest strain readings had to be restricted as the necked surface became rough and after a certain stage accurate measurements could no longer be made.

It was decided to use the Bridgman correction factor since this has been used in many more investigations than the other.

Compression Test and Correction for Friction

As mentioned in Chapter IV, two kinds of specimens had to be used for compression test; one kind for small strains, and the other for larger strains where elastic strains can be neglected. Hence, it is possible to take the specimen out from the machine to measure its reduction in length. To reduce friction, the ends of the specimens were lubricated with a commercial preparation of MoS_2 which worked very well, even though friction cannot possibly be entirely eliminated. According to Alexander[72] a coefficient of friction of 0.0056 will cause an error of about 1.4% for a diameter to height ratio of 5. To estimate the coefficient of friction encountered while using MoS_2 as a lubricant, a near accident during the compressive prestraining may be mentioned.

A cylinder of about 4-1/2 inches in diameter was being compressed with a spherically seated compression head, using MoS_2 as a lubricant. Slight misalignment of the piece caused it to slip and it shot out of the machine. The two faces had become non-parallel, and the maximum difference in length on a diameter was found to be only .050 inch. Therefore, the friction angle was $\tan^{-1} \frac{0.050}{2 \times 4.5}$; i.e., the friction coefficient was only about 0.0056. The error due to so small friction is negligible and hence no correction is required.

Plain Strain Test

The plane strain test is a biaxial stress test. As explained in Chapter IV, the direction of zero strain of such a test specimen SXY is X and it is loaded in the Y direction. Therefore, the stress on a Y plane is given by the load divided by the cross-sectional area and that on a X plane is given by

$$\sigma_{xx} = -\mu_{xy}\sigma_{yy}$$

where μ_{xy} is the plastic Poisson's ratio in the X direction for uniaxial loading in Y direction.

Stress-Strain Curves

Since the primary interest in the present investigation is in the plastic stress-strain relations, not much emphasis is given to the elastic range of the stress-strain diagram. Although a few tension specimens were tested with the help of SR-4 post-yield strain gages, most of the work was done with an electromechanical clip-on gage.

The primary reason for using electromechanical clip-on gages is the ease with which they can be handled to give good results cheaply and quickly. While at very small strains of the order of 10^{-5} or 10^{-4} in./in. SR-4 gages are more reliable, at larger strains, the accuracy of both type of gages are comparable. Furthermore, it is rather difficult to properly fix the SR-4 gages on specimens of very small diameters as used in this investigation.

The stress-strain curves are plotted on log-log co-ordinates, rather than in linear Cartesian co-ordinates. If plotted in Cartesian

co-ordinates, most of the curves look very similar and the differences are not clearly visible. At large strains, all the curves become so flat that hardly any strain hardening is noticeable. On the other hand, at small strain, differences in strain at any stress level become obliterated, and two curves plotted together for comparison become too close to comparison. Also, since the stress-strain relation for an annealed material can approximately be expressed as a power relation, the curve is a straight line on logarithmic co-ordinates, while no such visual effect is possible when plotted in Cartesian co-ordinates.

Flow stresses at different strain levels for the tests are given in Table V-I. This gives the average of results obtained from two tests of each kind. The tension test data has been corrected with the help of modified Bridgman correction factor and the expression for the corrected true stress now is:

$$\sigma = \frac{\frac{L}{A}}{\left(1 + \frac{2}{\epsilon - \epsilon_m}\right) \ln \left(1 + \frac{\epsilon - \epsilon_m}{2}\right)}$$

where L is the load, and A the instantaneous cross-sectional area.

General Remarks

The results of various tension and compression tests for different prestrain states are presented in different combinations for comparison purposes in Figures V-2 to V-77. A few general remarks may be made before the comparative discussion.

TABLE V-I

FLOW STRESS IN KSI

Annealed Material; ϵ_p = 0.000

Strain	.002	.003	.004	.005	.007	.01	.02	.03	.05	.07	0.1	.15	.2	.25	.3	.35	.4	.45	.5	.6	.7	.8	.9	1.0
TX	3.5	4.0	4.5	4.9	5.5	6.3	8.2	9.4	10.9	11.8	12.5	13.5	14.4	15.2	15.9	16.5	17.1	17.6	18.2	19.0	19.8	20.4	21.1	21.8
TY	3.3	3.7	4.1	4.5	5.1	6.0	7.8	9.0	10.4	11.1	12.0	13.5	14.5	15.5	16.4	17.0	17.7	18.3	18.9	19.8	20.7	21.5	22.3	23.0
TZ	3.5	4.0	4.4	4.8	5.4	6.3	8.4	9.7	11.1	11.7	12.9	14.4	15.5	16.4	17.2	17.9	18.5	19.1	19.6	20.5	21.4	22.3	22.9	23.5
CX	3.5	4.0	4.4	4.8	5.5	6.3	8.3	9.3	10.7	11.7	12.6	13.8	14.8	15.4	16.5	17.1	17.7	18.4	18.8	19.8	20.7	21.5	22.3	23.0
CY	3.6	4.1	4.5	4.9	5.5	6.3	8.3	9.3	10.6	11.6	12.7	14.0	15.1	16.0	16.7	17.4	18.0	18.5	19.1	20.0	20.7	21.5	22.1	22.7
CZ	4.1	4.5	5.0	5.4	6.1	6.9	8.7	9.6	10.9	11.8	13.0	14.4	15.4	16.3	16.9	17.5	18.3	18.7	19.3	20.2	21.0	21.7	22.4	23.0

Prestrain State T11; ϵ_p = 0.1098

TX	10.5	11.2	11.5	11.8	12.0	12.2	12.4	12.5	12.5	12.8	13.1	13.4	13.9	14.4	14.7	15.2	15.6	15.9	16.3	17.1	17.7			
TY	11.4	12.0	12.4	12.5	12.5	12.6	12.7	12.8	12.8	12.9	13.2	13.3	14.0	14.5	15.1	15.4	16.0	16.5	16.9	17.4	18.2	19.1		
TZ	12.2	12.3	12.4	12.5	12.6	12.8	13.4	13.7	14.2	14.5	15.2	16.0	16.5	17.1	17.7	18.3	18.8	19.3	19.8	20.6	12.5			
CX	11.2	12.1	12.5	12.6	12.9	13.2	13.6	13.8	14.1	14.5	14.8	15.5	16.2	16.8	17.4	17.9	18.4	18.9	19.4	20.1	20.9	21.5	22.2	22.9
CY	12.2	12.6	12.9	13.0	13.1	13.3	13.5	13.7	14.1	14.4	14.8	15.5	16.2	16.8	17.4	17.9	18.4	18.7	19.3	20.0	20.7	21.5	22.3	23.0
CZ	9.5	10.2	10.7	11.0	11.5	11.9	12.2	12.3	12.4	12.5	12.8	13.6	14.6	15.5	16.4	17.0	17.6	18.2	18.7	19.7	20.5	21.2	21.8	22.4

Prestrain State T15; ϵ_p = 0.152

TX	10.9	11.9	12.4	12.6	13.0	13.2	13.4	13.4	13.4	13.5	13.8	14.1	14.5	14.8	15.3	15.7	16.0	16.6	17.0	17.8	18.7			
TY	12.2	12.9	13.2	13.4	13.4	13.5	13.7	13.9	13.9	14.0	14.2	14.8	15.4	15.7	16.3	16.7	17.0	17.5	17.9	18.7				
TZ	12.6	12.8	12.9	12.9	13.0	13.2	13.5	13.8	14.4	14.6	15.4	16.0	16.7	17.3	17.7	18.4	18.7	19.2	19.6	20.5	21.3	21.9	22.6	23.4
CX	13.0	13.4	13.5	13.7	13.8	14.0	14.4	14.5	14.7	14.9	15.3	15.9	16.5	17.1	17.6	18.2	18.7	19.3	19.7	20.5	21.4	22.1	22.7	23.4
CY	13.1	13.7	14.0	14.0	14.0	14.1	14.2	14.4	14.7	15.2	15.5	16.2	16.5	17.4	17.8	18.3	18.6	19.1	19.5	20.4	21.2	22.0	22.7	23.5
CZ	10.7	11.5	12.1	12.4	12.7	13.0	13.3	13.3	13.4	13.4	13.5	14.1	14.8	15.6	16.5	17.2	17.8	18.4	19.0	20.0	20.8	21.5	22.3	23.0

Prestrain State T20; ϵ_p = .206

TX	11.5	12.7	13.5	13.8	14.2	14.3	14.5	14.6	14.6	14.7	14.9	15.2	15.6	15.8	16.3	16.6	16.9	17.2	17.6	18.3	19.3			
TY	12.7	13.9	14.3	14.4	14.5	14.6	14.9	15.1	15.1	15.2	15.4	15.9	16.2	16.6	17.2	17.6	18.0	18.4	18.9	19.8	20.7			
TZ	13.6	13.9	14.0	14.2	14.3	14.4	14.7	15.0	15.5	15.7	16.3	16.9	17.5	18.0	18.5	19.0	19.5	19.9	20.4	21.3	22.1	22.7	23.5	24.3
CX	13.3	14.3	14.6	14.7	14.9	15.0	15.4	15.5	15.8	16.0	16.3	16.8	17.4	18.0	18.5	19.0	19.5	19.9	20.4	21.3	21.9	22.7	23.4	24.1
CY	14.1	14.7	15.1	15.2	15.3	15.4	15.5	15.6	15.8	16.0	16.4	16.8	17.4	17.9	18.4	18.8	19.4	19.7	20.2	21.0	21.6	22.4	23.1	23.7
CZ	10.9	12.0	12.6	13.2	13.6	14.0	14.4	14.4	14.4	14.1	14.0	14.4	14.8	15.6	16.4	17.1	17.8	18.4	18.9	19.9	20.8	21.6	22.4	23.0

TABLE V-I CONT'D

Prestrain State T25; ϵ_p = 0.245

TX	12.3	13.5	14.0	14.4	14.6	14.8	14.9	15.0	15.1	15.2	15.2	15.6	15.9	16.3	16.6	17.0	17.4	17.7	18.1	18.7	19.4				
TY	13.4	14.4	14.6	15.0	15.2	15.4	15.4	15.4	15.4	15.5	15.8	16.1	16.6	17.0	17.4	17.9	18.3	18.8	19.2	20.0					
TZ	14.8	15.2	15.3	15.3	15.4	15.5	16.0	16.2	16.5	16.8	17.1	17.6	18.3	18.8	19.3	19.7	20.2	20.6	21.0	21.7	22.6	23.4			
CX	14.4	15.1	15.5	15.6	15.9	16.0	16.2	16.4	16.5	16.6	17.0	17.5	18.0	18.5	18.9	19.4	19.9	20.3	20.7	21.5	22.2	22.8	23.5	24.1	
CY	14.1	15.4	15.7	15.8	15.9	16.0	16.2	16.2	16.3	16.5	16.6	17.2	17.6	18.2	18.6	19.1	19.5	19.9	20.3	21.0	21.7	22.4	23.1	23.7	
CZ	10.4	11.7	12.5	13.0	13.6	14.2	14.6	14.7	14.8	14.7	14.6	14.9	15.3	15.8	16.5	17.3	17.8	18.4	18.9	19.8	20.7	21.5	22.4	23.0	

Prestrain State C2; ϵ_p = 0.106

Strain	.002	.003	.004	.005	.007	.01	.02	.03	.05	.07	0.1	.15	.2	.25	.3	.35	.4	.45	.5	.6	.7	.8	.9	1.0
TX	12.1	12.5	12.6	12.7	12.9	13.1	13.4	13.5	13.7	14.1	14.3	14.9	15.3	15.7	16.2	16.5	17.0	17.4	17.7	18.6	19.5	20.2		
TY	12.5	12.9	13.1	13.2	13.3	13.4	13.6	13.7	14.0	14.1	14.4	15.0	15.6	16.2	16.8	17.3	17.7	18.1	18.4	19.2	20.0	20.7		
TZ	9.2	10.0	10.4	10.6	11.2	11.5	11.8	12.0	12.1	12.3	12.5	13.1	13.7	14.4	15.1	15.7	16.3	16.9	17.5	18.5	19.2	20.1	20.8	21.6
CX	10.5	11.5	11.8	12.2	12.5	12.7	13.0	13.3	13.5	13.6	14.1	14.6	15.4	15.9	16.5	17.1	17.6	18.1	18.5	19.5	20.4	21.2	21.9	22.6
CY	12.0	12.6	13.0	13.3	13.4	13.5	13.9	14.1	14.4	14.5	14.8	15.5	16.0	16.6	17.3	17.7	18.4	18.9	19.5	20.4	21.4	22.2	22.9	23.7
CZ	12.4	12.6	12.8	12.9	13.1	13.4	13.7	14.0	14.4	14.9	15.5	16.5	17.3	17.9	18.5	19.0	19.5	19.9	20.4	21.2	21.8	22.5	23.1	23.6

Prestrain State C3; ϵ_p = 0.1494

TX	12.9	13.2	13.3	13.4	13.5	13.7	14.0	14.2	14.4	14.5	14.6	15.0	15.4	15.8	16.4	16.8	17.1	17.7	18.1	18.9	19.4	20.0	20.5	21.0	
TY	13.0	13.6	14.2	14.3	14.3	14.4	14.6	14.7	15.0	15.1	15.1	15.5	15.9	16.5	17.1	17.6	18.0	18.5	19.0	19.8	20.4				
TZ	9.8	10.8	11.5	12.0	12.4	12.6	13.1	13.3	13.5	13.6	13.7	14.1	14.9	15.1	15.7	16.3	16.9	17.5	17.9	18.8	19.7	20.6	21.5	22.1	
CX	12.5	13.3	13.8	14.0	14.4	14.5	14.7	14.9	15.1	15.3	15.4	15.9	16.4	16.9	17.5	18.0	18.6	19.0	19.5	20.4	21.2	21.8	22.5	23.3	
CY	12.9	13.5	13.9	14.3	14.5	14.6	14.8	14.9	15.1	15.3	15.6	16.2	16.7	17.2	17.7	18.2	18.6	19.1	19.6	20.6	21.4	22.0	22.5	23.2	
CZ	13.2	13.4	13.5	13.7	13.9	14.1	14.5	14.7	15.3	15.6	16.1	16.8	17.5	18.2	18.7	19.2	19.7	20.2	20.6	21.5	22.3	23.0	23.6	24.3	

TABLE V-I CONT'D

Prestrain State C4 $\epsilon_p = 0.204$

Strain	.002	.003	.004	.005	.007	.01	.02	.03	.05	.07	.1	.15	.2	.25	.3	.35	.4	.45	.5	.6	.7	.8	.9	1.0
TX	13.3	13.8	14.1	14.3	14.4	14.4	14.5	14.5	14.8	15.1	15.3	15.9	16.2	16.5	17.0	17.3	17.8	18.1	18.5	19.3	19.9	20.5	21.0	
TY	14.3	15.1	15.5	15.6	15.7	15.8	16.0	16.2	16.3	16.3	16.7	17.1	17.6	18.1	18.7	19.0	19.5	19.9	20.3	21.0	21.7			
TZ	10.1	11.1	11.6	12.2	12.6	13.1	13.5	13.5	13.5	13.5	13.8	14.2	14.8	15.2	15.6	16.0	16.9	17.4	17.9	18.8	19.5	20.4		
CX	12.7	13.5	13.8	14.2	14.5	14.7	15.2	15.3	15.3	15.5	15.6	16.2	16.6	17.1	17.5	18.0	18.5	19.0	19.5	20.4	21.3	22.0	22.6	23.4
CY	14.4	15.3	15.6	15.9	16.0	16.2	16.3	16.4	16.5	16.6	16.7	17.2	17.6	18.1	18.5	19.0	19.4	19.8	20.2	21.0	21.6	22.4	22.9	
CZ	14.2	14.5	14.6	14.7	14.9	15.1	15.5	15.7	15.9	16.3	16.7	17.4	18.0	18.5	19.0	19.5	20.0	20.4	20.8	21.5	22.3	23.0	23.7	24.5

Prestrain State C5; $\epsilon_p = 0.244$

Strain	.002	.003	.004	.005	.007	.01	.02	.03	.05	.07	.1	.15	.2	.25	.3	.35	.4	.45	.5	.6	.7	.8	.9	1.0
TX	14.0	14.6	14.9	15.0	15.1	15.2	15.4	15.5	15.6	15.8	16.1	16.5	16.8	17.2	17.4	17.9	18.4	18.7	19.1	19.9	20.4	21.0	21.7	
TY	15.2	15.8	16.2	16.4	16.5	16.6	16.7	16.7	16.8	16.8	17.0	17.4	17.8	18.2	18.5	19.0	19.4	19.8	20.2	20.9	21.6	22.0		
TZ	11.1	12.1	12.6	13.0	13.5	13.9	14.5	14.6	14.6	14.7	14.8	15.1	15.5	15.9	16.4	16.8	17.3	17.9	18.4	19.2	20.1	20.7	21.3	
CX	12.7	14.0	14.7	15.2	15.6	15.9	16.2	16.4	16.6	16.8	16.9	17.1	17.6	18.0	18.4	18.7	19.1	19.5	19.9	20.5	21.4	22.2	22.8	23.5
CY	12.6	14.4	15.3	15.6	16.0	16.1	16.4	16.6	16.9	17.0	17.3	17.5	18.0	18.5	18.9	19.3	19.7	20.1	20.5	21.3	22.0	22.6	23.4	24.0
CZ	14.5	15.0	15.3	15.4	15.5	15.6	16.0	16.3	16.5	16.6	17.0	17.6	18.4	18.8	19.4	19.8	20.2	20.6	21.0	21.7	22.5	23.1	23.8	24.4

Prestrain State C6; $\epsilon_p = 0.30$

TX	14.5	15.3	15.5	15.7	15.9	16.0	16.3	16.5	16.6	16.6	16.7	17.0	17.5	17.8	18.2	18.7	19.0	19.4	19.7	20.3	20.9			
TY	14.9	16.4	16.9	17.0	17.1	17.2	17.2	17.3	17.3	17.3	17.6	18.0	18.5	18.8	19.2	19.6	20.0	20.3	20.7	21.4	22.0			
TZ	11.4	12.7	13.5	14.0	14.6	15.3	15.6	15.8	16.0	16.1	16.2	16.3	16.7	17.1	17.5	18.1	18.7	19.1	19.7	20.7	21.5	22.2		
CX	14.7	15.9	16.3	16.5	16.9	17.1	17.3	16.9	16.8	16.8	17.0	17.5	17.9	18.3	18.6	19.0	19.4	19.6	20.0	20.6	21.3	22.0	22.5	23.4
CY	13.9	15.3	15.9	16.3	16.6	16.9	17.0	17.2	17.4	17.5	17.6	18.0	18.4	18.7	19.0	19.4	19.7	20.1	20.4	21.1	21.9	22.5	23.1	23.7
CZ	15.3	16.0	16.4	16.5	16.6	16.8	17.1	17.2	17.4	17.6	18.0	18.5	19.0	19.5	20.0	20.5	21.0	21.4	21.7	22.5	23.2	23.8	24.5	25.1

Prestrain State C7; $\epsilon_p = 0.455$

TX	15.3	16.7	17.0	17.0	17.1	17.2	17.4	17.5	17.6	17.6	17.7	17.9	18.2	18.5	18.7	19.1	19.6	19.8	20.1	20.7	21.2			
TY	16.6	18.2	18.5	18.6	18.7	18.8	18.9	19.0	19.0	19.0	19.1	19.3	19.7	20.1	20.5	20.8	21.3	21.7	22.0	22.8	23.6	24.1	24.5	
TZ	12.5	13.9	14.6	15.2	15.9	16.5	17.2	17.3	17.3	17.3	17.4	17.6	17.9	18.4	18.6	19.0	19.4	19.7	20.2	21.1	22.0	22.9	23.9	
CX	14.8	16.4	17.0	17.5	18.1	18.3	18.5	18.5	18.5	18.5	18.6	18.9	19.1	19.4	19.6	19.9	20.3	20.6	21.0	21.6	22.4	23.3	23.7	24.4
CY	15.9	17.5	18.3	18.6	19.0	19.3	19.4	19.2	19.1	19.0	19.0	19.3	19.5	19.7	20.1	20.4	20.6	20.9	21.3	21.9	22.5	23.0	23.6	24.1
CZ	16.5	17.5	17.7	17.9	18.0	18.2	18.5	18.7	18.9	19.0	19.3	19.7	20.1	20.5	20.9	21.2	21.5	21.9	22.2	22.8	23.4	24.0	24.5	25.1

TABLE V-I CONT'D

Prestrain State C8; ϵ_p = 0.673

TX	16.0	17.5	18.0	18.0	18.3	18.5	18.8	19.0	19.2	19.3	19.3	19.5	19.7	20.0	20.3	20.7	21.0	21.3	21.6	22.3	22.7				
TY	17.2	19.0	19.6	19.9	20.3	20.5	20.6	20.6	20.7	20.8	20.8	20.9	21.3	21.5	22.0	22.5	22.8	23.2	23.6	24.3					
TZ	12.2	14.2	15.2	15.7	16.6	17.4	18.3	18.5	18.8	19.1	19.2	19.2	19.4	19.7	20.2	20.4	20.7	21.2	21.6	22.4	23.5				
CX	14.1	16.4	17.5	18.0	18.8	19.3	19.5	19.4	19.4	19.4	19.4	19.5	19.6	19.9	20.2	20.5	20.7	21.0	21.4	22.0	22.6	23.3	23.9	24.6	
CY	16.5	18.7	19.7	20.2	20.4	20.5	20.5	20.5	20.6	20.6	20.6	20.6	20.8	21.1	21.4	21.6	21.9	22.2	22.5	23.0	23.6	24.4	24.9	25.5	
CZ	17.2	18.6	19.0	19.2	19.5	19.6	20.0	20.1	20.4	20.5	20.8	21.2	21.5	21.9	22.1	22.5	22.7	23.0	23.3	23.9	24.3	24.8	25.3	26.0	

Prestrain State C9; ϵ_p = 1.953

TX	17.7	21.2	22.7	23.6	24.4	24.9	25.2	25.2	25.2	25.2	25.2	25.5	25.7	26.0	26.2	26.4	26.6	26.9	27.1	27.7					
TY	20.3	22.9	24.0	24.5	25.2	25.7	25.9	26.2	26.2	26.2	26.3	26.5	26.8	26.9	27.1	27.4	27.8	28.1	28.3	29.1	29.8	30.4			
CX	16.0	19.0	20.8	21.7	23.1	24.0	25.2	25.7	25.7	25.4	25.1	24.8	24.7	24.7	24.8	24.9	24.9	25.1	25.2	25.5	25.9	26.4	27.0	27.7	
CY	16.5	20.2	22.5	23.6	25.0	26.0	26.8	27.1	27.0	26.8	26.5	26.1	26.0	25.9	25.9	25.9	25.9	26.0	26.0	26.3	26.7	27.3	27.9	28.6	
CZ				26.4	26.5	26.5	26.7	26.9	27.0	27.2	27.3	27.5	27.6	27.8	28.0	28.3	28.5	28.7	29.0	29.5	29.9	30.3	30.9	31.3	

Prestrain State C10; ϵ_p = 1.01

TX	16.5	18.3	18.8	19.2	19.5	19.8	20.1	20.2	20.3	20.3	20.3	20.7	21.0	21.3	21.6	21.9	22.3	22.6	22.9	23.5	24.2				
TY	17.6	20.1	20.7	21.0	21.4	21.5	21.8	21.9	22.0	22.1	22.1	22.3	22.5	22.8	23.1	23.4	23.8	24.2	24.6	25.2	25.7				
TZ	13.6	15.5	16.7	17.5	18.5	19.4	20.4	20.5	20.6	20.7	20.7	20.8	20.8	21.1	21.4	21.7	22.0	22.4	22.8	23.5	24.6				
CX	15.9	18.1	19.1	19.5	20.1	20.5	21.2	21.4	21.5	21.5	21.4	21.3	21.4	21.5	21.7	22.0	22.2	22.4	22.6	23.3	23.9	24.5	25.1	25.8	
CY	15.2	18.0	19.5	20.5	21.5	22.2	22.6	22.9	23.3	23.2	22.8	22.6	22.6	22.7	22.9	23.0	23.3	23.5	23.8	24.5	25.1	25.8	26.5	27.3	
CZ	17.9	20.1	20.7	21.2	21.7	22.0	22.2	22.5	22.9	23.1	23.2	23.5	23.9	24.2	24.4	24.7	24.9	25.2	25.5	26.0	26.6	27.1	27.6	28.1	

Prestrain State C11; ϵ_p = 1.49

TX	17.5	19.9	20.9	21.3	21.7	22.0	22.4	22.5	22.6	22.7	22.8	23.2	23.5	23.7	23.9	24.2	24.4	24.7	24.8	25.2	25.7	26.0			
TY	18.3	21.2	22.3	22.7	23.3	23.6	24.0	24.2	24.3	24.3	24.4	24.7	24.9	25.2	25.6	25.9	26.1	26.2	26.4	26.7	26.8				
TZ	14.6	16.6	18.0	18.9	20.0	21.1	22.5	22.8	22.8	22.7	22.7	22.6	22.7	23.0	23.2	23.6	23.9	24.1	24.4	25.1					
CX	14.6	17.3	18.9	20.0	21.3	22.2	23.0	23.6	24.3	24.0	23.9	23.6	23.6	23.5	23.6	23.7	23.9	24.1	24.3	24.7	25.2	25.7	26.3	26.8	
CY	16.6	19.5	21.3	22.3	23.5	24.4	24.4	25.1	25.0	25.0	24.7	24.5	24.4	24.4	24.5	24.6	24.7	24.8	25.0	25.4	25.9	26.3	26.7	27.3	
CZ	17.3	20.7	22.4	23.0	23.6	24.1	24.6	24.9	25.2	25.4	25.5	25.7	26.0	26.2	26.5	26.7	26.9	27.1	27.4	27.7	28.1	28.5	28.9	29.2	

Common materials do not show any sharp yield point. A transition zone connects the elastic part of the curve with the plastic part. It appears that the random variations in this transition zone are rather large. When the straining in a subsequent test is of the same sign, either positive or negative, and direction as the prior strain, this transition region is rather short and the curve has a small radius of curvature. On the other hand when they are of different signs, the transition range is much larger and the transition from elastic to plastic range is very gradual.

The stress-strain relationship is rather widely variable for small strains, e.g., $\epsilon < 0.01$. The reason may be the different amounts of residual stresses present in the finished specimens. By the time the material has undergone a strain of about 0.01, it is believed all the grains have yielded in the direction of loading and hence the stress-strain diagram is reliable. Hence, for all subsequent discussions in this chapter, when any comparison is made between two curves, it is always assumed that the strains are greater than 0.01 unless specifically mentioned. A true strain of 0.01 is equivalent to 1% cold work.

Prestraining increases the strength of the material in all directions, in tension and as well as in compression. In general, the differences in flow stress are only of the order of 1 ksi, or about 4-5%, except when the direction of stresses is reversed. In most cases, the difference between two tests is less than 200 psi, but in a few cases it has been as high as 600 psi. Hence, a difference in flow stress of 1 ksi is possibly significant, but a difference

of a few hundred psi is not. Whenever it is mentioned that a certain difference is "slight" or "small", it is understood that the difference is less than 500 psi. Differences shown as percents are rounded figures only.

Stress-Strain Curve for Annealed Material

Figures V-2 and V-3 show the plastic stress-strain relations for testing in the X, Y and Z directions in tension and in compression respectively. It is seen that the curves are not straight lines on log-log co-ordinates in the whole plastic range. In other words, the relation $\sigma = \sigma_o \epsilon^m$ is not valid for constant m over the range investigated. However, this relation holds good from about $\epsilon = 0.1$ to $\epsilon = 1.0$. Fortunately, we are primarily interested in this region only, since the smallest prestrains in tension and in compression are 0.1098 and 0.106 respectively. Although the general relationship is valid for each of the tests the flow constants σ_o and m vary from test to test as shown in Table V-II. It is noticed from Figure V-2 that the flow stress in tension in the Z direction is about 1 ksi higher than that in the X direction. The flow stress in the Y direction is the same as that in the X direction at $\epsilon = .15$ and is intermediate between those in the X and Y directions. It is seen in Figure V-3 that the flow stresses for the compression tests are very close to each other.

Figures V-4, V-5 and V-6 show the comparison between tension and compression tests in the X, Y and Z directions respectively. Although there are slight differences between the tensile and compressive

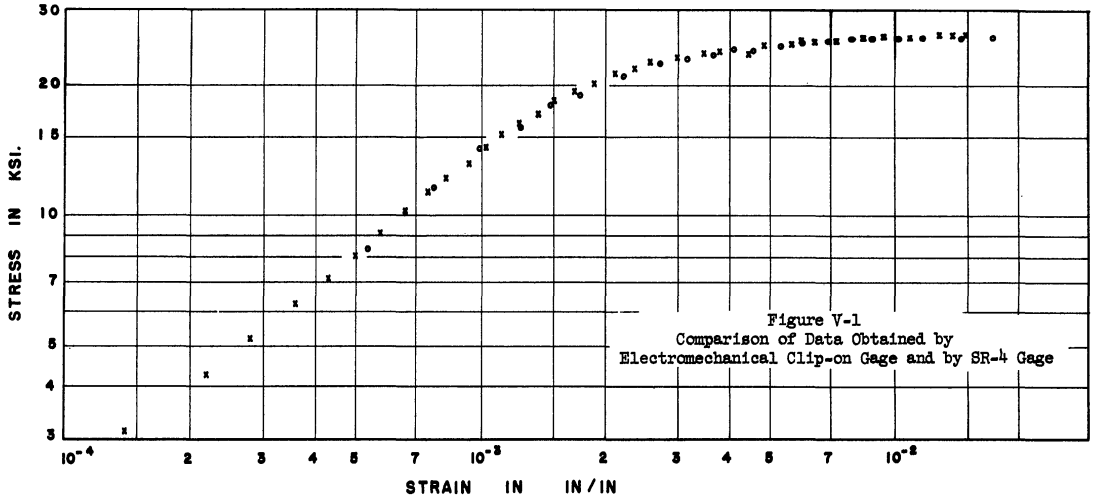

Figure V-1
Comparison of Data Obtained by
Electromechanical Clip-on Gage and by SR-4 Gage

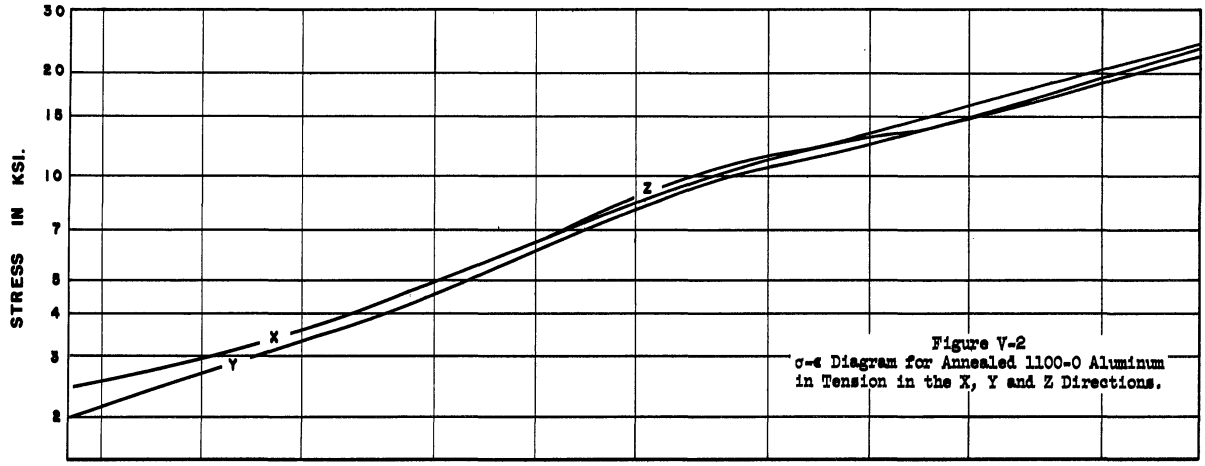

Figure V-2
σ-ε Diagram for Annealed 1100-0 Aluminum
in Tension in the X, Y and Z Directions.

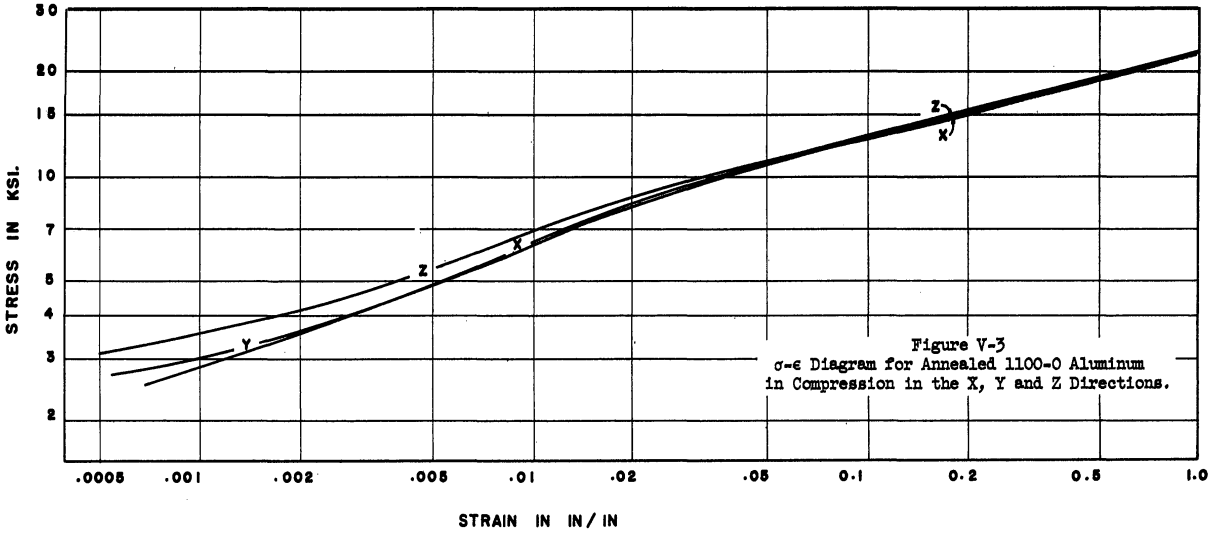

Figure V-3
σ-ε Diagram for Annealed 1100-0 Aluminum
in Compression in the X, Y and Z Directions.

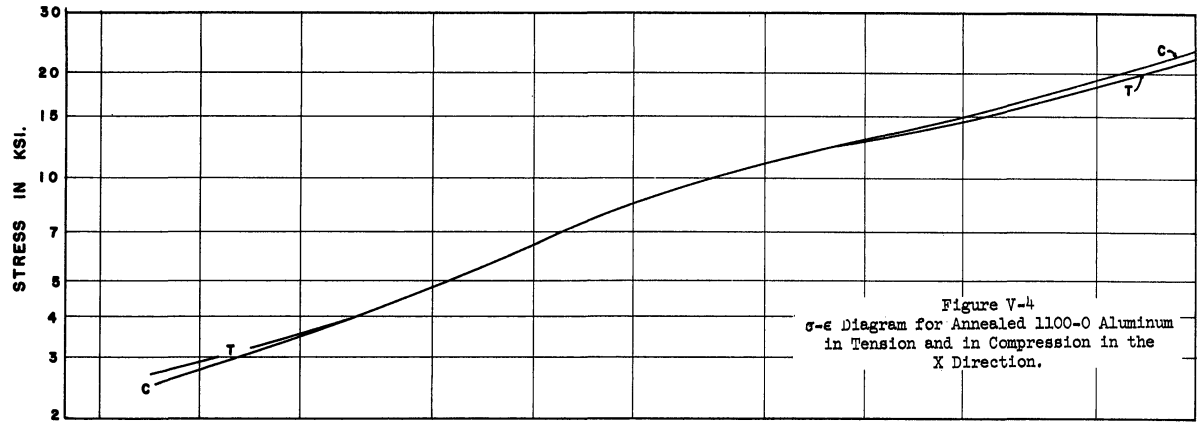

Figure V-4
σ-ε Diagram for Annealed 1100-0 Aluminum in Tension and in Compression in the X Direction.

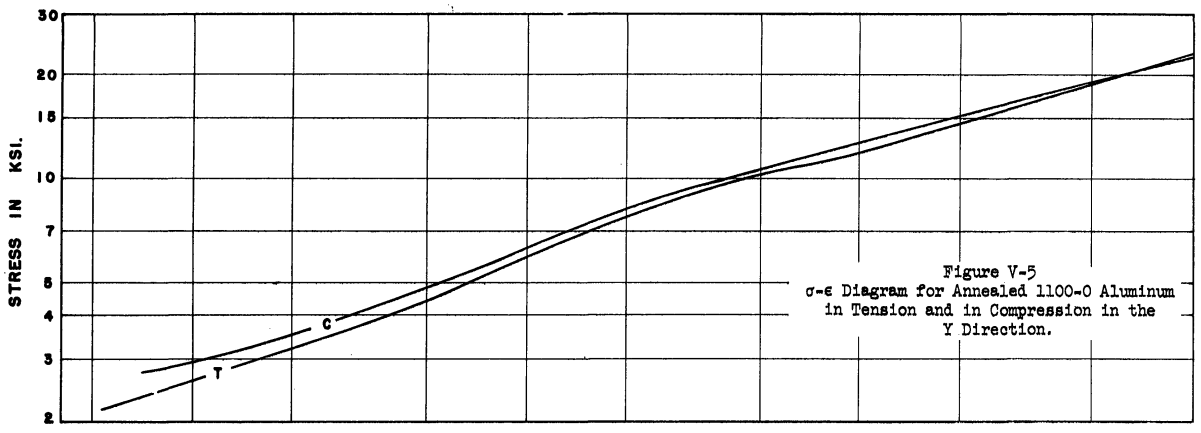

Figure V-5
σ-ε Diagram for Annealed 1100-0 Aluminum in Tension and in Compression in the Y Direction.

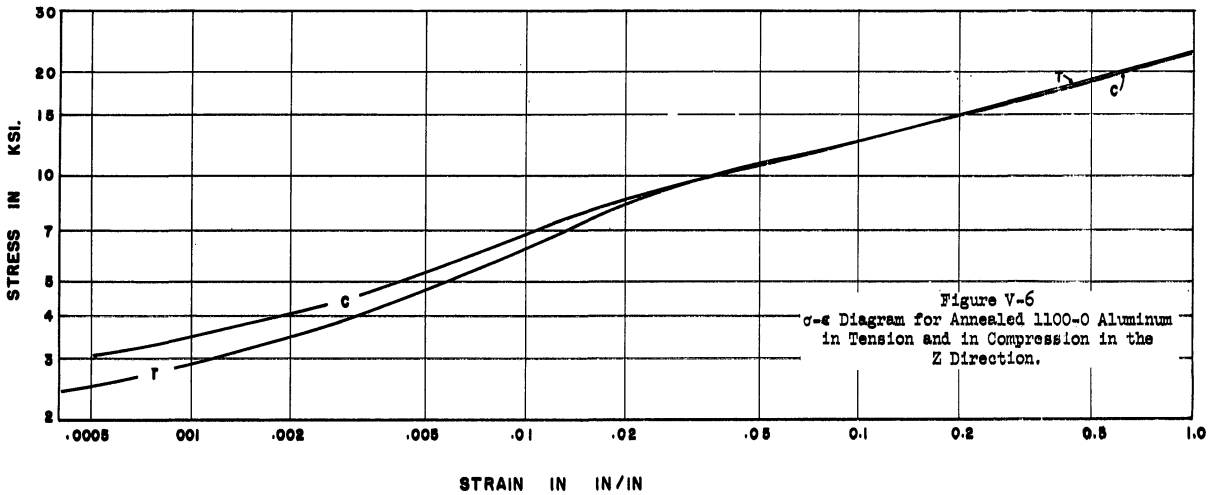

Figure V-6
σ-ε Diagram for Annealed 1100-0 Aluminum in Tension and in Compression in the Z Direction.

flow stresses for each of the three directions tested, they are within the range of experimental error and random variations.

TABLE V-II

PLASTIC CONSTANTS FOR ANNEALED 1100-0 ALUMINUM
(Average of two tests of each kind)

Kind of Test	Direction	σ_o in ksi	m
Tension	X	21.8	0.260
Tension	Y	23.0	0.280
Tension	Z	23.4	0.262
Compression	X	23.0	0.275
Compression	Y	22.7	0.255
Compression	Z	23.0	0.250

Stress-Strain Relations for Tension Tests After Tensile Prestrain for Individual Prestrain States

Figures V-7 to V-10 show the stress-strain relations for tension tests in X, Y and Z directions for different tensile prestrain states. It appears that the flow stresses in the X and Y directions are more or less the same and are lower than that in the Z direction by 0 to 3 ksi, i.e., by about 0 to 20%. The differences between the flow stresses in the different directions is least at about $\epsilon = 0.01$ and continuously increases with increasing strain. During uniaxial tensile loading, the transverse strains are compressive. Consequently, a tensile specimen cut out in the X or Y direction has compressive prestrain, and so the differences in the flow stresses may be due to the "Bauschinger Effect."

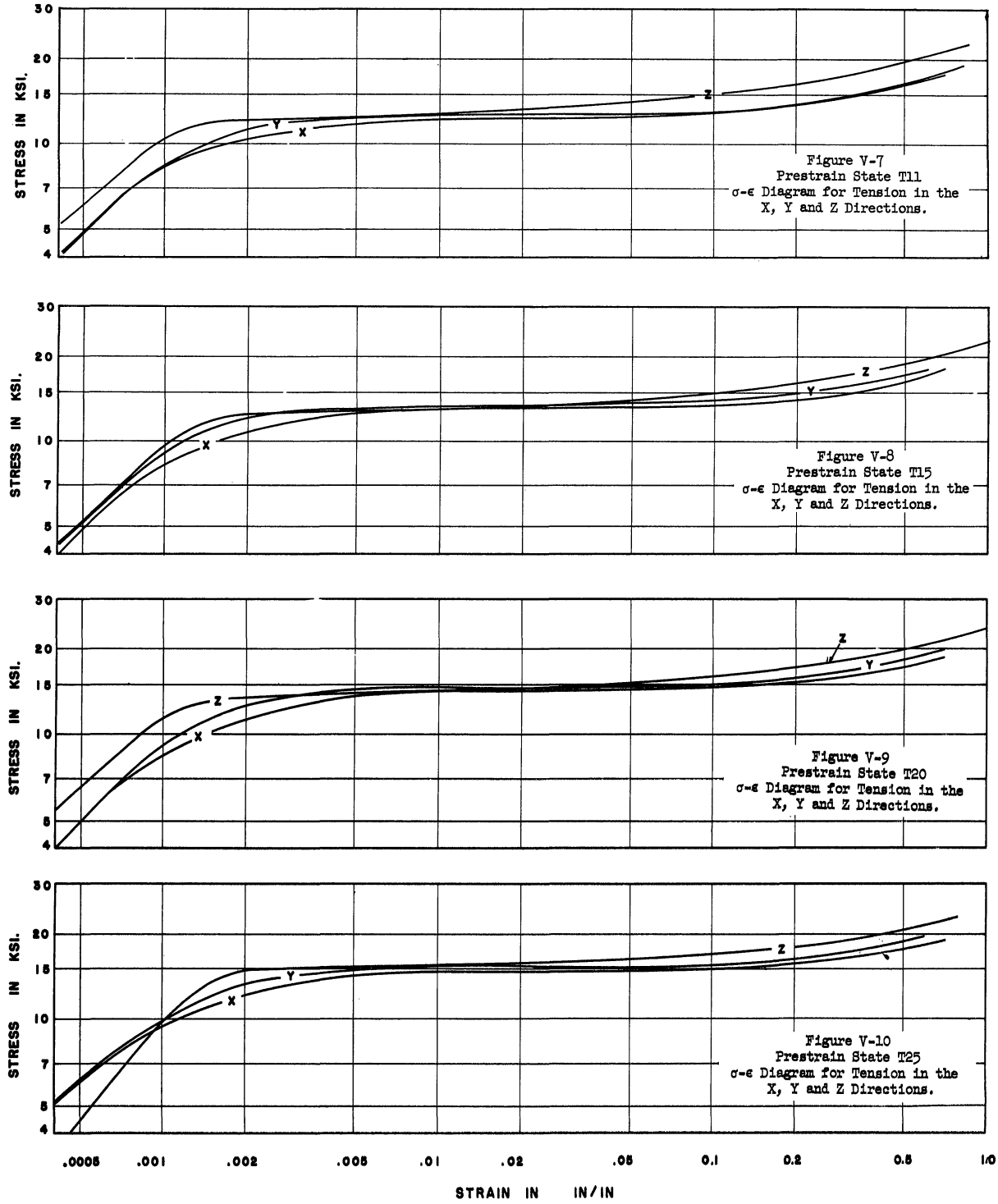

Figure V-7
Prestrain State T11
σ-ε Diagram for Tension in the
X, Y and Z Directions.

Figure V-8
Prestrain State T15
σ-ε Diagram for Tension in the
X, Y and Z Directions.

Figure V-9
Prestrain State T20
σ-ε Diagram for Tension in the
X, Y and Z Directions.

Figure V-10
Prestrain State T25
σ-ε Diagram for Tension in the
X, Y and Z Directions.

Stress-Strain Relations in Compression After Tensile Prestrain for Individual Prestrain States

Figures V-11 to V-14 compare the stress-strain relations in compression in the X, Y and Z directions for tensile prestrains. Here the flow stresses in the X and Y directions are identical. The flow stress in the Z direction is 1 to 3 ksi, or about 5 to 20% lower than in the other two directions up to a strain of about 0.2. The differences gradually decrease after that until the flow stresses are about the same for all directions at $\epsilon = 1.0$.

Since the flow stresses in the X and Y directions are higher than in the Z direction, it supports the findings in the previous section on tensile loading. Here again is the evidence of a Bauschinger effect of an equal magnitude to that in the previous section.

Tensile Relations After Compressive Prestrain for Individual Prestrain States

Figures V-15 to V-24 presents comparisons between the tensile stress-strain curves in the three directions for compressive prestrains. It is found that the curves for the Z direction are always lower than those for the X and Y directions. For the prestrain state $\epsilon_p = 0.106$, the flow stress in the X direction is slightly higher than that in the Y direction. Except for this, the flow stress in the Y direction is the highest and that in the X direction is intermediate between those in the Y and Z directions. The differences however, become smaller with increasing prestrains.

As was true in the two previous cases of tensile prestrain a Bauschinger type effect is evident here for compressive

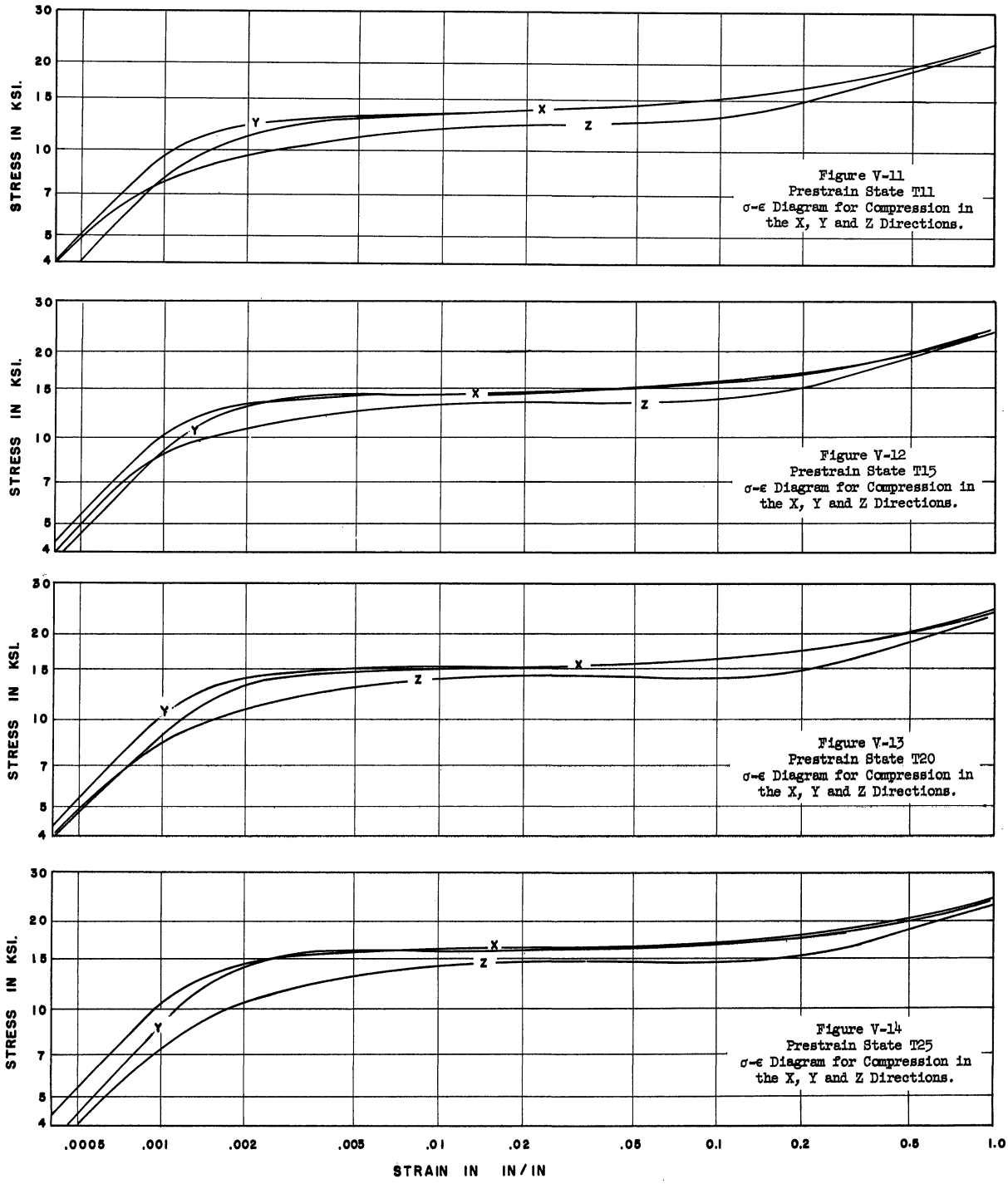

Figure V-11
Prestrain State T11
σ-ε Diagram for Compression in the X, Y and Z Directions.

Figure V-12
Prestrain State T15
σ-ε Diagram for Compression in the X, Y and Z Directions.

Figure V-13
Prestrain State T20
σ-ε Diagram for Compression in the X, Y and Z Directions.

Figure V-14
Prestrain State T25
σ-ε Diagram for Compression in the X, Y and Z Directions.

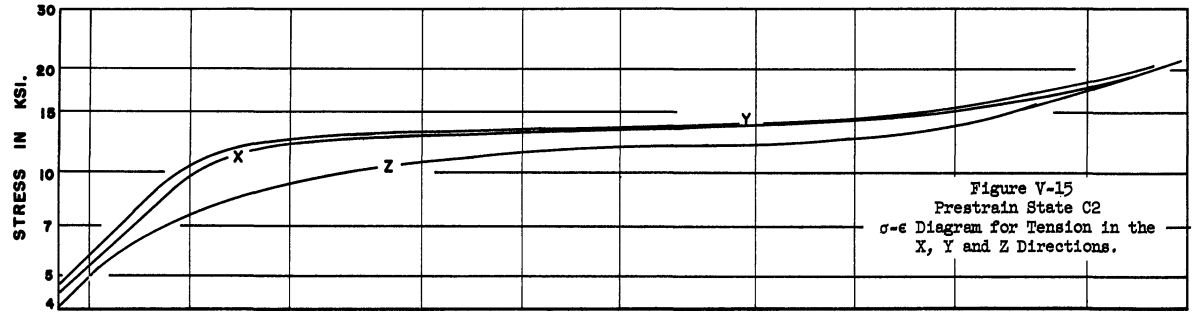

Figure V-15
Prestrain State C2
σ-ε Diagram for Tension in the
X, Y and Z Directions.

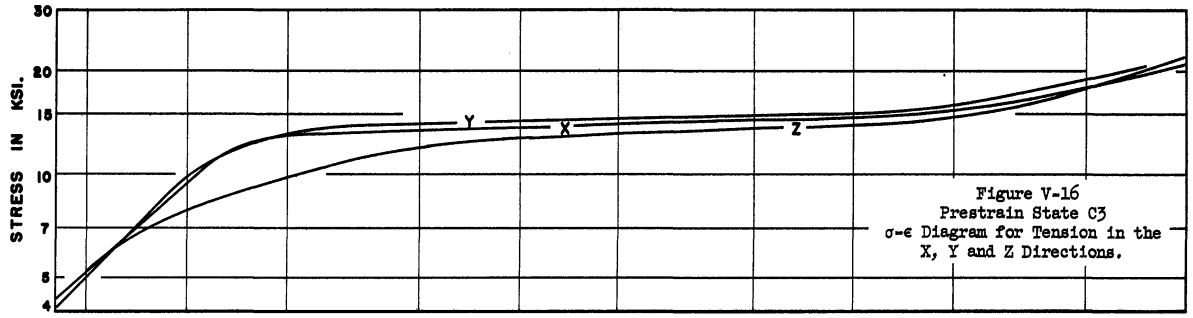

Figure V-16
Prestrain State C3
σ-ε Diagram for Tension in the
X, Y and Z Directions.

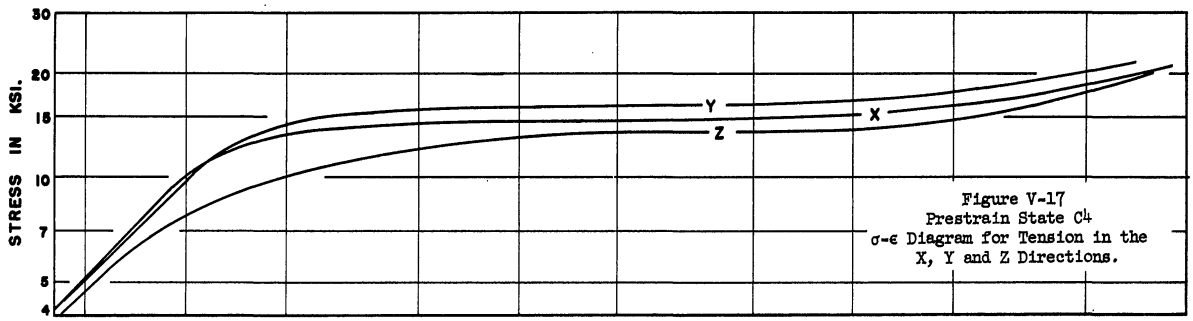

Figure V-17
Prestrain State C4
σ-ε Diagram for Tension in the
X, Y and Z Directions.

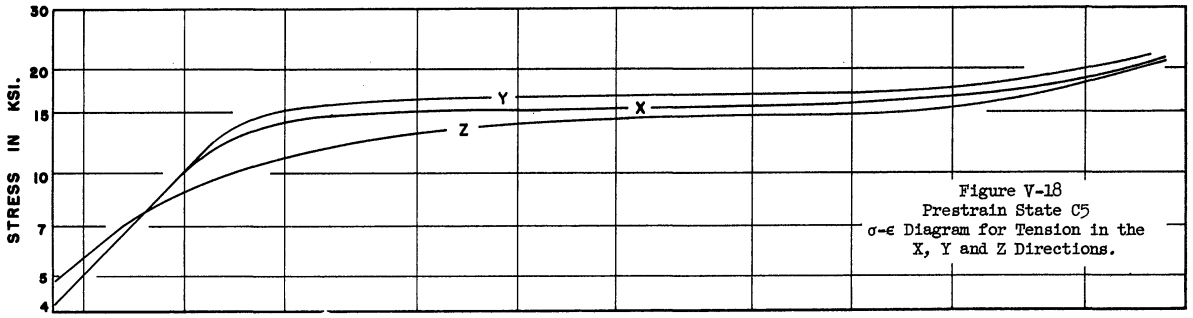

Figure V-18
Prestrain State C5
σ-ε Diagram for Tension in the
X, Y and Z Directions.

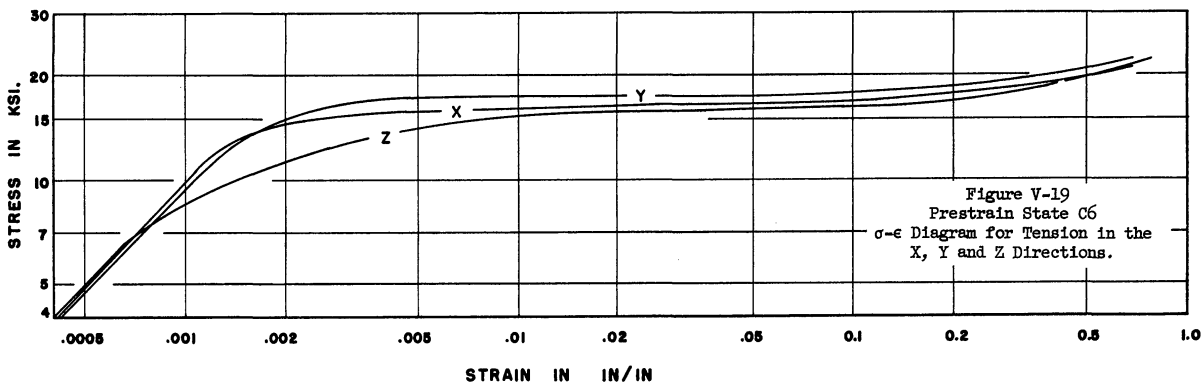

Figure V-19
Prestrain State C6
σ-ε Diagram for Tension in the
X, Y and Z Directions.

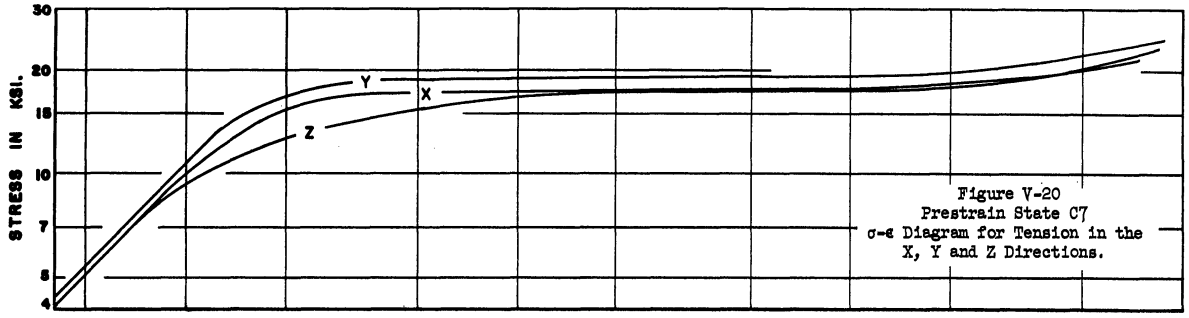

Figure V-20
Prestrain State C7
σ-ε Diagram for Tension in the
X, Y and Z Directions.

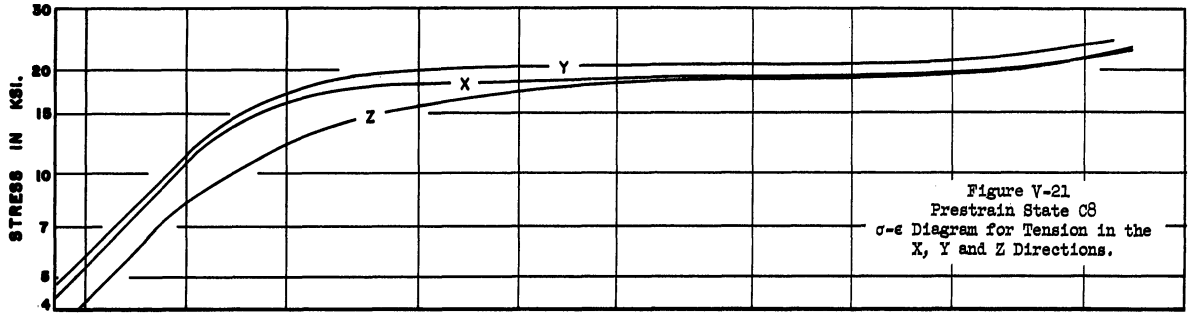

Figure V-21
Prestrain State C8
σ-ε Diagram for Tension in the
X, Y and Z Directions.

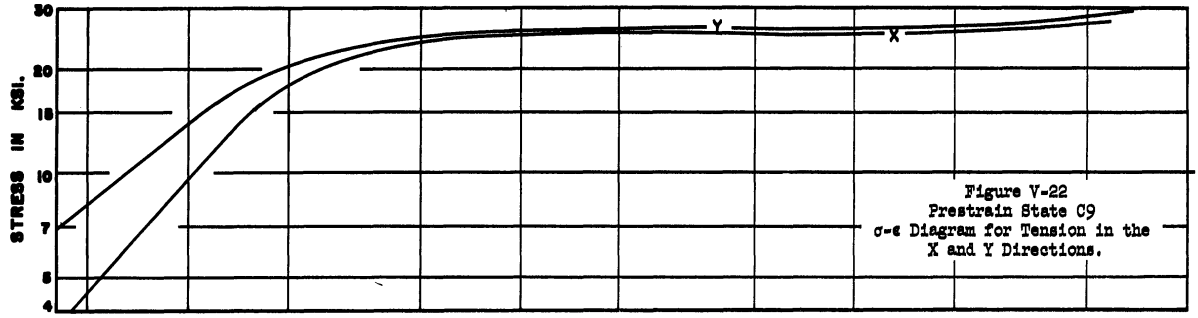

Figure V-22
Prestrain State C9
σ-ε Diagram for Tension in the
X and Y Directions.

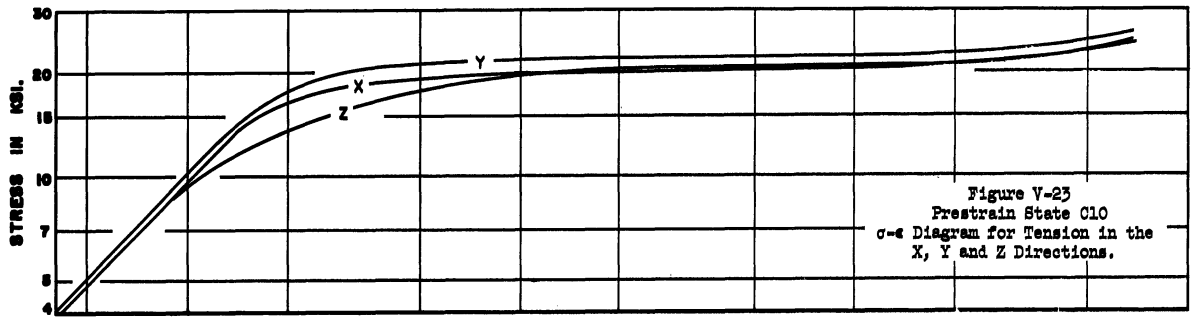

Figure V-23
Prestrain State C10
σ-ε Diagram for Tension in the
X, Y and Z Directions.

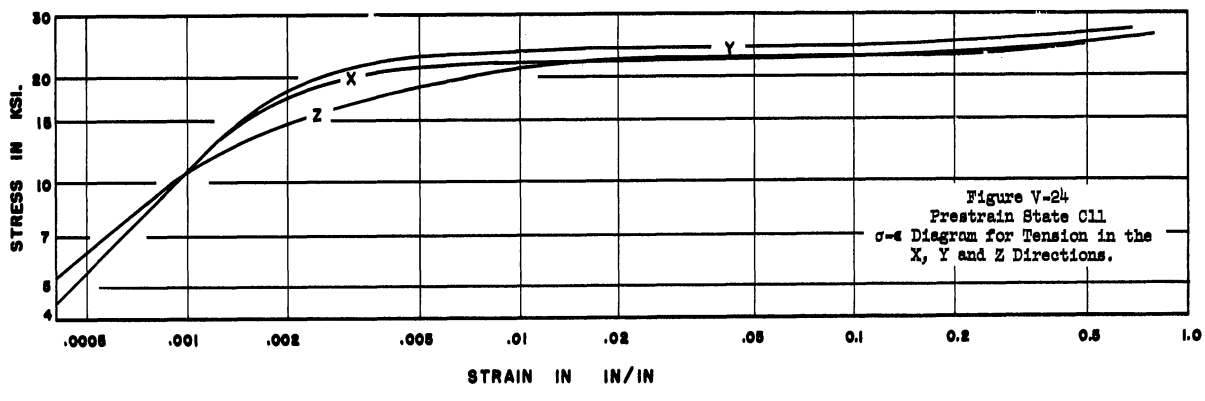

Figure V-24
Prestrain State C11
σ-ε Diagram for Tension in the
X, Y and Z Directions.

prestrain in the Z direction. Tensile strains are induced in the X and Y directions. Consequently, tensile specimens cut out in the X and Y directions should be expected to have higher flow stresses in the Z direction. This is borne out. However, the magnitude of the Bauschinger type effect appears to decrease with increasing prestrain.

Compression Tests After Compressive Prestrains for Individual Prestrain States

Stress-strain diagrams for compression tests after compressive prestrains are shown in Figures V-25 to V-34. The flow stresses in the X direction are found, in general, to be lower than those in the other directions, although the differences are rather small. Flow stresses in the Y and Z directions are almost identical for strains up to 0.1 and for higher strains the flow stress in the Y direction is, in general, lower than that in the Z direction.

The data presented in the curves from these tests are consistant with all the previous tests. Here again a Bauschinger type effect is evident, although the effect is small. During compressive prestrain, the strains in the X and Y directions are tensile. Specimens cut out with their axes in these directions, on subsequent compressive loading, have flow stresses that are lower than those in the Z direction. This trend is identical in all the above discussed cases.

Comparison Between Tension and Compression Tests for Prestrains of Nominally Equal Magnitude

The prestrains had been planned in such a way that the first four compressive prestrain states have approximately the same numerical values of prestrains as the tensile prestrain states. This made it

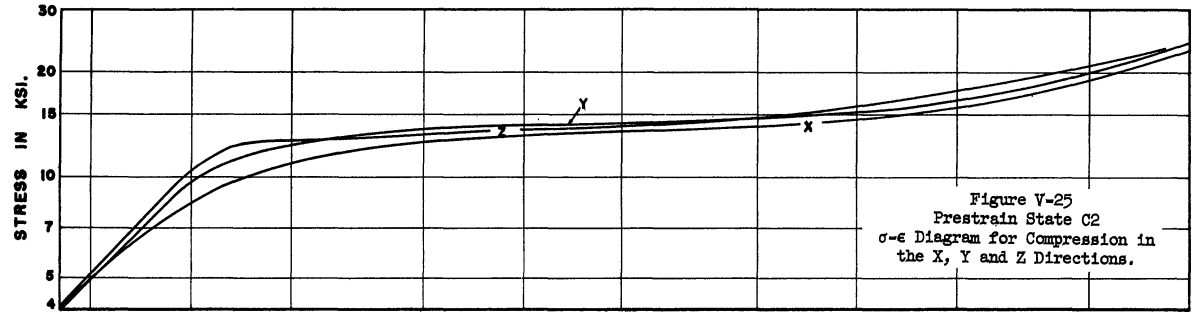

Figure V-25
Prestrain State C2
σ-ε Diagram for Compression in
the X, Y and Z Directions.

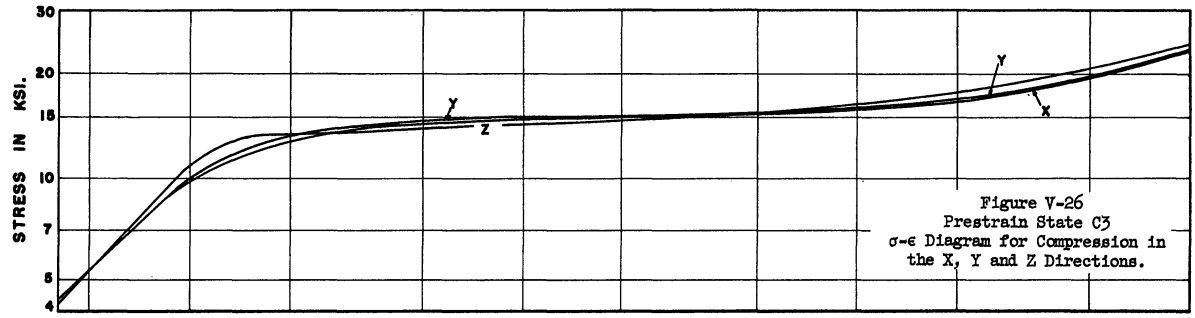

Figure V-26
Prestrain State C3
σ-ε Diagram for Compression in
the X, Y and Z Directions.

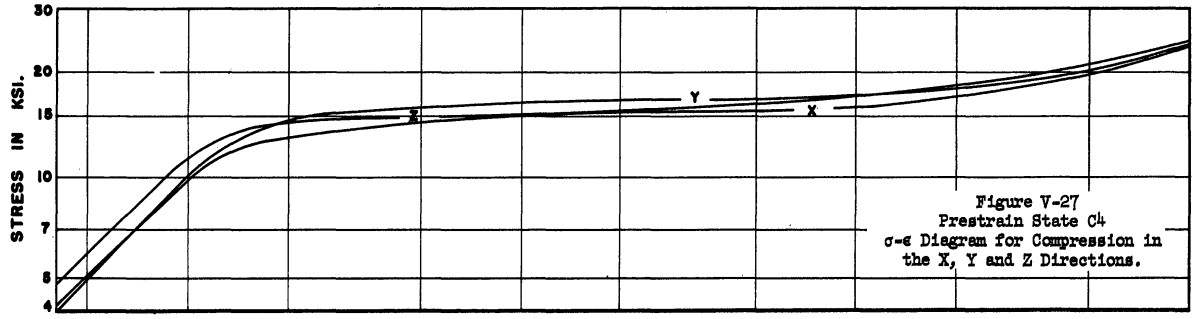

Figure V-27
Prestrain State C4
σ-ε Diagram for Compression in
the X, Y and Z Directions.

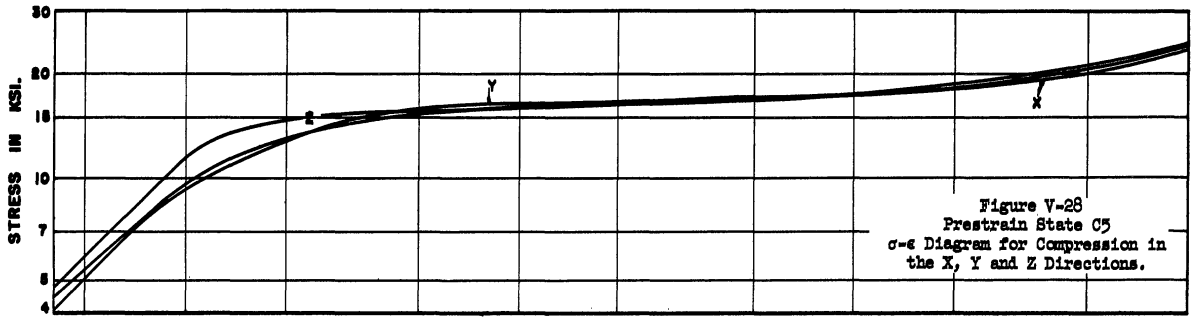

Figure V-28
Prestrain State C5
σ-ε Diagram for Compression in
the X, Y and Z Directions.

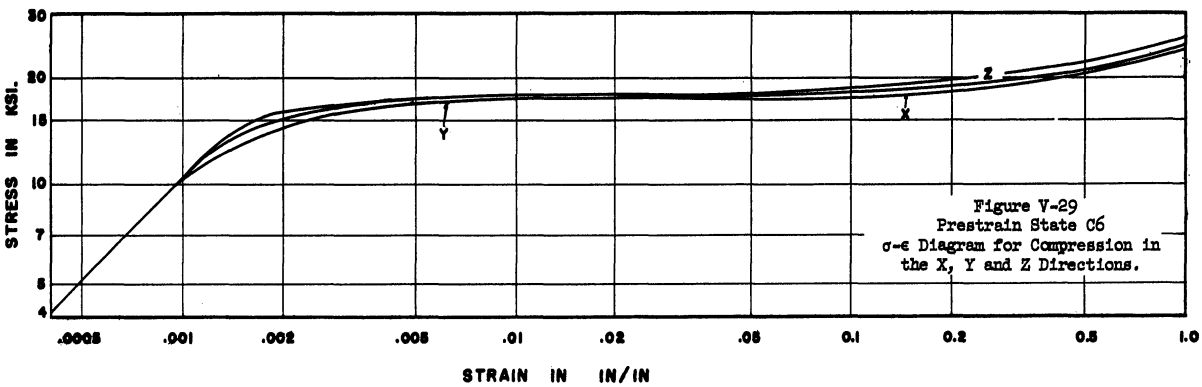

Figure V-29
Prestrain State C6
σ-ε Diagram for Compression in
the X, Y and Z Directions.

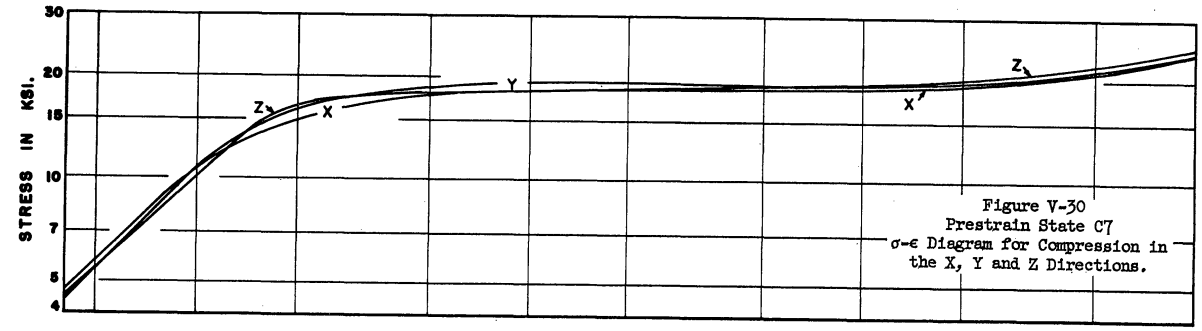

Figure V-30
Prestrain State C7
σ-ε Diagram for Compression in the X, Y and Z Directions.

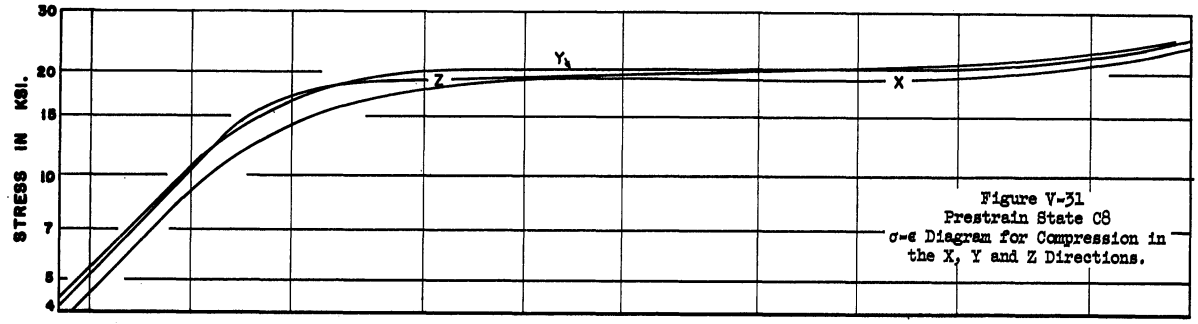

Figure V-31
Prestrain State C8
σ-ε Diagram for Compression in the X, Y and Z Directions.

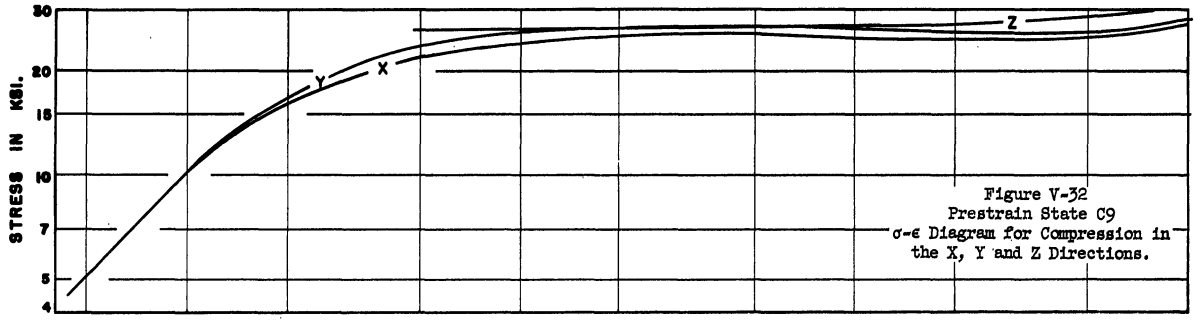

Figure V-32
Prestrain State C9
σ-ε Diagram for Compression in the X, Y and Z Directions.

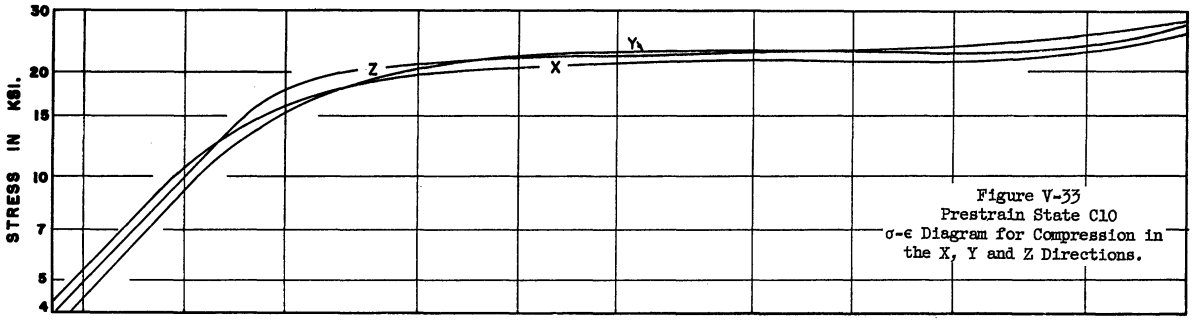

Figure V-33
Prestrain State C10
σ-ε Diagram for Compression in the X, Y and Z Directions.

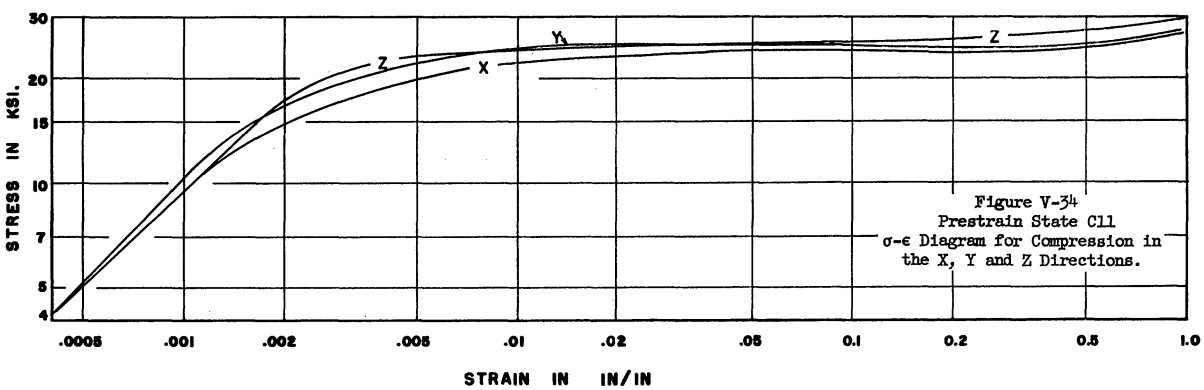

Figure V-34
Prestrain State C11
σ-ε Diagram for Compression in the X, Y and Z Directions.

possible to compare the stress-strain curves of the material prestrained to approximately the same amount in tension and in compression.

Figures V-35 to V-38 show the results of tension and compression tests in the X direction for both tensile and compressive prestrains of nominally the same magnitude. It appears that for compressive prestrain the tension and compression curves are very close to each other, tension curve being slightly lower. For tensile prestrain, the curves for tension tests are 1 to 3 ksi, or 5 to 20% lower than that in compression. Also, curves for compression tests in the X direction are about the same whether the material is prestrained in tension, or in compression, but for tension tests the flow stress is lower by 1/2 to 2 ksi, or up to 10% for tensile prestrain than for compressive prestrain.

Figures V-39 to V-44 show the comparison between tension and compression tests in the X direction for compressive prestrains greater than 0.25. For strains more than 0.1, the flow stresses are practically the same, and between $\epsilon = 0.01$ and 0.1, the material seems to be slightly stronger in compression.

Figures V-45 to V-48 show the stress-strain curves in tension and in compression in the Y direction for $\epsilon_p < 0.25$, prestrained both in tension and in compression. Observations here are similar to those for the X direction. At strains greater than 0.005, the curves for the compression tests for both kinds of prestrain and that for the tension after compressive prestrain are all very close to each other, while the curves for the tension tests in the Y direction after tensile prestrain are 0 to 2 ksi, i.e., up to 15% lower than the other three.

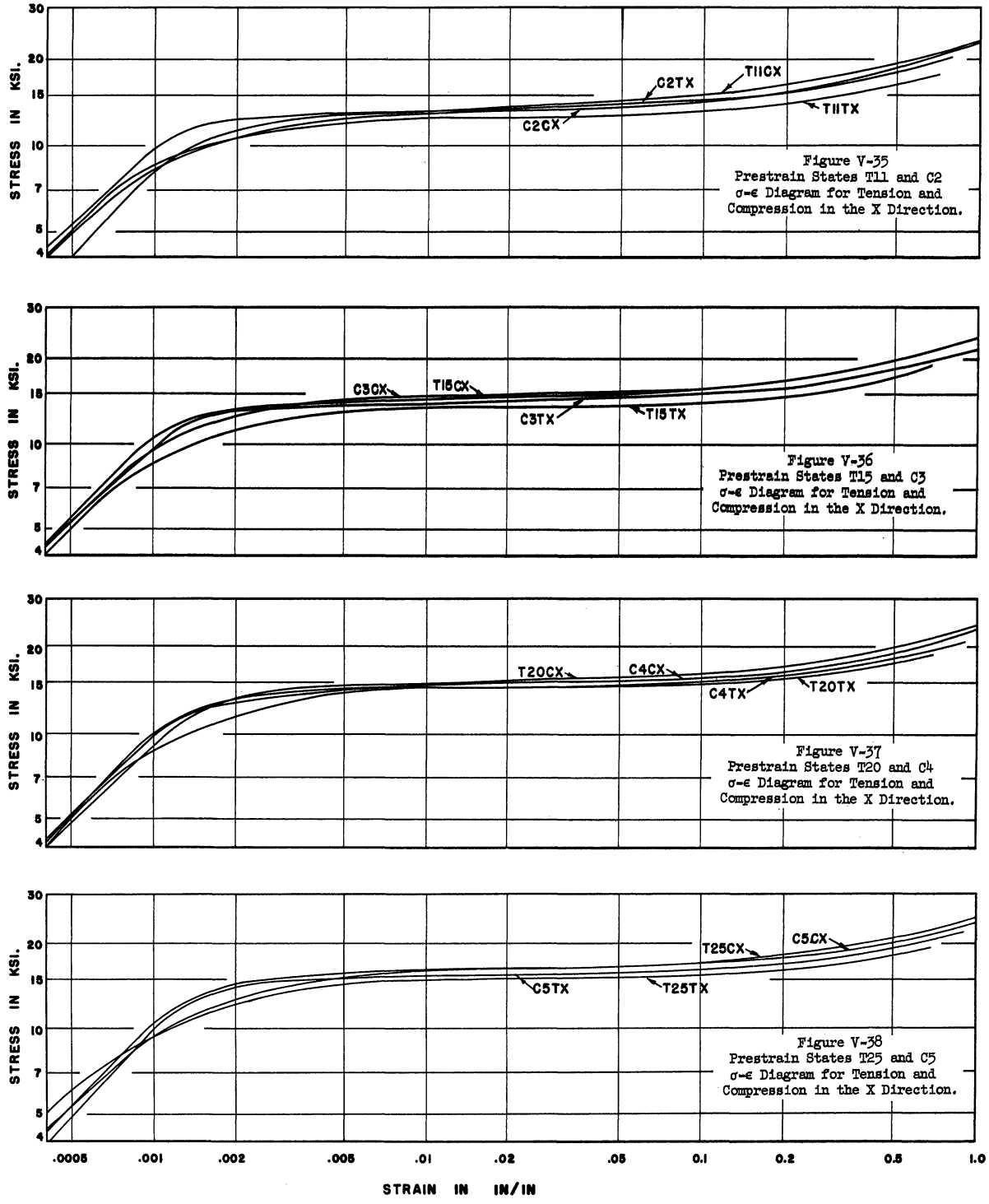

Figure V-35
Prestrain States T11 and C2
σ-ε Diagram for Tension and
Compression in the X Direction.

Figure V-36
Prestrain States T15 and C3
σ-ε Diagram for Tension and
Compression in the X Direction.

Figure V-37
Prestrain States T20 and C4
σ-ε Diagram for Tension and
Compression in the X Direction.

Figure V-38
Prestrain States T25 and C5
σ-ε Diagram for Tension and
Compression in the X Direction.

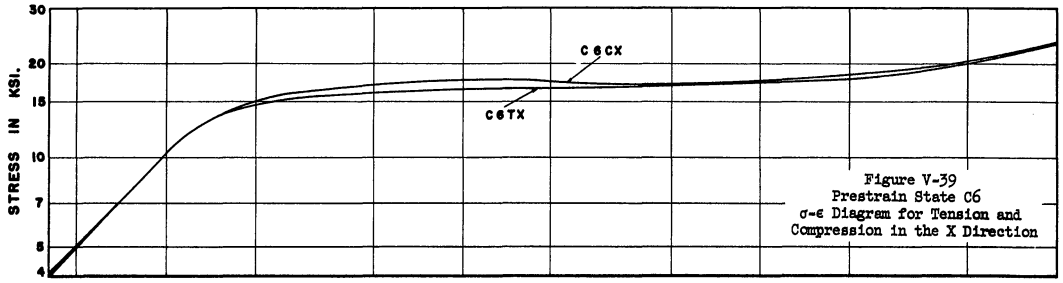

Figure V-39
Prestrain State C6
σ-ε Diagram for Tension and
Compression in the X Direction

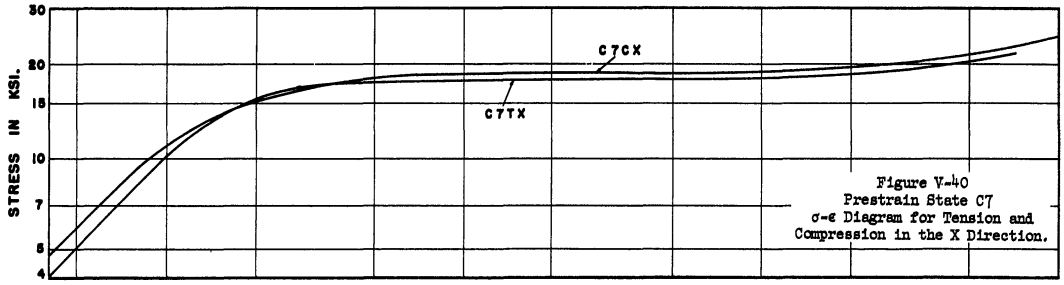

Figure V-40
Prestrain State C7
σ-ε Diagram for Tension and
Compression in the X Direction.

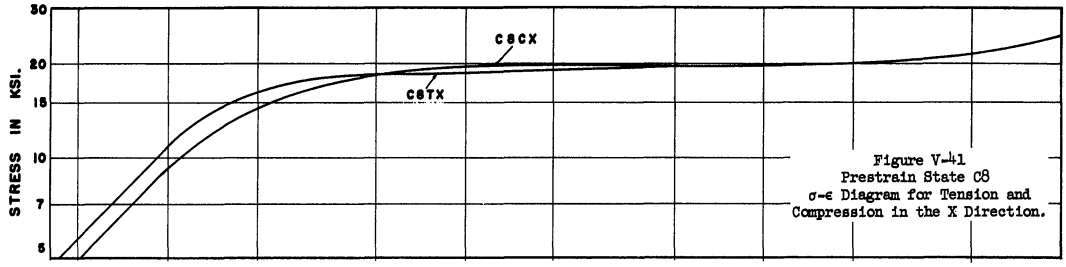

Figure V-41
Prestrain State C8
σ-ε Diagram for Tension and
Compression in the X Direction.

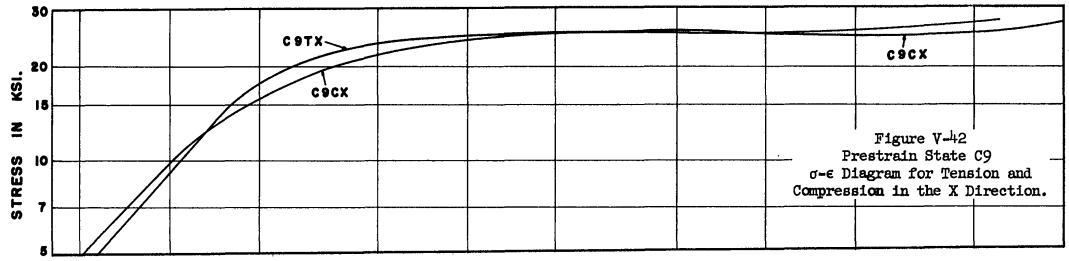

Figure V-42
Prestrain State C9
σ-ε Diagram for Tension and
Compression in the X Direction.

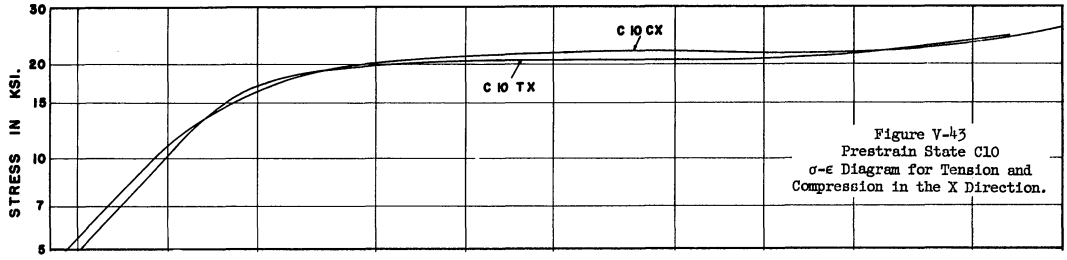

Figure V-43
Prestrain State C10
σ-ε Diagram for Tension and
Compression in the X Direction.

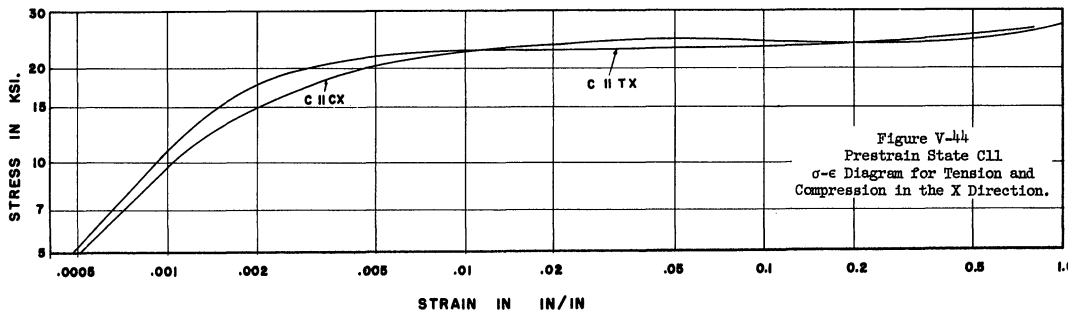

Figure V-44
Prestrain State C11
σ-ε Diagram for Tension and
Compression in the X Direction.

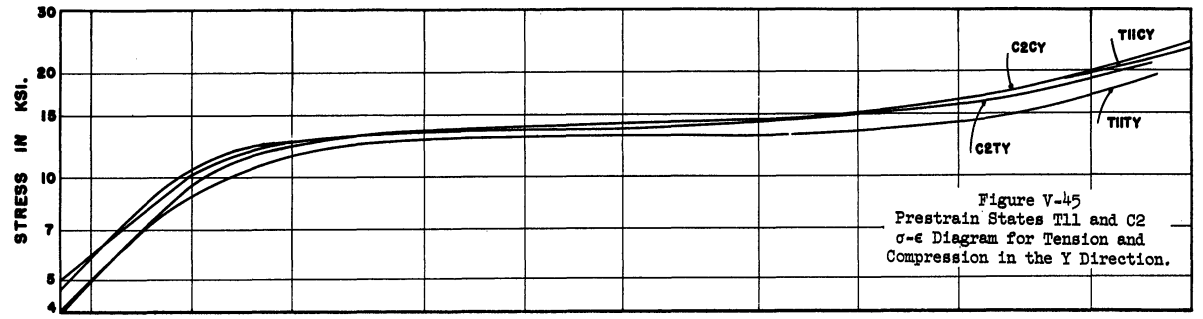

Figure V-45
Prestrain States T11 and C2
σ-ε Diagram for Tension and
Compression in the Y Direction.

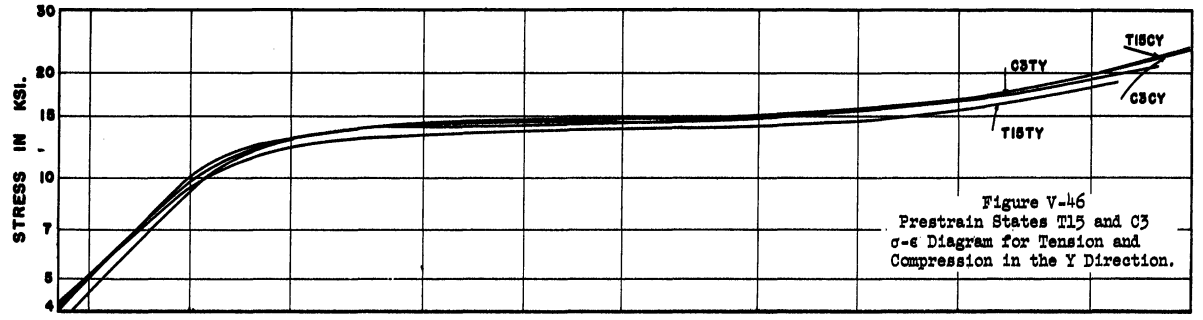

Figure V-46
Prestrain States T15 and C3
σ-ε Diagram for Tension and
Compression in the Y Direction.

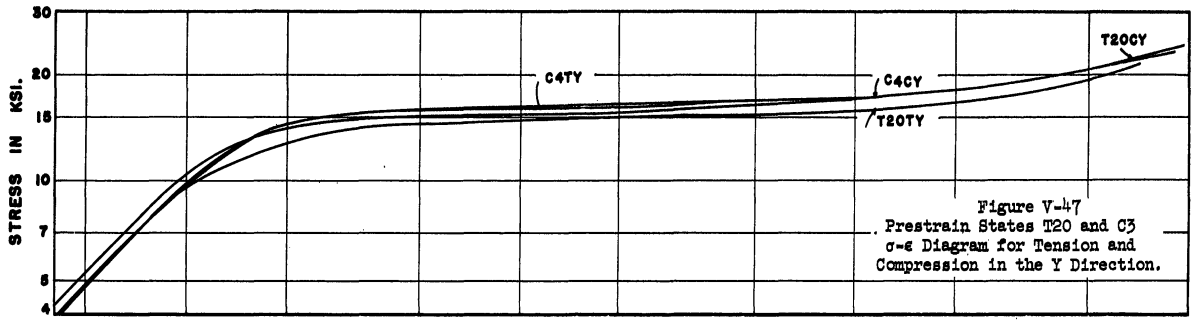

Figure V-47
Prestrain States T20 and C3
σ-ε Diagram for Tension and
Compression in the Y Direction.

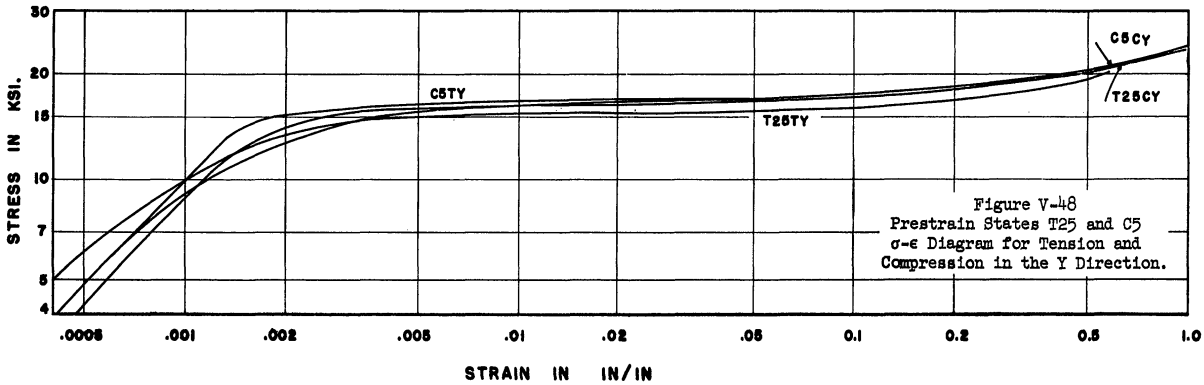

Figure V-48
Prestrain States T25 and C5
σ-ε Diagram for Tension and
Compression in the Y Direction.

Figures V-49 to V-54 show the comparison between tension and compression tests for compressive prestrains greater than 0.25. The flow stresses are practically identical except for prestrain states $\epsilon_p > 0.4$ and strains greater than 0.2, in which case, the compression curve is 0 to 1-1/2 ksi, i.e., up to 8% lower than the tension curve.

An interesting phenomenon was observed during compression tests in the X and the Y directions. In the X direction, for prestrains $\epsilon_p \geq 0.45$, the flow stress reaches a maximum, and then decreases slightly with increasing strain before beginning to increase monotonically. This strain-softening is only a fraction of a ksi at lower prestrains, increasing to about 1 ksi at $\epsilon_p = 1.95$. This phenomenon was observed by Bridgman[51] and by Ebert,[56] but it seems that they did not put any importance to them or dismissed as experimental error. This effect has been consistently encountered in the present investigation, and it seems to be a regular phenomenon.

As a possible explanation of this phenomenon, it is recalled that when the material is prestrained in compression in the Z direction, strains in the X and Y direction are tensile, while the subsequent testing is compressive. It is likely that while prestraining, certain crystallographic planes were active for slip and dislocations were pinned down by different obstacles while moving on those planes. During subsequent testing, some of them, although they were sessile in one plane, found mobility possible in other planes which became active on change of direction of strain, and hence a drop in flow stress.

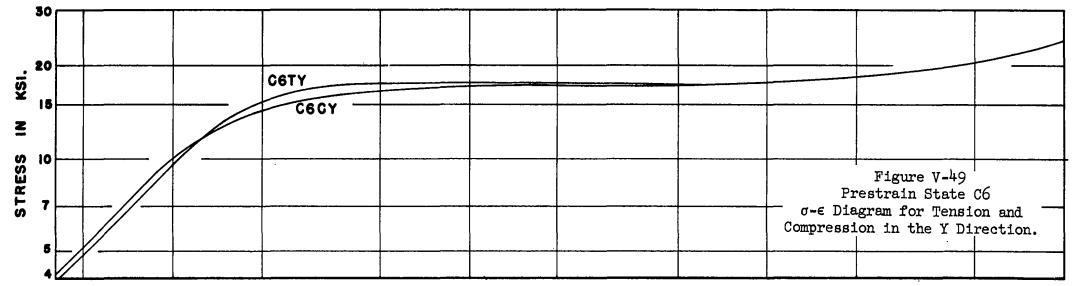

Figure V-49
Prestrain State C6
σ-ε Diagram for Tension and
Compression in the Y Direction.

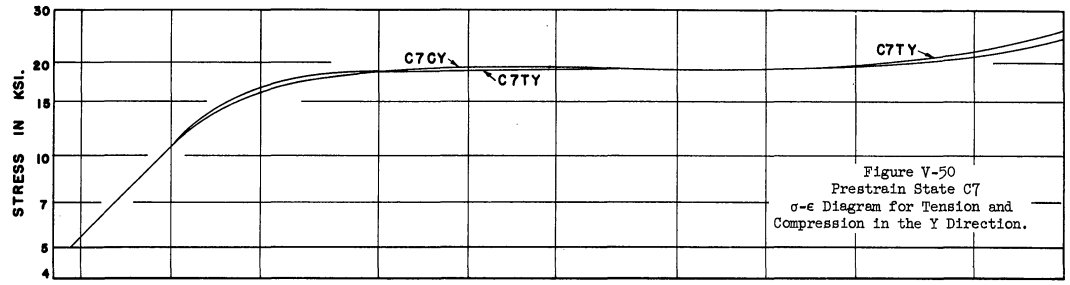

Figure V-50
Prestrain State C7
σ-ε Diagram for Tension and
Compression in the Y Direction.

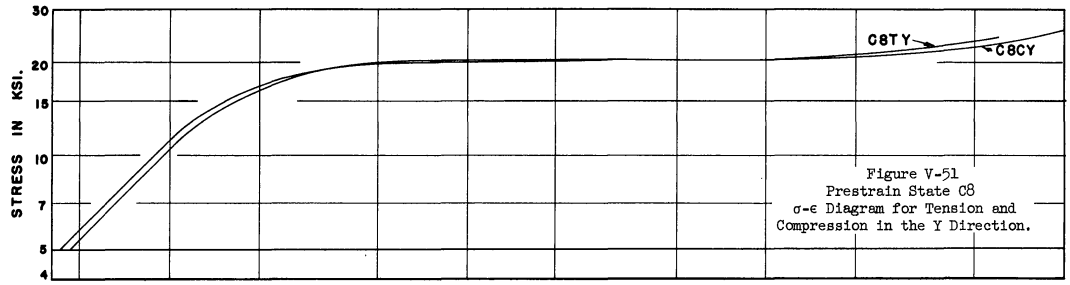

Figure V-51
Prestrain State C8
σ-ε Diagram for Tension and
Compression in the Y Direction.

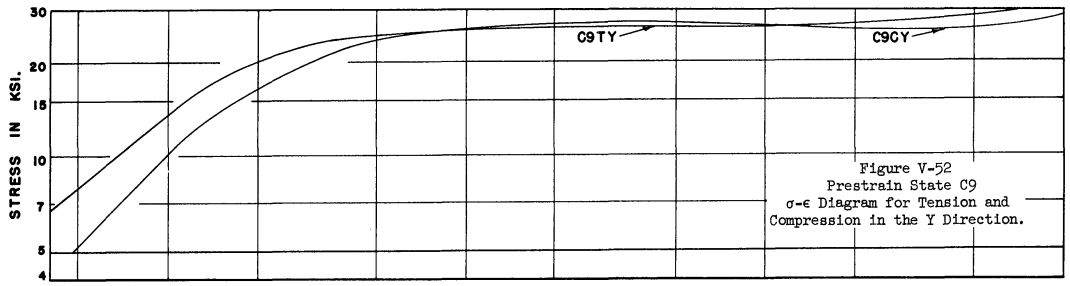

Figure V-52
Prestrain State C9
σ-ε Diagram for Tension and
Compression in the Y Direction.

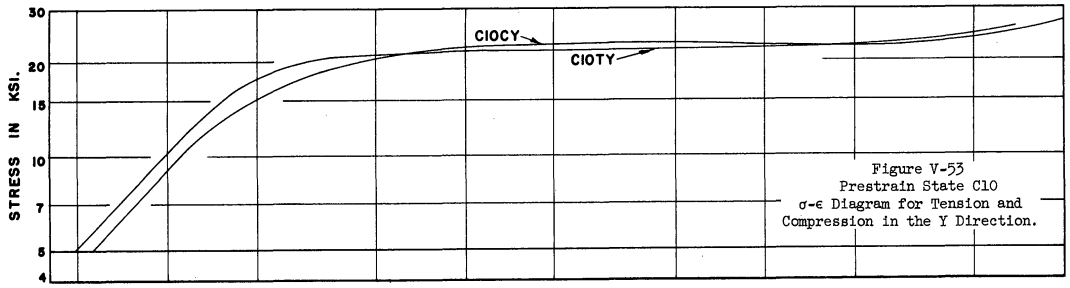

Figure V-53
Prestrain State C10
σ-ε Diagram for Tension and
Compression in the Y Direction.

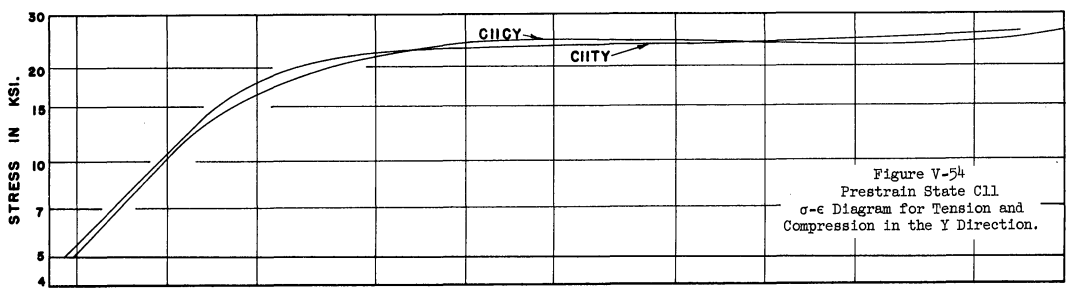

Figure V-54
Prestrain State C11
σ-ε Diagram for Tension and
Compression in the Y Direction.

The flow stress increases until a maxima is reached between ϵ = 0.01 and 0.05. It then decreases to a minima at about ϵ = 0.15 to 0.25, before it starts increasing monotonically.

The difference between flow stresses in tension and in compression in the X and Y directions is always rather small, but that in the Z direction is appreciable. Figures V-55 to V-58 show the stress-strain curves in tension and in compression in the Z direction for both tensile and compressive prestrains of the same nominal magnitudes for $\epsilon_p < .25$. It is apparent that the flow stress is 5 to 20% lower when the direction of testing is reversed. The effects are similar for both tensile and compressive prestrains, although probably the reduction in flow stress is slightly lesser for tensile prestrains than for compressive prestrains.

From Figures V-55 to V-63 it is apparent that the Bauschinger effect is much more pronounced for stresses near the elastic limit than for stresses associated with, say, 0.2% offset. From Figure V-55, the elastic limit is about 32% lower when measured in a sense opposite to the preload, but for a 0.4 offset, the yield strength is only about 15% lower in the opposite sense. In some cases this value is only 10% lower.

Figures V-59 to V-63 show the comparison between tension and compression tests in the Z direction after compressive prestrains $\epsilon_p > 0.25$. The flow stress in tension is always less than that in compression. The minimum difference of about 8% occurs at a strain of about 0.02 and the maximum between 0.2 to 0.4. The maximum difference is about 3 ksi or about 15%. The difference tends to become

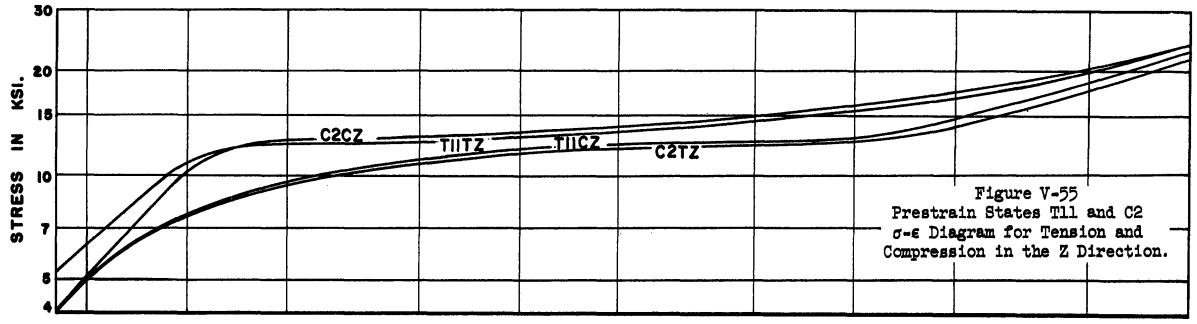

Figure V-55
Prestrain States T11 and C2
σ-ε Diagram for Tension and
Compression in the Z Direction.

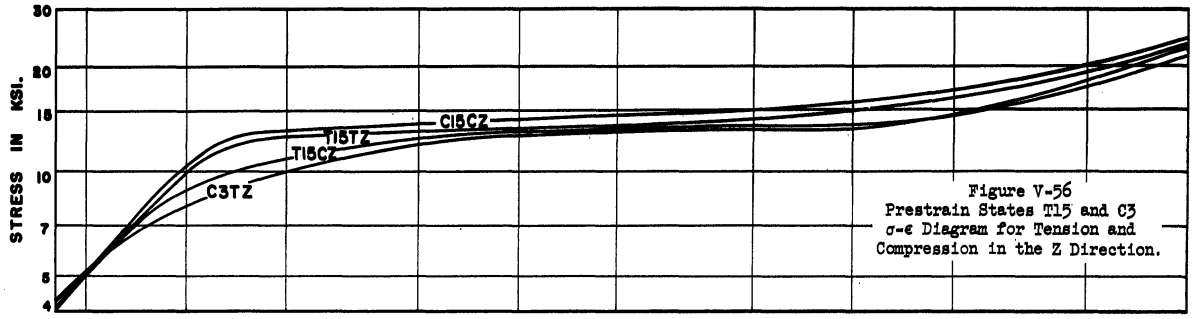

Figure V-56
Prestrain States T15 and C3
σ-ε Diagram for Tension and
Compression in the Z Direction.

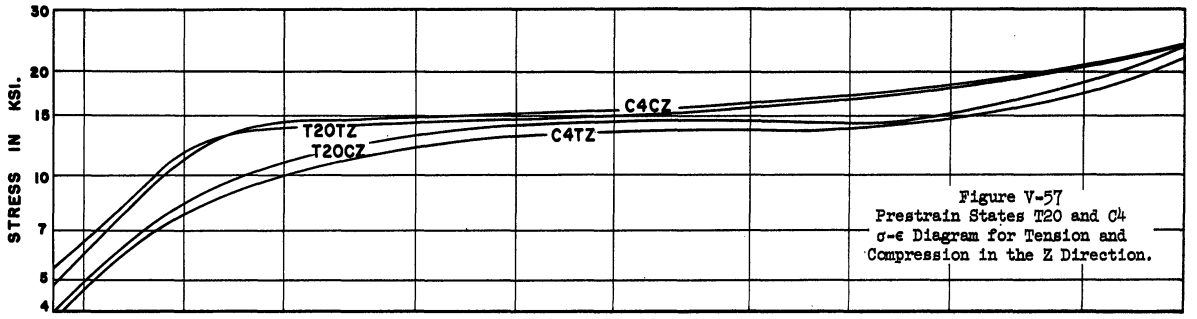

Figure V-57
Prestrain States T20 and C4
σ-ε Diagram for Tension and
Compression in the Z Direction.

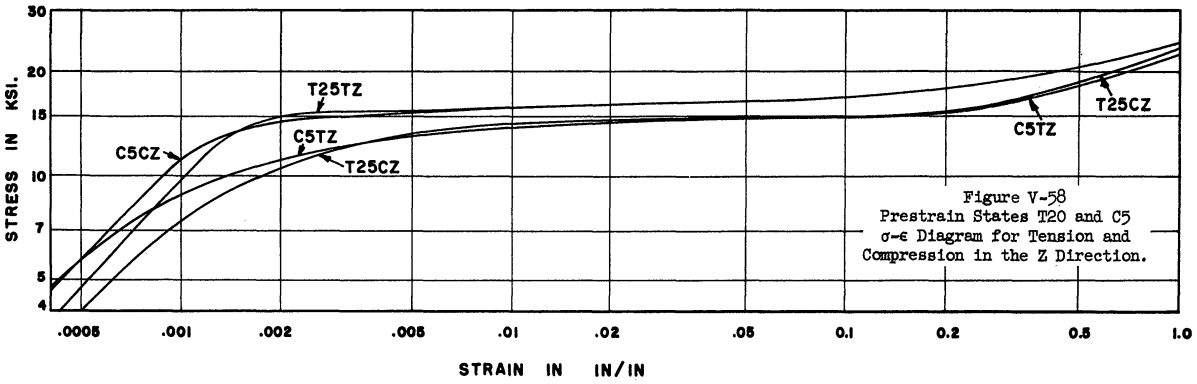

Figure V-58
Prestrain States T20 and C5
σ-ε Diagram for Tension and
Compression in the Z Direction.

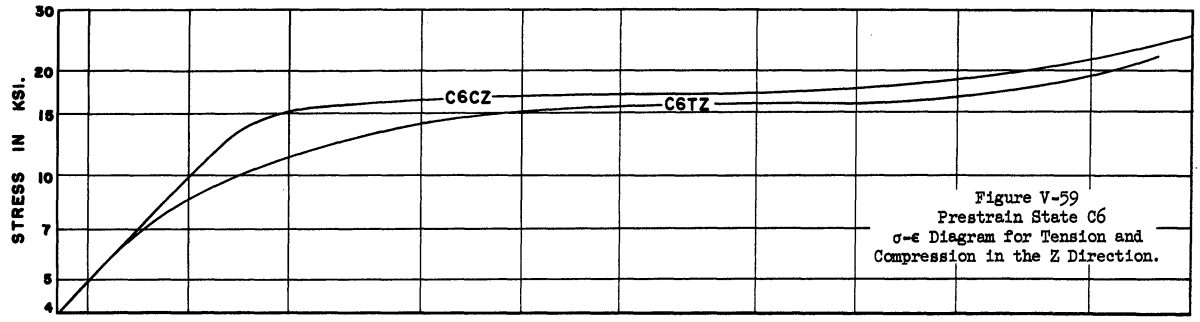

Figure V-59
Prestrain State C6
σ-ε Diagram for Tension and
Compression in the Z Direction.

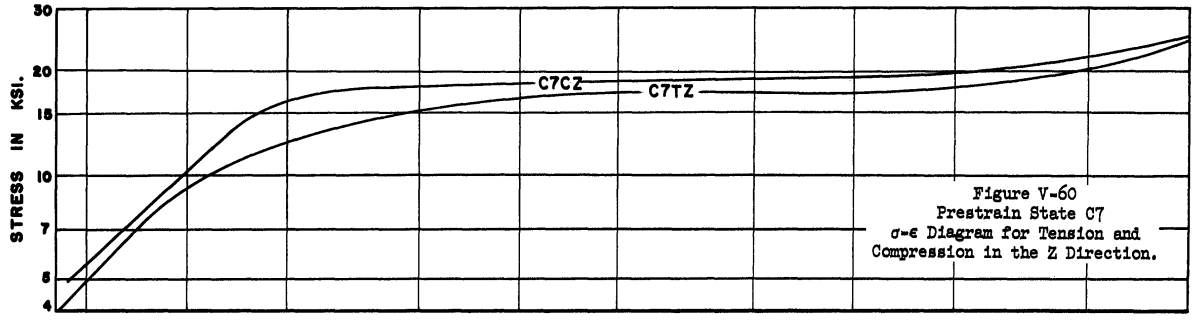

Figure V-60
Prestrain State C7
σ-ε Diagram for Tension and
Compression in the Z Direction.

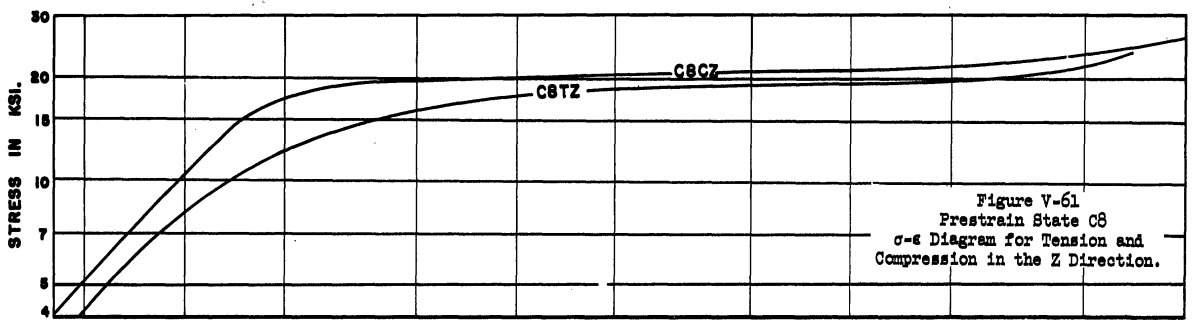

Figure V-61
Prestrain State C8
σ-ε Diagram for Tension and
Compression in the Z Direction.

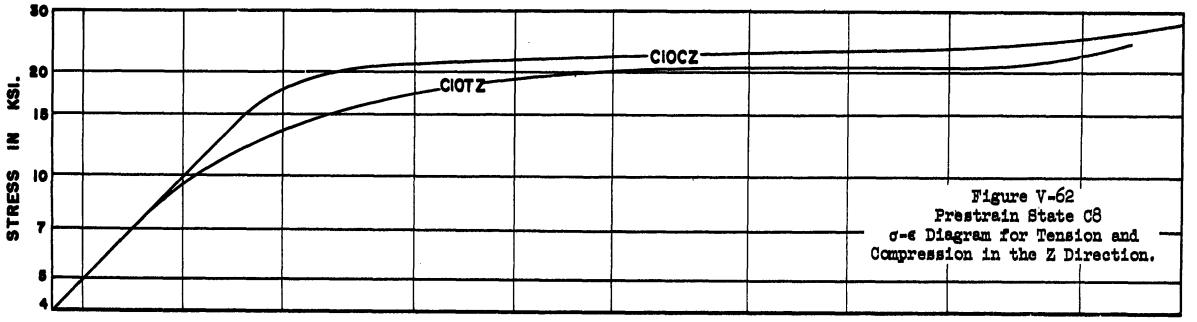

Figure V-62
Prestrain State C8
σ-ε Diagram for Tension and
Compression in the Z Direction.

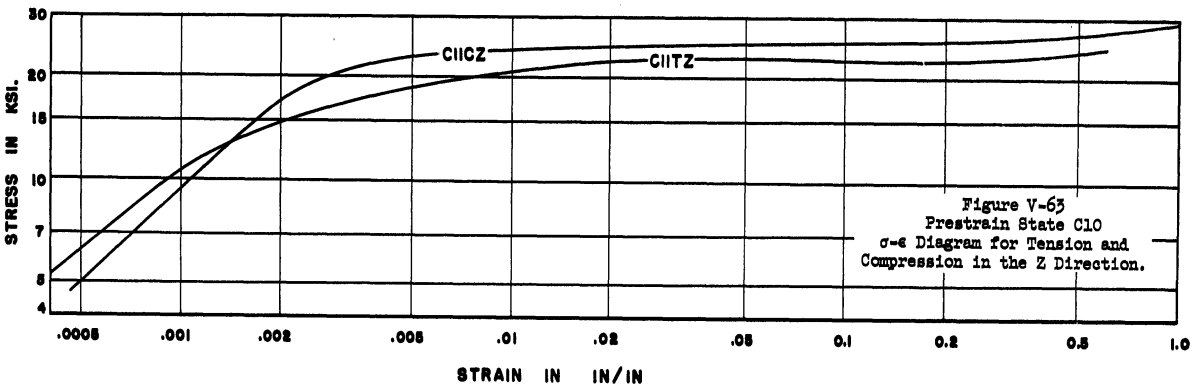

Figure V-63
Prestrain State C10
σ-ε Diagram for Tension and
Compression in the Z Direction.

smaller at higher strain, but whether this reduction in difference is actual or is only apparent depends on the validity of the correction that has been applied to find the true stress at the necked down region.

Tension Tests After Tensile Prestrains

Figure V-64 shows the stress-strain relations in tension in the X direction after tensile prestrain. The curves show increasing flow stresses for increasing prestrains. However, it is also seen that all the curves intersect the stress-strain curve for the X direction in the annealed state. This means that although the material is strengthened in the X direction for lower strains, beyond a certain value of strain, the material is weaker than in initially annealed material. In other words, prestrain in the Z direction is not additive to strain in subsequent testing in the X direction. Also, it is apparent from this behavior that the concept of "effective strain" which is a positive definite quantity is not applicable, at least for large finite strains.

Figure V-65 is similar to Figure V-64, except that the curves are for the Y direction. The same conclusions as above are reached from this.

Figure V-66 shows the results of tension test after tensile prestrain, both in the Z direction. Here the subsequent testing should be only a continuation of the prestraining process, and as expected, all the curves are above that for the annealed state. To check that the tension tests are just a continuation of the prestrain

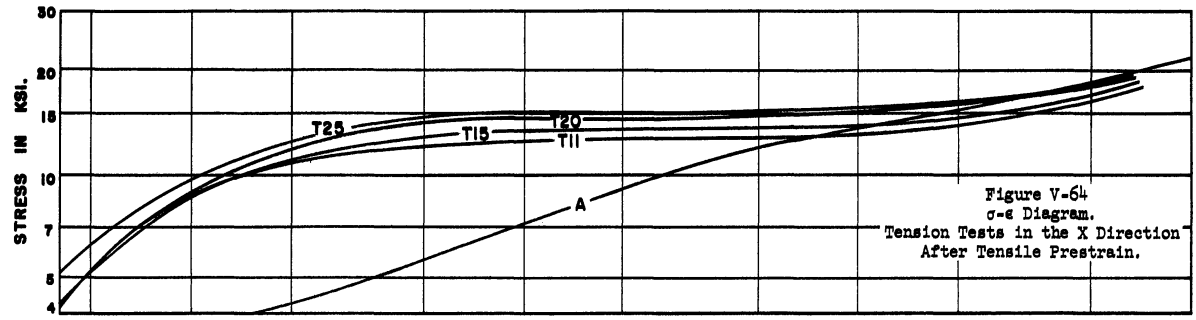

Figure V-64
σ-ε Diagram.
Tension Tests in the X Direction
After Tensile Prestrain.

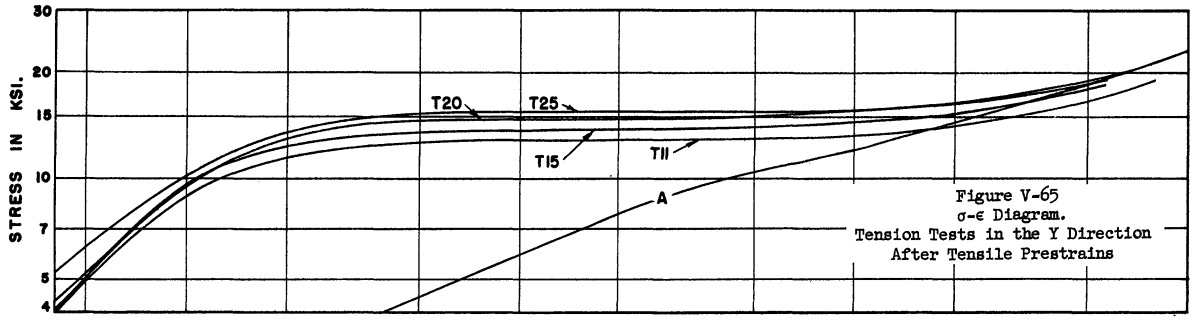

Figure V-65
σ-ε Diagram.
Tension Tests in the Y Direction
After Tensile Prestrains

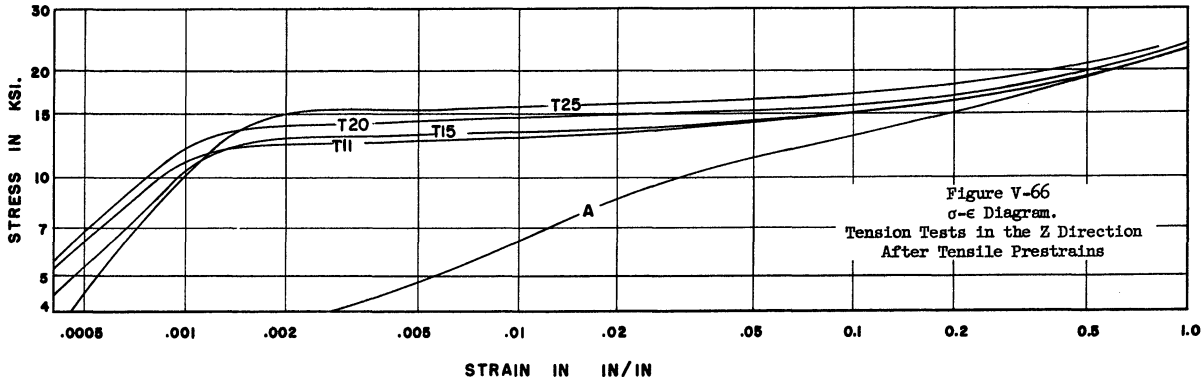

Figure V-66
σ-ε Diagram.
Tension Tests in the Z Direction
After Tensile Prestrains

process, stress against ($\epsilon_p + \epsilon$) for plastic ranges only were plotted in Figure V-67. The best straight line drawn gives a stress-strain relation as

$$\sigma = 22.4\ \epsilon^{0.262}$$

This is about 4.3% lower than that obtained by testing annealed specimens, and is within the range of experimental error.

Compression Tests After Tensile Prestrains

Figures V-68 and V-69 show the results of compression tests in the X and Y directions respectively for tensile prestrains. Since the material underwent compressive strains in the X and Y directions during prestraining, it is expected that the flow stress would be greater than in the annealed state for all strains. This expectation is confirmed. Flow stresses increase with increasing prestrain as is expected.

Figure V-70 shows the results of compression test in the Z direction after prestraining in tension. This set of curves are interesting in that although flow stress increases with increasing prestrain for strains up to about 0.25, they all converge at that strain to the flow stress value of annealed material, and for higher strains, the curves are practically coincident, irrespective of the prestrain value. In other words, for any tensile prestrain, the material behaves like an annealed material for compressive strains greater than 0.25.

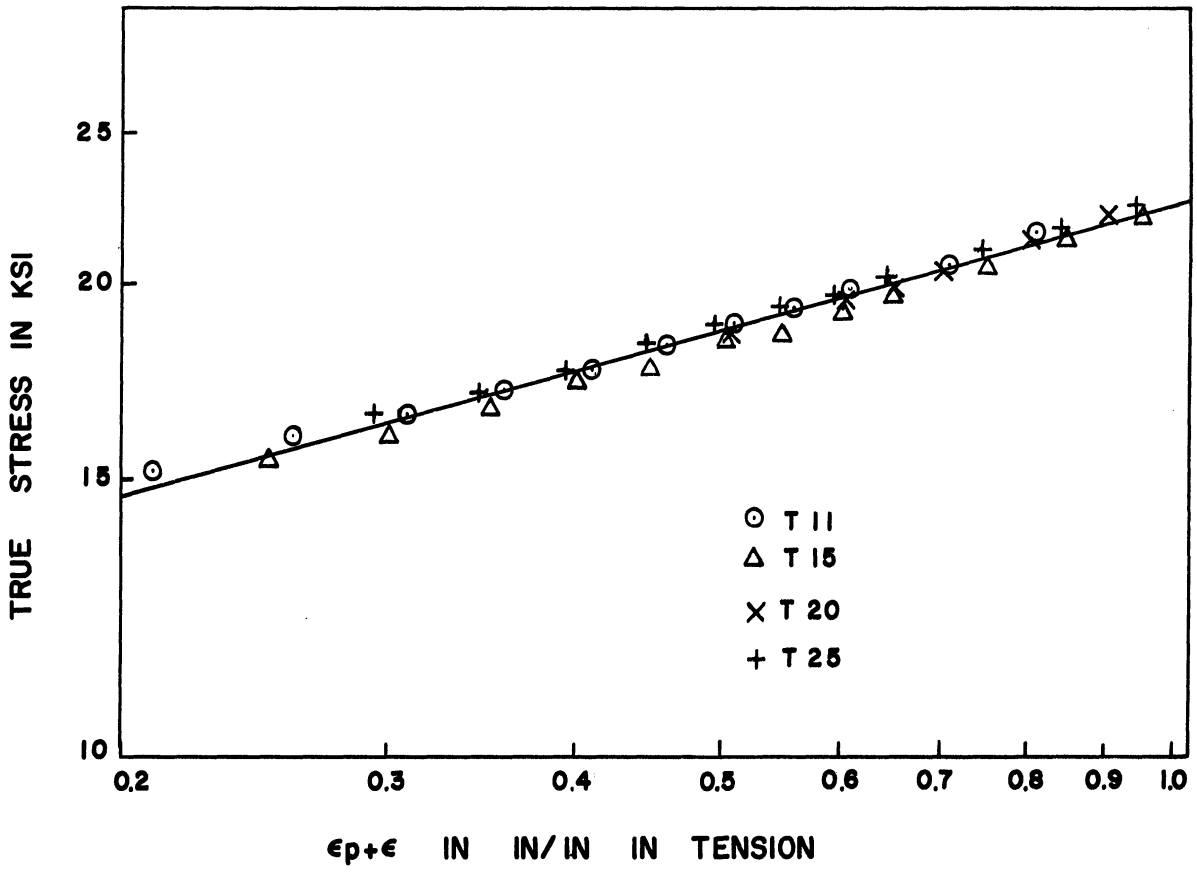

Figure V-67. σ-ϵ Diagram. Tension Test in Z Direction as Continuation of Tensile Prestrain.

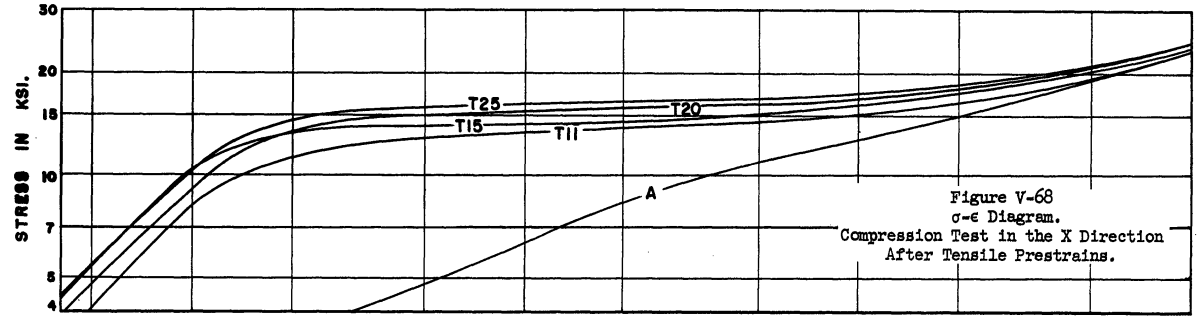

Figure V-68
σ-ε Diagram.
Compression Test in the X Direction
After Tensile Prestrains.

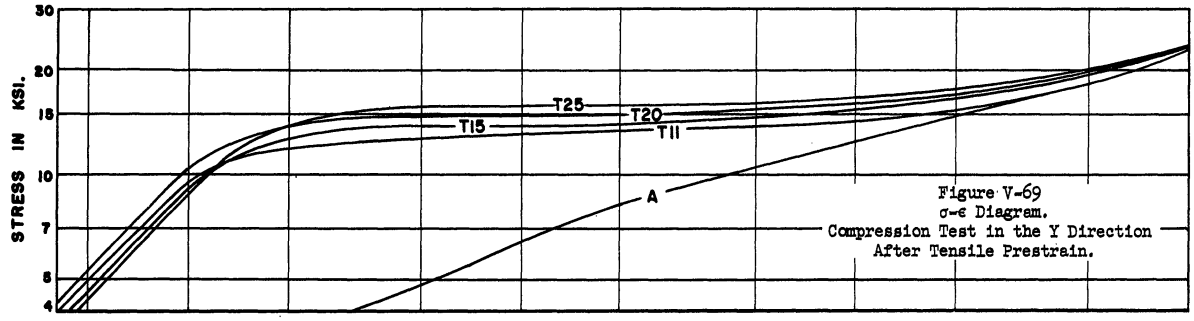

Figure V-69
σ-ε Diagram.
Compression Test in the Y Direction
After Tensile Prestrain.

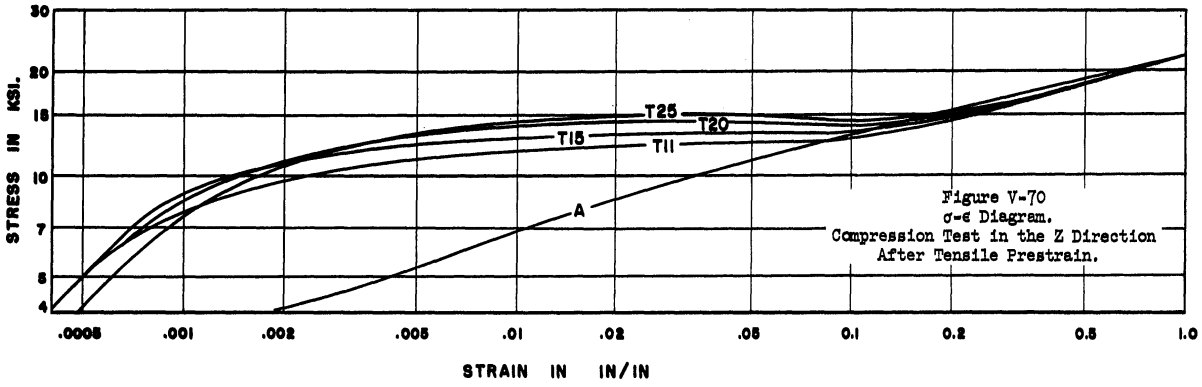

Figure V-70
σ-ε Diagram.
Compression Test in the Z Direction
After Tensile Prestrain.

Tension Test After Compressive Prestrain

Figures V-71 and V-72 show the stress-strain curves for tension in the X and Y directions after compressive prestrain. By the same token as for Figures V-68 and V-69, it is expected that the curves should all lie above that for annealed material. However, the curve for annealed material crosses first two or three curves for low prestrain values below $\epsilon = 1.0$. The cross over is slight and may be due to some experimental error or the factor used to correct for the triaxiality of stresses at the neck.

Figure V-73 shows stress-strain curves for different prestrain states when tested in tension in the Z direction after prestraining in compression. They seem to be converging toward the curves for annealed material, but data could not be obtained for sufficiently large strains to verify it.

Compression Test After Compressive Prestrain

Figures V-74 and V-75 presents the results of compression tests in the X and Y directions respectively after compressive prestraining. In the same way as in Figures V-64 and V-65, they should cross the curve for annealed material. It is not obvious from the diagrams, since sufficiently high strains could not be attained. The interesting phenomenon of strain softening has been discussed before and can be clearly seen in specimens C6 and C9. However, it is not so pronounced in all the specimens.

Figure V-76 gives the comparison between stress-strain diagrams for compression tests in the Z direction after compressive

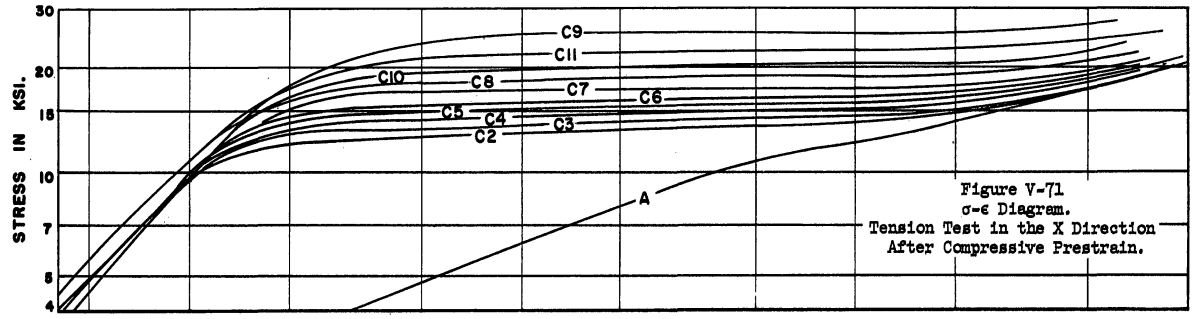

Figure V-71
σ-ε Diagram.
Tension Test in the X Direction
After Compressive Prestrain.

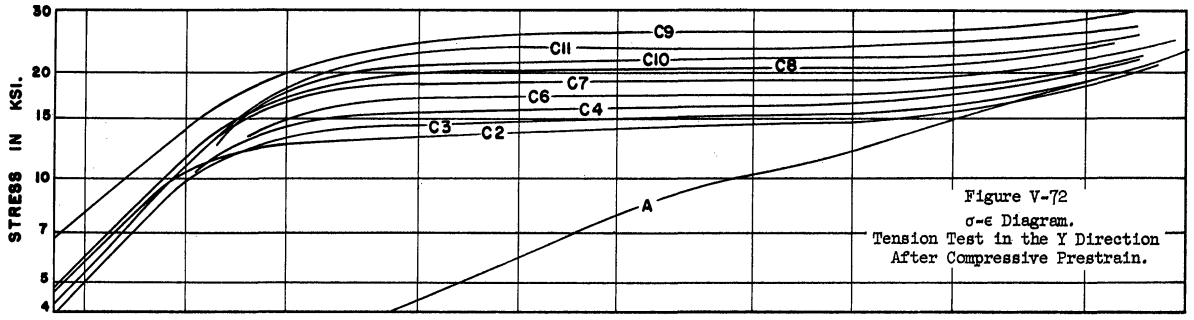

Figure V-72
σ-ε Diagram.
Tension Test in the Y Direction
After Compressive Prestrain.

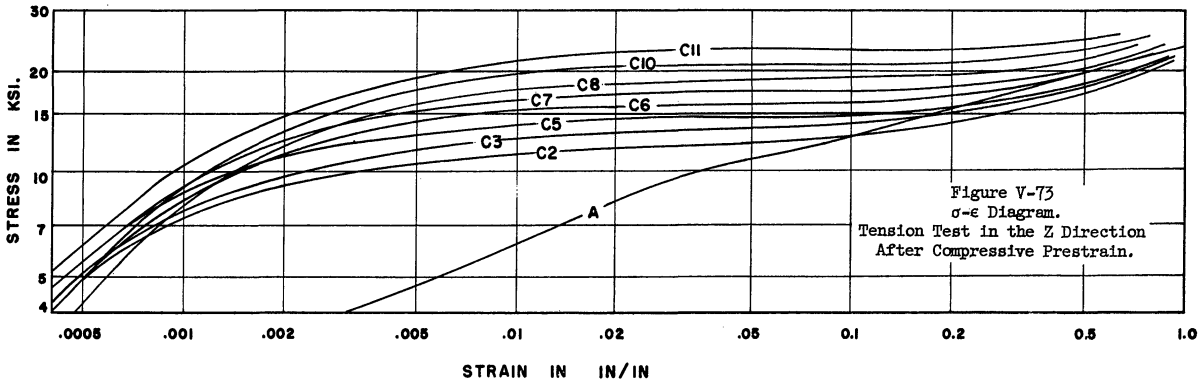

Figure V-73
σ-ε Diagram.
Tension Test in the Z Direction
After Compressive Prestrain.

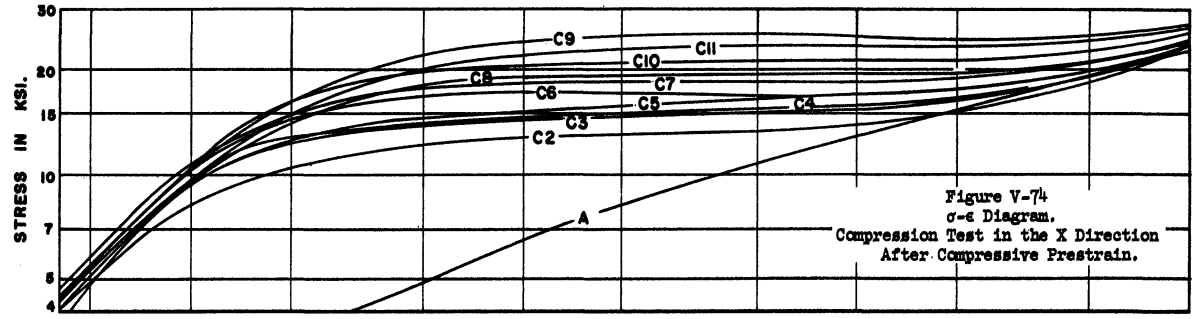

Figure V-74
σ-ε Diagram.
Compression Test in the X Direction
After Compressive Prestrain.

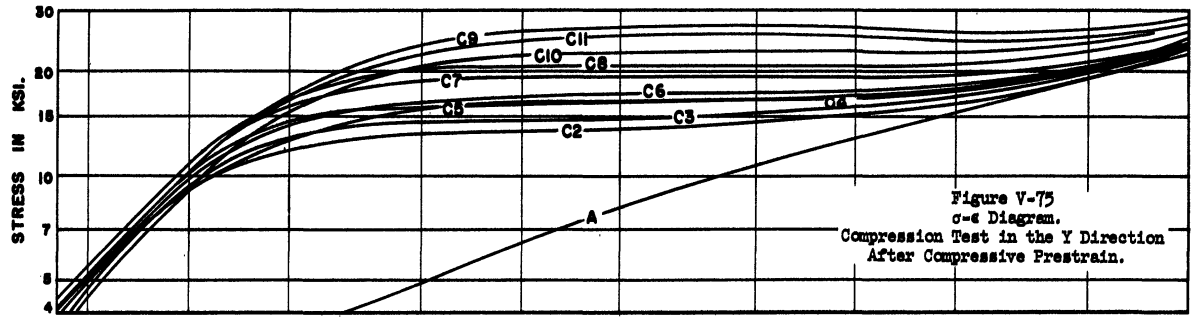

Figure V-75
σ-ε Diagram.
Compression Test in the Y Direction
After Compressive Prestrain.

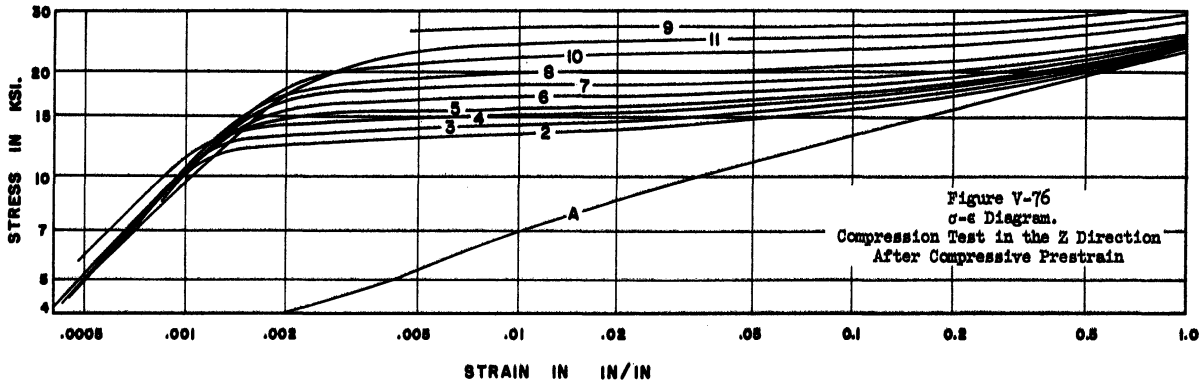

Figure V-76
σ-ε Diagram.
Compression Test in the Z Direction
After Compressive Prestrain

prestrains. As in the case of Figure V-66 the subsequent testing is only a continuation of the prestraining process. To check this, stress was plotted against $(\epsilon_p + \epsilon)$ in Figure V-77, and it was found that the data points were indeed on an approximately straight line on log-log co-ordinates showing a stress-strain relation:

$$\sigma = 22.9\ \epsilon^{0.254}\ \text{ksi.}$$

which is almost identical to that for the annealed material and for the tensile prestrain specimens.

It is rather difficult to compare quantitatively such a large number of stress-strain diagrams as are present in this investigation; particularly since each curve is an average of only two tests and, therefore, no statistical analysis for each kind of curve is possible. Variations in flow stresses at low, intermediate and large strains are not similar and hence no single figure can adequately describe the difference between two curves. However, in an attempt to make the picture a little more clear Tables V-III, V-IV and V-V have been prepared.

0.2% Offset Yield Stress

Table V-III shows the stresses at 0.2% plastic strain for the different tests and the percent difference between these stresses and the same for tension or compression test in the Z direction according as whether the prestrain is tensile or compressive.

For tensile prestrains, it is observed that compared to the yield stress for the tension tests in the Z direction, the yield stress:

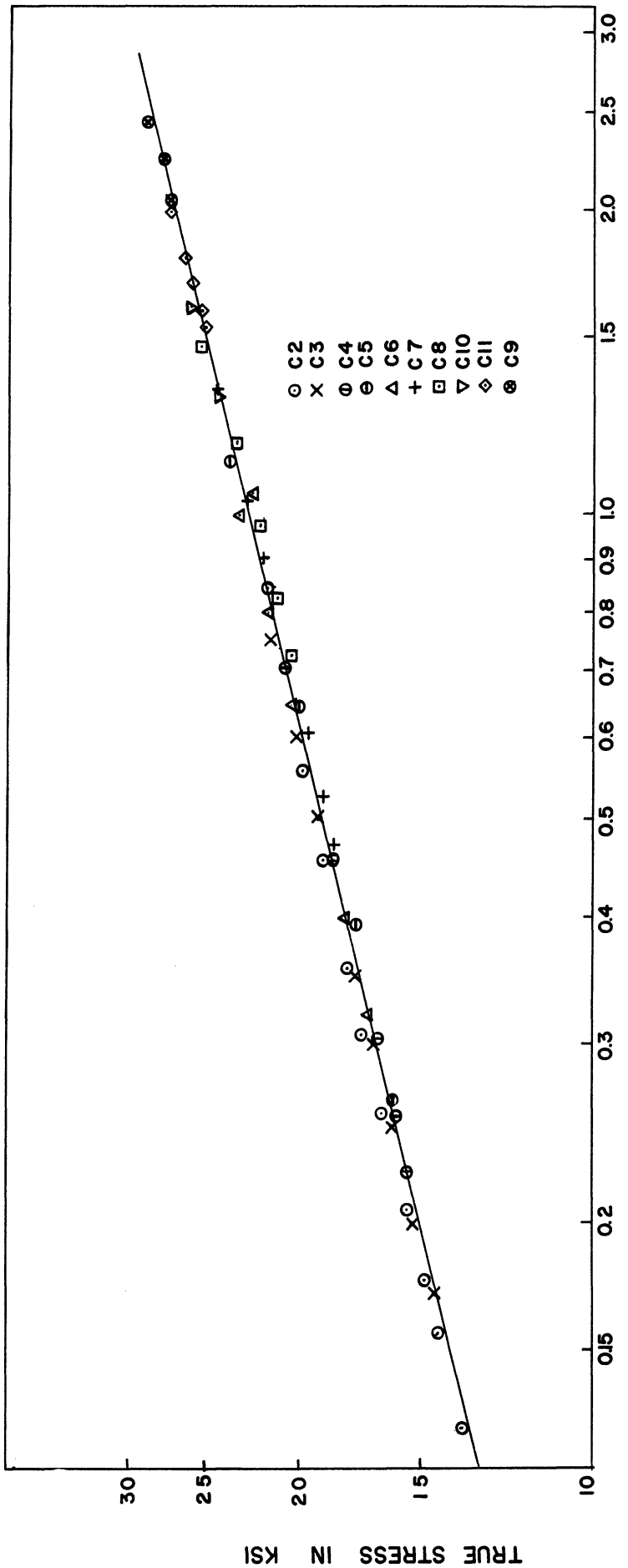

Figure V-77. σ-ϵ Diagram. Compression Test in Z Direction as Continuation of Compressive Prestrain.

TABLE V-III

0.2% OFFSET YIELD STRESS AND DIFFERENCE FROM $\sigma_{(.2\%)z}$

(a) Tensile Prestrains

		TX	TY	TZ	CX	CY	CZ
T11	ksi	11.3	12.0	12.4	12.3	12.6	10.2
	Diff in %	-8.9	-3.2	0	-0.8	1.6	-17.7
T15	ksi	12.0	13.0	12.8	13.6	13.9	11.6
	Diff in %	-6.3	1.6	0	6.3	8.6	-9.4
T20	ksi	13.1	14.2	14.0	14.5	15.0	12.2
	Diff in %	-6.4	1.4	0	3.6	7.1	-12.9
T25	ksi	13.6	14.5	15.3	15.4	15.6	12.0
	Diff in %	-11.1	-5.2	0	0.7	2.0	-20.6

(b) Compressive Prestrains

C2	ksi	12.5	13.0	10.0	11.5	12.7	12.6
	Diff in %	-0.8	3.2	-20.6	-8.7	0.8	0
C3	ksi	12.8	14.0	11.0	13.5	13.7	13.5
	Diff in %	-5.2	3.7	-18.5	0	1.5	0
C4	ksi	14.0	15.3	11.2	13.6	15.5	14.5
	Diff in %	-3.4	5.5	-22.8	-6.2	6.9	0
C5	ksi	14.8	16.0	12.3	14.4	14.8	15.1
	Diff in %	-2.0	6.0	-18.5	-4.6	-2.0	0
C6	ksi	15.4	16.7	13.0	16.1	15.6	16.4
	Diff in %	-6.1	1.8	-20.7	-1.8	-4.9	0
C7	ksi	16.9	18.5	14.4	16.9	18.1	17.7
	Diff in %	-4.5	4.5	-18.6	-14.5	2.3	0
C8	ksi	18.0	19.6	14.6	17.1	19.7	19.0
	Diff in %	-5.3	3.2	-23.2	-10.0	3.7	0
C10	ksi	18.7	20.8	16.4	19.0	19.5	20.8
	Diff in %	-10.1	0	-21.2	-8.7	-6.3	0
C11	ksi	21.0	22.4	17.7	18.7	21.4	22.5
	Diff in %	-6.7	-0.4	-21.3	-16.9	-4.9	0
C9	ksi	23.0	24.2	-	20.9	22.9	26.4
	Diff in %	-12.9	-8.3	-	-20.8	-13.3	0

TABLE V-IV

AVERAGE FLOW STRESS AND % DIFFERENCE FROM $\sigma_{z(av)}$

(a) Tensile Prestrains

		TX	TY	TZ	CX	CY	CZ
T11	ksi	13.1	13.5	14.8	14.8	14.8	13.4
	Diff in %	-10.5	-8.8	0	0	0	-9.5
T15	ksi	13.9	14.4	14.9	15.4	15.4	14.0
	Diff in %	-6.7	-3.4	0	3.4	3.4	-6.0
T20	ksi	15.0	15.5	16.0	16.3	16.4	14.7
	Diff in %	-6.3	-3.1	0	1.9	2.5	-8.0
T25	ksi	15.4	16.0	17.0	17.0	16.9	15.0
	Diff in %	-9.4	-5.9	0	0	-0.6	-11.8

(b) Compressive Prestrains

C2	ksi	14.2	14.5	12.6	14.0	14.9	15.2
	Diff in %	-7.2	-4.6	-17.1	-7.9	-2.0	0
C3	ksi	14.8	15.4	13.9	15.6	15.8	15.9
	Diff in %	-6.9	-3.1	-12.6	-1.9	-0.6	0
C4	ksi	15.4	16.8	14.0	15.8	17.0	16.6
	Diff in %	-7.2	1.2	-15.7	-4.8	2.4	0
C5	ksi	16.1	17.3	14.9	17.0	17.2	17.1
	Diff in %	-5.9	1.2	-12.9	-0.6	0.6	0
C6	ksi	16.9	17.5	16.1	17.4	17.7	18.0
	Diff in %	-6.1	-2.8	-10.5	-3.3	-1.7	0
C7	ksi	17.8	19.3	17.3	19.0	19.3	19.2
	Diff in %	-7.3	0.5	-10.0	-1.0	0.5	0
C8	ksi	19.2	21.0	18.6	19.5	20.7	20.6
	Diff in %	-6.8	1.9	-9.7	-5.3	0.5	0
C10	ksi	20.5	22.2	20.3	21.2	22.9	23.0
	Diff in %	-10.9	-3.5	-11.7	-7.8	-0.4	0
C11	ksi	22.7	24.3	22.2	23.2	24.4	25.1
	Diff in %	-9.6	-3.2	-11.5	-7.6	-2.8	0
C9	ksi	25.2	26.2	-	24.6	26.1	27.2
	Diff in %	-7.4	-3.7	-	-9.6	-4.0	0

TABLE V-V

FLOW STRESS AT $\epsilon = 0.6$ AND % DIFFERENCE FROM $\sigma_{(0.6)z}$

(a) Tensile Prestrain

		TX	TY	TZ	CX	CY	CZ
T11	ksi	17.1	17.4	20.6	20.1	20.0	19.7
	Diff in %	-17.0	-15.5	0	-2.4	-2.9	-4.4
T15	ksi	17.8	18.7	20.5	20.5	20.4	20.0
	Diff in %	-13.2	-8.8	0	0	-0.5	-2.4
T20	ksi	18.3	19.8	21.3	21.3	21.0	19.9
	Diff in %	-14.1	-7.0	0	0	-1.4	-6.6
T25	ksi	18.7	20.0	21.7	21.5	21.0	19.8
	Diff in %	-13.8	-7.8	0	-0.9	-3.2	-8.8

(b) Compressive Prestrain

C2	ksi	18.6	19.2	18.5	19.5	20.4	21.2
	Diff in %	-12.3	-9.4	-12.7	-8.0	-3.8	0
C3	ksi	18.9	19.8	18.8	20.4	20.6	21.5
	Diff in %	-12.1	-7.9	-12.6	-5.1	-4.2	0
C4	ksi	19.3	21.0	18.8	20.4	21.0	21.5
	Diff in %	-10.2	-2.3	-12.6	-5.1	-2.3	0
C5	ksi	19.9	20.9	19.2	20.5	21.3	21.7
	Diff in %	-8.3	-3.7	-11.5	-5.5	-1.8	0
C6	ksi	20.3	21.4	20.7	20.6	21.1	22.5
	Diff in %	-9.8	-4.9	-8.0	-8.4	-6.2	0
C7	ksi	20.7	22.8	21.1	21.6	21.9	22.8
	Diff in %	-9.2	0	-7.5	-5.3	-4.0	0
C8	ksi	22.3	24.3	22.4	22.0	23.0	23.9
	Diff in %	-6.7	1.6	-6.3	-8.0	-3.8	0
C10	ksi	23.5	25.2	23.5	23.3	24.5	26.0
	Diff in %	-9.6	-3.1	-9.6	-10.4	-5.8	0
C11	ksi	25.2	26.7	25.1	24.7	25.4	27.7
	Diff in %	-9.0	-3.6	-9.4	-10.8	-8.3	0
C9	ksi	27.7	29.1	-	25.5	26.3	29.5
	Diff in %	-5.4	-1.4	-	-13.6	-10.9	0

(a) In tension in the Y direction is the same;

(b) In compression in the X and Y directions is about 5% higher;

(c) In tension in the X direction is about 8% lower;

(d) In compression in the Z direction is about 10 to 20% lower.

For compressive prestrains, when compared with the yield stress for compression in the Z direction, it is found that

(a) The yield stress in tension and in compression in the X direction are up to 13% and 20% lower respectively.

(b) Except for the prestrain state C9 the tensile yield stress in the Y direction is slightly higher and the compressive yield stress in the Y direction is about the same as the yield stress in compression in the Z direction.

(c) Yield stress in tension in the Z direction is about 22% lower than the compressive stress in the same direction.

These observations are consistant with the previous remarks concerning the Bauschinger effect.

Average Flow Stress

Table V-IV shows the "average" flow stresses and the percent difference from that for strains of the same direction and sense as the prestrain. This average flow stress is the average of flow stresses at the following strains:

0.005, 0.007, 0.01, 0.02, 0.03, 0.05, 0.07, 0.1, 0.2, 0.3 and 0.5 .

This average flow stress is used in an attempt to correct for any irregularities that may be present in the stress-strain curves.

It is seen from this table that the comments on Table V-III are in general valid for Table V-IV also, except that the differences are smaller. Also, from Figures V-7 to V-63 it is seen that the variations in the flow stresses is the largest at small strains and it gradually diminishes with increasing strains to a minimum at about $\epsilon = 0.01$.

Flow Stress at $\epsilon = 0.6$

Table V-V is similar to Table V-III, except that the flow stresses are taken at $\epsilon = 0.6$. This is done to show the differences at larger strains. It is seen that the Bauschinger effect is smaller for the Z direction, and is not very consistant for the other directions. However, it may be recalled that the modified Bridgman correction factor has been used to find the flow stress at large strains. The uncertainties inherent in the correction may have affected the numerical results at $\epsilon = 0.6$.

Concluding the discussion on Figures V-2 to V-77 it may be stated as a general comment that the Bauschinger effect, defined as the difference between the tensile and the compressive flow stresses, is present at all prestrain states. It is present not only in the direction of prior loading, but also in the transverse directions. If the strain in the transverse direction is, say, tensile during prestraining, flow stress in this direction will be higher in tension than that in compression. Similarly for compressive strains. It also

appears that, in general, the flow stresses for uniaxial testing in the Y direction, the direction of smaller transverse strains, is higher than those in the X direction, the direction of larger transverse strains. It was also noticed that, in general, for the range of strain of about 0.003 to about 0.05 the highest flow stresses occur in the Y direction. In fact, the flow stresses in the Y direction in this range of strain is higher than that in the Z direction even when the tests in these two directions are both of the same sense as that of the prestrain.

Yield Stress and Strain Hardening Exponent

Cold worked materials do not, in general, show a sharp yield point. Therefore, it is necessary to define a yield strength (or stress) for the purpose of engineering application to design. A very common definition of yield strength is the flow stress at an arbitrary plastic strain, usually 0.2%. A similar definition will be used in the present investigation, with slight modification.

It is well known that when a material is strained, unloaded, and loaded again, yielding occurs at a stress lower than that originally applied. A noticeable amount of plastic deformation occurs before the previous highest stress state is reached. Since in this investigation an attempt is made to relate the subsequent properties to the previous history, it is attempted to define yield stress in such a way that when the material is reloaded in the same direction and sense, the yield stress obtained is the same as the maximum stress applied during prestraining. From Figures V-67 and V-77 and Table V-I it is found that

the flow stress at a strain of about 0.01 satisfies such conditions. Hence, the yield stress may now be defined as the flow stress at $\epsilon = 0.01$.

The stress-strain diagrams for testing in the same direction as the prestrain has an increasing slope; but it is possible to approximate certain parts of the curves by straight lines. In all other cases, there appears to be a portion of the curve that is reasonably straight. The slope of the curve gives the strain hardening exponent in that range.

Table V-VI gives the yield stress, slope m and the strength constant σ_o for the different tests, and the range of strains over which the exponential form of relation is valid. The table does not include the properties of the annealed material, as this definition of yield stress is not identical to the published values of yield strength. Also, for the annealed material, plastic flow starts at very low stress, and a relation of the form $\sigma = \sigma_o \epsilon^m$ is valid only for strains greater than $\epsilon = 0.1$, as mentioned before.

The proportional limit has also been recorded, but the scatter is very large due to the difficulty of actually deciding where on the curve it is that proportionality ceases.

Poisson's Ratio

The plastic Poisson's Ratios for the tension tests are shown in Table V-VII. In this table, $\mu_{\alpha\beta}$ means the ratio of strain in the α direction to that in the β direction when loaded uniaxially in the β direction. Since $\mu_{\alpha\beta} + \mu_{\gamma\beta} = -1$ where α, β and γ are three orthotropic directions, it is necessary to find only three independent Poisson's ratios. Since two complimentary Poisson's ratios cannot

TABLE V-VI (a)

FLOW CONSTANTS FOR TENSION TESTS IN X-DIRECTION

	Yield Stress in ksi	σ_o in ksi	m	Valid in the Range of Strain from	to	Prop. Limit in ksi	Remarks
Tensile Prestrain							
T11	12.2	13.7	0.0235	.0055	0.11	6.8	
T15	13.2	14.6	0.0219	.0055	0.15	6.0	
T20	14.3	15.7	0.0203	.0055	0.19	5.8	
T25	14.8	16.2	0.0182	.0055	0.18	4.9	
Compressive Prestrain							
C2	13.1	15.5	0.0359	.0025	0.14	9.0	
C3	13.7	15.9	0.0337	.002	0.18	10.0	
C4	14.4	16.0	0.0236	.0035	0.13	9.7	
C5	15.2	16.8	0.0213	.0035	0.14	10.0	
C6	16.0	17.9	0.0238	.0035	0.20	10.9	
C7	17.2	18.9	0.0200	.0035	0.23	9.6	
C8	18.5	20.4	0.0202	.0035	0.30	11.4	
C10	19.8	21.7	0.0192	.006	0.25	12.3	
C11	22.0	24.1	0.0153	.007	0.25	12.6	
C9	24.9	26.2	0.0091	.009	0.35	13.9	

TABLE V-VI (b)

FLOW CONSTANTS FOR TENSION TESTS IN Y-DIRECTION

	Yield Stress in ksi	σ_o in ksi	m	Valid in the Range of Strain from	to	Prop. Limit in ksi	Remarks
Tensile Prestrain							
T11	12.6	13.8	0.015	.0035	0.15	7.0	
T15	13.5	15.0	0.0197	.003	0.12	9.0	
T20	14.6	16.1	0.0218	.0035	0.14	8.0	
T25	15.4	16.4	0.0213	.0045	0.15	6.3	
Compressive Prestrain							
C2	13.4	15.0	0.0252	.0025	0.09	9.2	
C3	14.4	16.0	0.0225	.003	0.15	9.8	
C4	15.8	17.5	0.0214	.0035	0.11	10.6	
C5	16.6	18.0	0.0189	.004	0.18	12.1	
C6	17.2	18.4	0.0158	.0035	0.17	11.1	
C7	18.8	20.0	0.121	.0035	0.24	12.0	
C8	20.5	21.7	0.0133	.006	0.23	12.6	
C10	21.5	23.6	0.0197	.0045	0.32	12.9	
C11	23.6	25.6	0.0162	.007	0.21	14.6	
C9	25.7	28.1	0.0148	.009	0.4	15.5	

TABLE V-VI(c)

FLOW CONSTANTS FOR TENSION TESTS IN Z-DIRECTION

	Yield Stress in ksi	σ_o in ksi	m	Valid in the Range of Strain from	to	Prop. Limit in ksi	Remarks
Tensile Prestrain							
T11	12.8	15.7	.0393	.0016	0.06	10.0	
T15	13.2	15.7	.0342	.0020	0.05	9.7	
T20	14.4	16.7	.0308	.0020	0.05	11.2	
T25	15.5	18.0	.0303	.0025	0.07	8.2	
Compressive Prestrain							
C2	11.5	13.8	.0396	.006	0.13	5.0	
C3	12.6	15.2	.0391	.007	0.16	5.5	
C4	13.1	14.8	.0245	.010	0.15	5.8	
C5	13.9	15.9	.0259	.010	0.18	6.8	
C6	15.3	17.1	.0229	.009	0.16	6.4	
C7	16.5	18.4	.0158	.010	0.22	7.4	
C8	17.4	20.1	.0244	.016	0.28	7.4	
C10	19.4	21.4	.0098	.016	0.28	7.9	
C11	21.1	23.0	.0032	.018	0.25	9.8	

TABLE V-VI (d)

FLOW CONSTANTS FOR COMPRESSION TESTS IN X-DIRECTION

	Yield Stress in ksi	σ_o in ksi	m	Valid in the Range of Strain from	to	Prop. Limit in ksi	Remarks
Tensile Prestrain							
T11	13.2	16.1	.0438	.004	0.09	7.9	
T15	14.0	16.2	.0319	.0025	0.10	9.5	
T20	15.0	17.1	.0279	.0035	0.10	10.2	
T25	16.0	17.4	.0177	.004	0.09	10.3	
Compressive Prestrain							
C2	12.7	15.0	.036	.006	0.10	6.6	
C3	14.5	16.4	.0282	.005	0.12	7.6	
C4	14.7	16.4	.0268	.006	0.13	9.8	
C5	15.9	17.8	.248	.009	0.15	8.6	
C6	17.1	18.5	.0189	.004	0.25	10.8	Inflected
C7	18.3	19.6	.0149	.006	0.25	8.9	
C8	19.3	20.0	.0083	.008	0.27	9.0	Inflected
C10	20.5	22.0	.0102	.011	0.33	9.6	Inflected
C11	22.2	24.3	.0067	.022	0.50	9.6	Inflected
C9	24.0	26.0	.0057	.016	0.72	10.4	Inflected

TABLE V-VI (e)

FLOW CONSTANTS FOR COMPRESSION TESTS IN Y-DIRECTION

	Yield Stress in ksi	σ_o in ksi	m	Valid in the Range of Strain from	to	Prop. Limit in ksi	Remarks
Tensile Prestrain							
T11	13.3	15.3	0.0271	0.003	0.06	9.1	
T15	14.1	15.5	0.0189	0.003	0.055	9.3	
T20	15.4	16.4	0.0139	0.0035	0.07	10.0	
T25	16.0	16.8	0.0098	0.0035	0.10	10.2	
Compressive Prestrain							
C2	13.5	15.6	0.0298	0.0045	0.09	8.4	
C3	14.6	16.0	0.0214	0.004	0.08	9.0	
C4	16.2	17.4	0.0167	0.004	0.15	10.2	
C5	16.1	18.1	0.0224	0.005	0.16	7.0	
C6	16.9	18.3	0.015	0.008	0.14	9.3	
C7	19.3	20.1	0.012	0.006	0.30	10.8	Inflected
C8	20.5	21.3	0.0084	0.005	0.30	11.0	
C10	22.2	23.5	0.0102	0.009	0.45	10.4	Inflected
C11	24.4	25.0	0.003	0.011	0.55	10.8	Inflected
C9	26.0	26.7	0.002	0.011	0.75	11.4	Inflected

TABLE V-VI (f)

FLOW CONSTANTS FOR COMPRESSION TESTS IN Z-DIRECTION

	Yield Stress in ksi	σ_o in ksi	m	Valid in the Range of Strain from	to	Prop. Limit	Remarks
Tensile Prestrain							
T11	11.9	14.0	0.0376	0.008	0.12	5.2	
T15	13.0	14.3	0.0206	0.007	0.14	7.4	
T20	14.0	15.1	0.0184	0.007	0.20	7.0	
T25	14.2	15.4	0.0130	0.010	0.18	6.2	
Compressive Prestrain							
C2	13.4	17.0	0.0516	0.0015	0.08	9.6	
C3	14.1	17.6	0.0461	0.0016	0.07	9.8	
C4	15.1	18.0	0.0385	0.0017	0.08	10.4	
C5	15.6	18.2	0.0317	0.0025	0.11	11.0	
C6	16.8	18.9	0.0259	0.0030	0.11	12.0	
C7	18.2	20.2	0.0241	0.0037	0.13	13.7	
C8	19.6	21.8	0.0230	0.0040	0.16	13.0	
C10	22.0	24.5	0.0230	0.0070	0.25	15.0	
C11	24.1	27.0	0.0230	0.0080	0.30	16.2	
C9	26.5	28.0	0.0107	-	0.25	-	

TABLE V-VII

PLASTIC POISSON'S RATIOS*

	μ_{xy}	μ_{zy}	μ_{yz}	μ_{xz}	μ_{zx}	μ_{yx}	μ_{xy}(calculated)
Tensile Prestrain							
T11	0.71	0.29	0.38	0.62	0.50	0.50	0.620
T15	0.62	0.38	0.40	0.60	0.50	0.50	0.600
T20	0.57	0.43	0.42	0.58	0.52	0.48	0.580
T25	0.63	0.37	0.42	0.58	0.50	0.50	0.580
Compressive Prestrain							
C2	0.66	0.34	0.35	0.65	0.48	0.52	0.619
C3	0.65	0.35	0.39	0.61	0.43	0.57	0.665
C4	0.64	0.36	0.395	0.605	0.42	0.58	0.675
C5	0.62	0.38	0.39	0.61	0.375	0.625	0.715
C6	0.60	0.40	0.35	0.65	0.45	0.55	0.643
C7	0.55	0.45	0.41	0.59	0.56	0.44	0.541
C8	0.52	0.48	0.42	0.58	0.56	0.44	0.541
C10	0.52	0.48	0.37	0.63	0.59	0.41	0.510
C11	0.52	0.48	0.39	0.61	0.65	0.35	0.447
C9	0.55	0.45	-	-	0.58	0.42	0.521

* The sign of Poisson's Ratios are always negative.

TABLE V-VIII

YIELD STRESS IN PLANE STRAIN TESTS
STRESS IN KSI

Specimen	SXY	SZY	SYZ	SXZ	SZX	SYX
Tensile Prestrain						
T11	14.7	14.1	14.4	15.8	13.5	13.5
T15	16.0	14.8	14.7	18.1	14.5	14.4
T20	17.0	16.1	16.5	17.5	15.6	15.5
T25	17.6	16.5	17.3	18.5	16.5	16.6
Compressive Prestrain						
C2	15.3	14.5	13.5	14.8	14.0	14.8
C3	17.0	15.7	14.7	15.0	15.5	16.1
C4	17.2	16.7	15.1	16.8	16.7	16.2
C5	18.2	18.0	16.5	17.6	17.8	17.2
C6	19.1	18.4	17.4	17.4	18.0	18.4
C7	21.6	20.1	19.2	20.9	19.3	19.8
C8	23.1	21.6	19.7	21.0	20.7	21.2
C10	25.5	24.2	22.7	24.9	23.6	22.3
C11	27.0	25.7	24.1	24.9	25.0	24.7

both be exponential functions of prestrain, it is assumed that they are polynomial functions of prestrain. For compressive prestrains, it was found by inspection of Table V-VII that the values of μ_{xz} is approximately a constant of value 0.6. Hence, it was necessary to find only two other Poisson's ratios, viz. μ_{xy} and μ_{yx} as functions of prestrain. Similarly, it was found that for tensile prestrain, $\mu_{zx} = \mu_{yx} = -0.5$. Hence, it was necessary to find only μ_{xy} and μ_{xz}. However, the Poisson's ratios must satisfy the relation

$$\frac{\mu_{xy}\mu_{yz}\mu_{zx}}{\mu_{yx}\mu_{zy}\mu_{xz}} = 1 \qquad \text{(V-1)}$$

This relation has been derived in Appendix A.

For tensile prestrains, we have,

$$\mu_{zy} = -1-\mu_{xy}$$

$$\mu_{yz} = -1-\mu_{xz}$$

and $$\mu_{zx} = \mu_{yx} = -0.50 \ .$$

Substituting these in Equation (V-1), we have

$$\mu_{xy}(-1-\mu_{xz}) = \mu_{xz}(-1-\mu_{xy})$$

or

$$\mu_{xy} = \mu_{xz}$$

Similarly, for compressive prestrains, we have

$$\mu_{zy} = -1-\mu_{xy}$$

$$\mu_{zx} = -1-\mu_{yx}$$

$$\mu_{xz} = -0.60$$

$$\mu_{yz} = -1-\mu_{xz} = -0.40$$

Substituting in Equation (V-1) we have,

$$-0.4\ \mu_{xy}(-1-\mu_{yx}) = -0.6\ \mu_{yx}(-1-\mu_{xy})$$

or $$\mu_{xy}(1 + \mu_{yx}) = 1.5\ \mu_{yx} + 1.5\ \mu_{xy}\mu_{yx}$$

or $$\mu_{xy}(1 - 0.5\ \mu_{yx}) = 1.5\ \mu_{yx}$$

or $$\mu_{xy} = \frac{1.5\ \mu_{yx}}{1 - 0.5\ \mu_{yx}} = \frac{3\ \mu_{yx}}{2 - \mu_{yx}} \qquad \text{(V-2)}$$

The last column of Table V-VII shows the calculated values of μ_{xy}. The calculated and experimental values of μ_{xy} are plotted against prestrain in Figure V-78. Although the plot shows considerable scatter of data, a trend curve was drawn to relate μ_{xy} with tensile and compressive prestrains.

Figures V-79 to V-82 show the yield stresses plotted against prestrain in tension and in compression on log-log co-ordinates.

Table V-VIII shows the yield stresses obtained in the plain strain tests, and in Figures V-83 and V-84 they are shown plotted on log-log co-ordinates.

The data from Figures V-79 to V-84 were used to draw the traces of the yield surfaces on the π plane for different prestrain states. The procedure for this construction is shown in Appendix B. Figures V-85 and V-86 show the yield surfaces thus obtained for tensile and compressive prestrains respectively. The stress scale has been shown $\frac{\sqrt{3}}{\sqrt{2}}$ times the actual on the π plane so that the values of stresses along the stress axes can be read directly off the diagram.

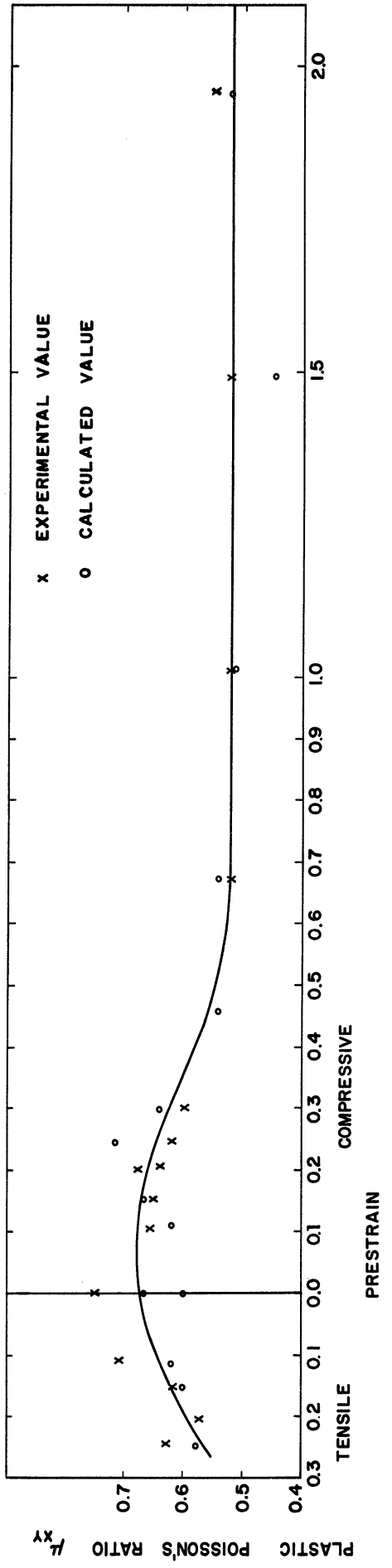

Figure V-78. Variation of Plastic Poisson's Ratio with Prestrain.

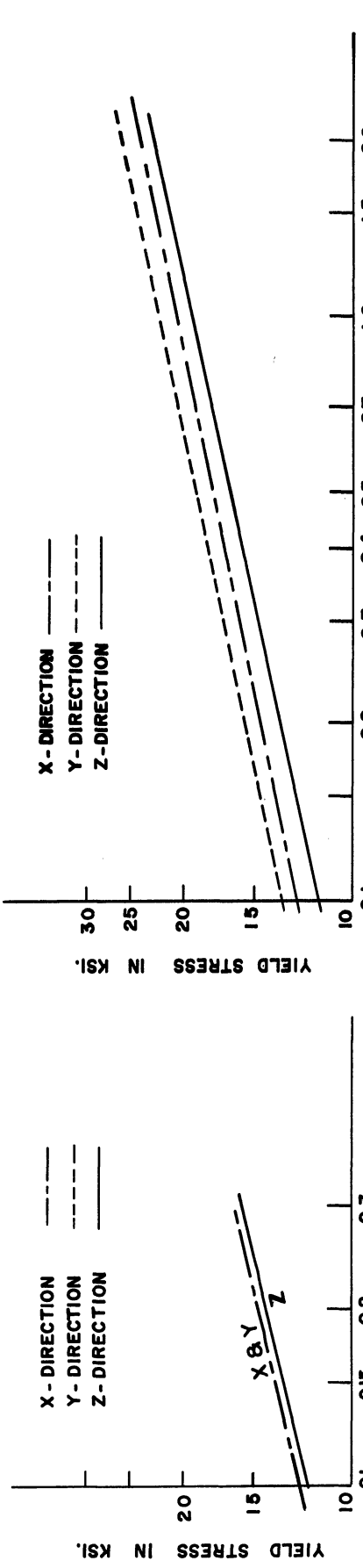

Figure V-79. Yield Stress in Tension After Tensile Prestrain.

Figure V-81. Yield Stress in Tension After Compressive Prestrain.

Figure V-80. Yield Stress in Compression After Tensile Prestrain.

Figure V-82. Yield Stress in Compression After Compressive Prestrain.

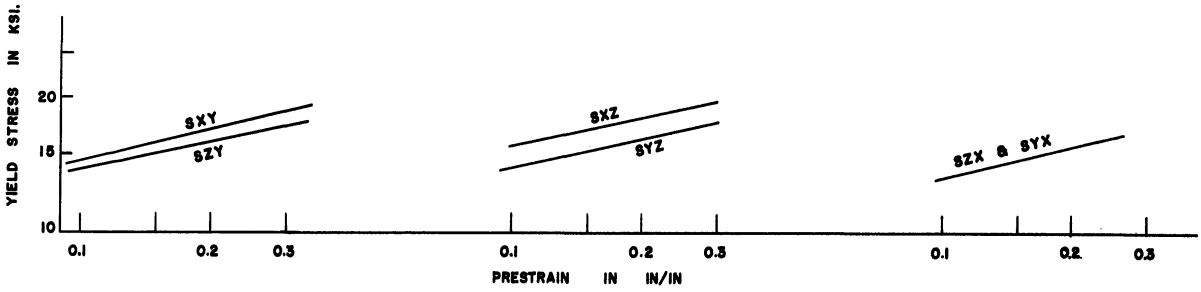

Figure V-83. Yield Stress in Plane Strain Test After Prestraining in Tension.

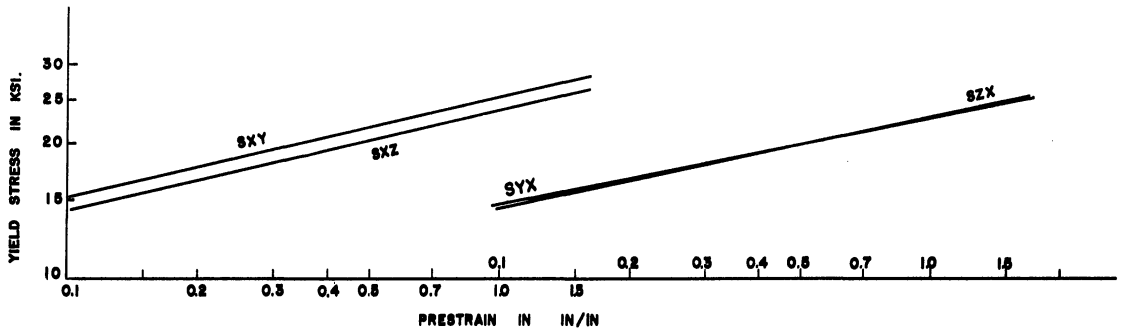

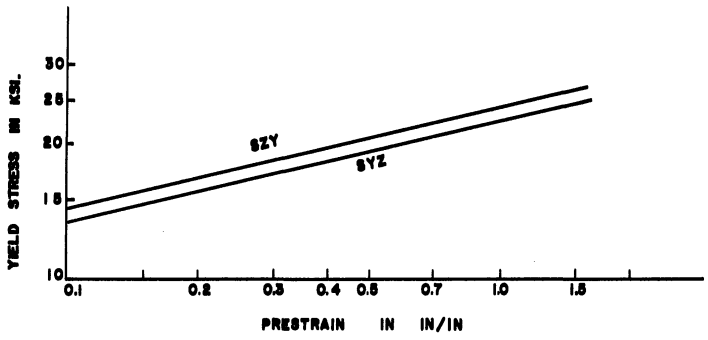

Figure V-84. Yield Stress in Plane Strain Test After Prestraining in Compression.

In Figure V-85 it is seen that with the increase of tensile prestrain the yield surface increases in size, i.e., strengthening occurs in all directions. The yield surface is not symmetrical about the normal to the π plane passing through the origin. Since the material was prestrained in tension in the Z direction, yield stress in compression in the Z direction is lesser than that in tension in the same direction, and the geometrical centers of the traces of yield surfaces is offset in the direction of tension in the Z direction by about 1/2 to 1-1/2 ksi. Since the shape of all the curves are closely similar, it appears that although a certain amount of kinemetric hardening occurred at the early stages of prestraining, at prestrains less than 0.1, subsequent hardening is primarily isotropic.

Figure V-86 shows yield surfaces for compressive prestrains. Similar comments as for Figure V-85 can be made in this case too.

It is apparent from Figures V-86 and V-86 that the yield criterion for cold worked aluminum is not satisfactorily described either by Tresca criterion, or by von Mises criterion. However, a corner seems to develop gradually at the loading point with increasing compressive prestrains, similar to what may be predicted by slip theory, but since the surfaces expand also, a combined effect of kinematic, isotropic and slip mechanisms of hardening seems likely at higher prestrains.

Residual Ductility

Of all the mechanical properties of materials, ductility shows the widest range of scatter, and the present investigation is

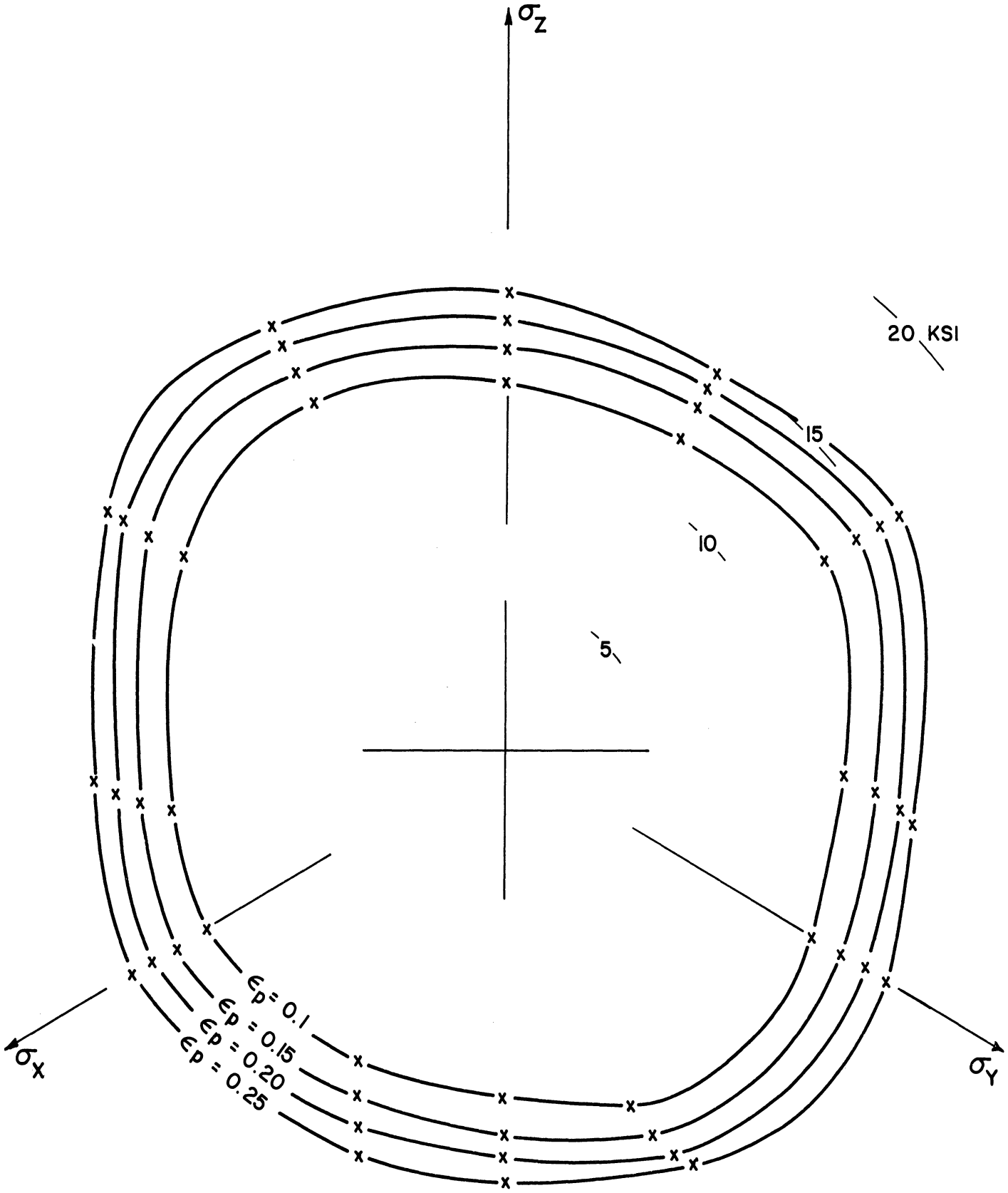

Figure V-85. Yield Surfaces for 1100 Aluminum Alloy After Tensile Prestrains.

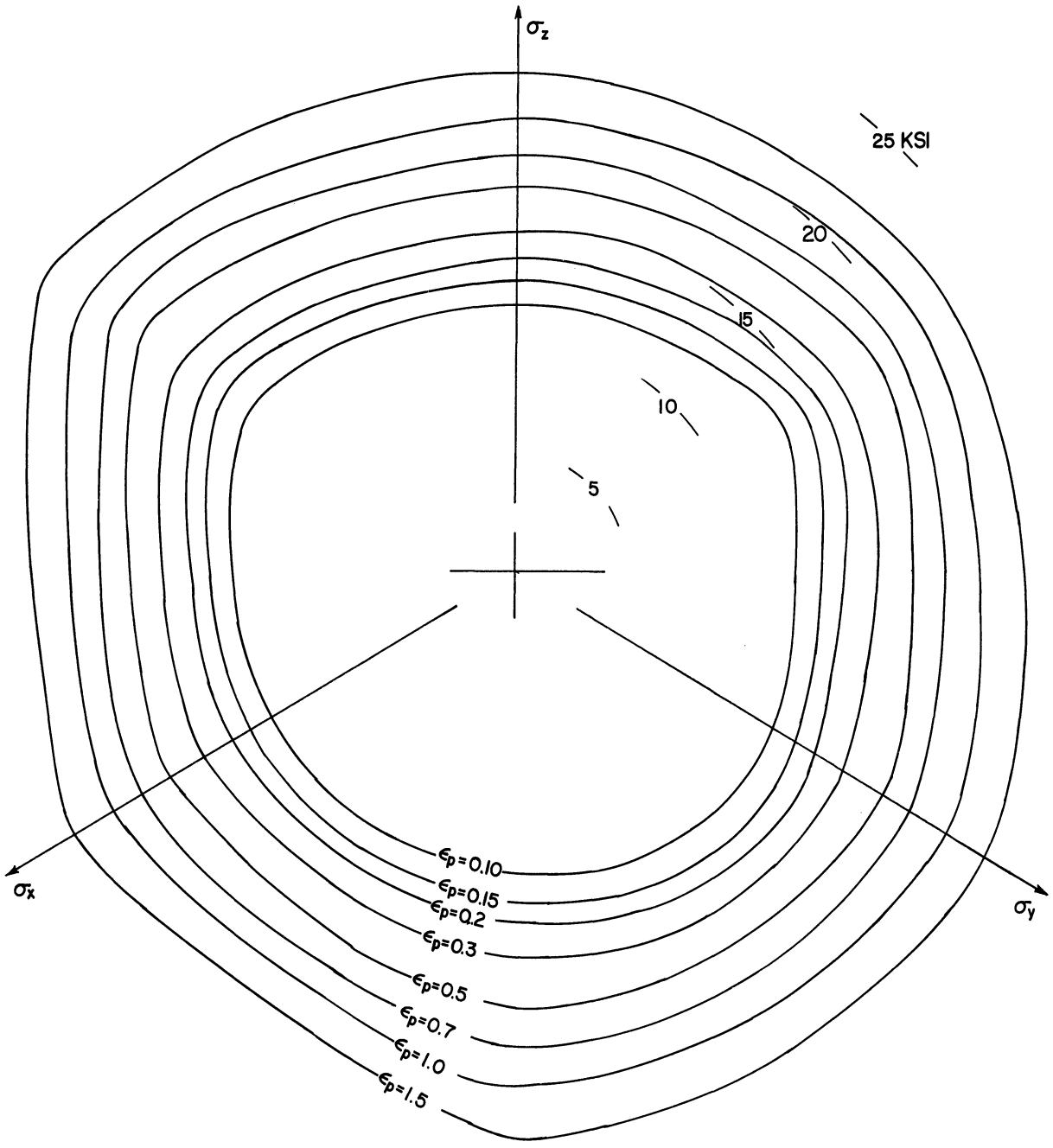

Figure V-86. Yield Surfaces for 1100 Aluminum Alloy After Compressive Prestrains.

no exception. The fracture strains in two transverse directions and the longitudinal strain at fracture for different prestrain states are tabulated in Table V-IX.

Assuming that the ductility of an annealed material is constant, and since a tension test in the Z direction is merely a continuation of the previous tensile prestrain, it is expected that we should find

$$\epsilon_p + \epsilon_d = \text{Const.}$$

where ϵ_p is the prestrain in tension, and ϵ_d the residual ductility for tension test in the Z direction. If ductility is plotted against prestrain in Cartesian co-ordinates, this relation will appear as a straight line. Therefore, although such a simple relation is not likely to be found for compressive prestrains, residual ductility for tension tests in X, Y and Z directions were plotted against prestrains in Cartesian co-ordinates in Figures V-87, V-88 and V-89 respectively. It is observed from these diagrams that the highest ductility in the X and Y directions are found in the annealed condition of the material. For testing in the Y direction, ductility falls off rather rapidly with increase in prestrain of either kind, but the curve seems to level off for compressive prestrains above 0.4. For testing in the X direction, ductility decreases almost uniformly for tension as well as in compression, the curve being steeper for tensile prestrains.

For testing in the Z direction, the slope of the curve for tensile prestrain is unity as is expected. With increasing compressive

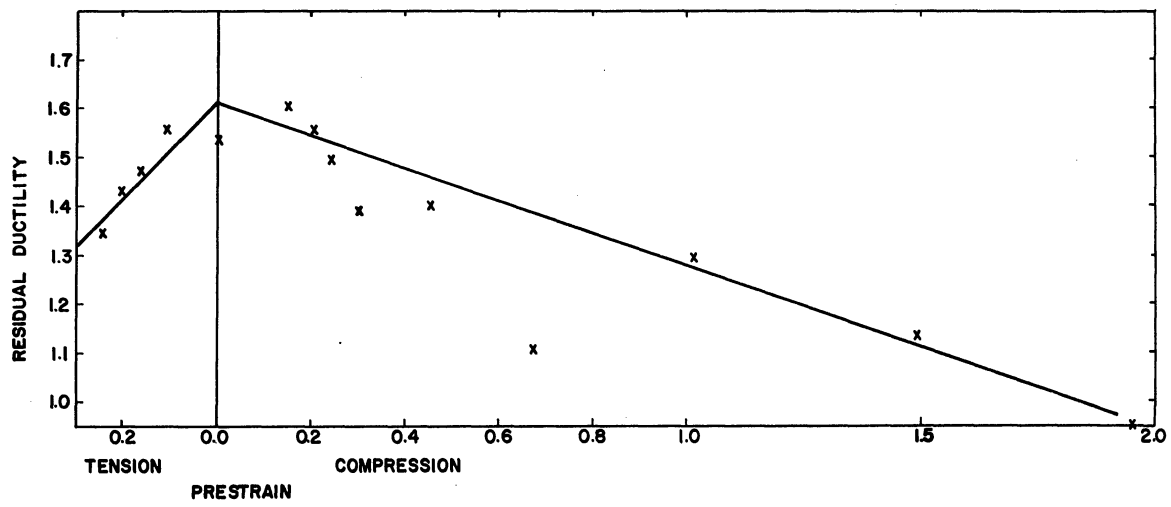

Figure V-87. Residual Ductility for Tension Test in the X Direction.

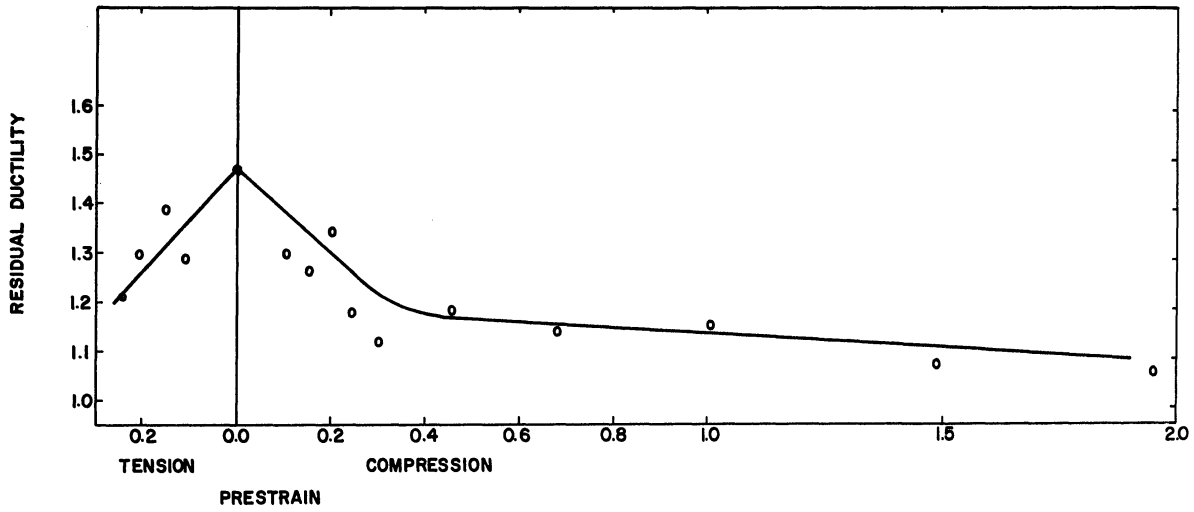

Figure V-88. Residual Ductility for Tension Test in the Y Direction.

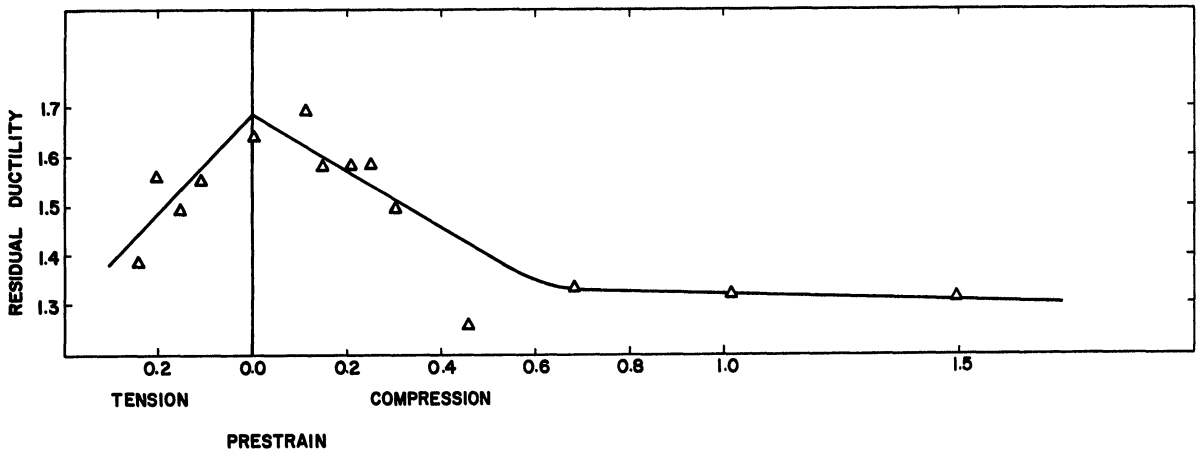

Figure V-89. Residual Ductility for Tension Test in the Z Direction.

TABLE V-IX

RESIDUAL DUCTILITY IN TENSION
TESTS SUBSEQUENT TO PRESTRAINING
(Av. of Two Tests)

Prestrain State	Direction of Testing	ϵ_x	ϵ_y	ϵ_z*
	X	1.530	1.009	0.521
Annealed	Y	1.092	1.466	0.374
	Z	0.959	0.681	1.640
T 11	X	1.558	0.999	0.559
(ϵ_p = 0.1098)	Y	0.891	1.285	0.394
	Z	0.925	0.637	1.562
T 15	X	1.476	0.991	0.485
(ϵ_p = 0.152)	Y	1.005	1.385	0.380
	Z	0.830	0.671	1.501
T 20	X	1.433	0.928	0.505
(ϵ_p = 0.206)	Y	0.869	1.289	0.420
	Z	0.857	0.701	1.558
T 25	X	1.351	0.826	0.525
(ϵ_p = 0.245)	Y	0.856	1.209	0.353
	Z	0.774	0.615	1.389
C 2	X	1.570	0.905	0.665
(ϵ_p = 0.106)	Y	0.873	1.289	0.416
	Z	1.027	0.668	1.695
C 3	X	1.606	0.944	0.662
(ϵ_p = 0.1494)	Y	0.850	1.266	0.416
	Z	0.947	0.636	1.583
C 4	X	1.553	0.863	0.690
(ϵ_p = 0.204	Y	0.931	1.346	0.415
	Z	0.907	0.677	1.584

TABLE V-IX (CONT'D)

Prestrain State	Direction of Testing	ϵ_x	ϵ_y	ϵ_z*
C 5	X	1.495	0.782	0.713
(ϵ_p = 0.244)	Y	0.720	1.182	0.462
	Z	0.932	0.650	1.582
C 6	X	1.389	0.735	0.654
(ϵ_p = 0.300))	Y	0.684	1.120	0.436
	Z	0.916	0.590	1.506
C 7	X	1.401	0.618	0.783
(ϵ_p = 0.455)	Y	0.739	1.174	0.435
	Z	0.838	0.421	1.259
C 8	X	1.105	0.480	0.625
(ϵ_p = 0.673)	Y	0.704	1.141	0.437
	Z	0.849	0.489	1.338
C 9	X	0.950	0.480	0.470
(ϵ_p = 1.953)	Y	0.547	1.053	0.506
	Z	-	-	-
C 10	X	1.290	0.554	0.736
(ϵ_p = 1.01)	Y	0.592	1.147	0.555
	Z	0.829	0.492	1.321
C 11	X	1.130	0.470	0.660
(ϵ_p = 1.49)	Y	0.523	1.074	0.551
	Z	0.790	0.526	1.316

*ϵ_x, ϵ_y and ϵ_z are the strains in the X, Y and Z directions respectively at fracture.

prestrain the residual ductility is reduced and the curve levels off at prestrains of about 0.7.

It is also noticed that the material has maximum ductility for tension tests in the annealed condition in the Z direction. This is as expected since commercial bars and plates, regardless of whether they are hot or cold rolled, have the inclusions elongated in the direction of rolling and consequently the ductility in the transverse direction is in general much lower than that in the longitudinal direction.

Limitations of the Present Investigation

Certain assumptions, tacit or expressed, are always part of experimental investigations. Some such assumptions made for this investigation are critically examined below.

(a) Continuity of Medium. This assumption is made in the treatment of certain branches of science, such as hydrodynamics. Even without going down to the atomic level, this assumption is not strictly valid for metals of commercial preparation and fabrication, since microdiscontinuities, cracks, inclusions, etc. are always present. They can easily be discerned under a microscope after polishing and etching.

(b) Homogeneity. Metals in general are not microscopically homogeneous, but their elastic and plastic properties are usually averaged out over macroscopic dimensions, at least for the annealed material. But in the cold worked condition of a material even macroscopic homogeneity is questionable. Figure V-90 shows[73] hardness

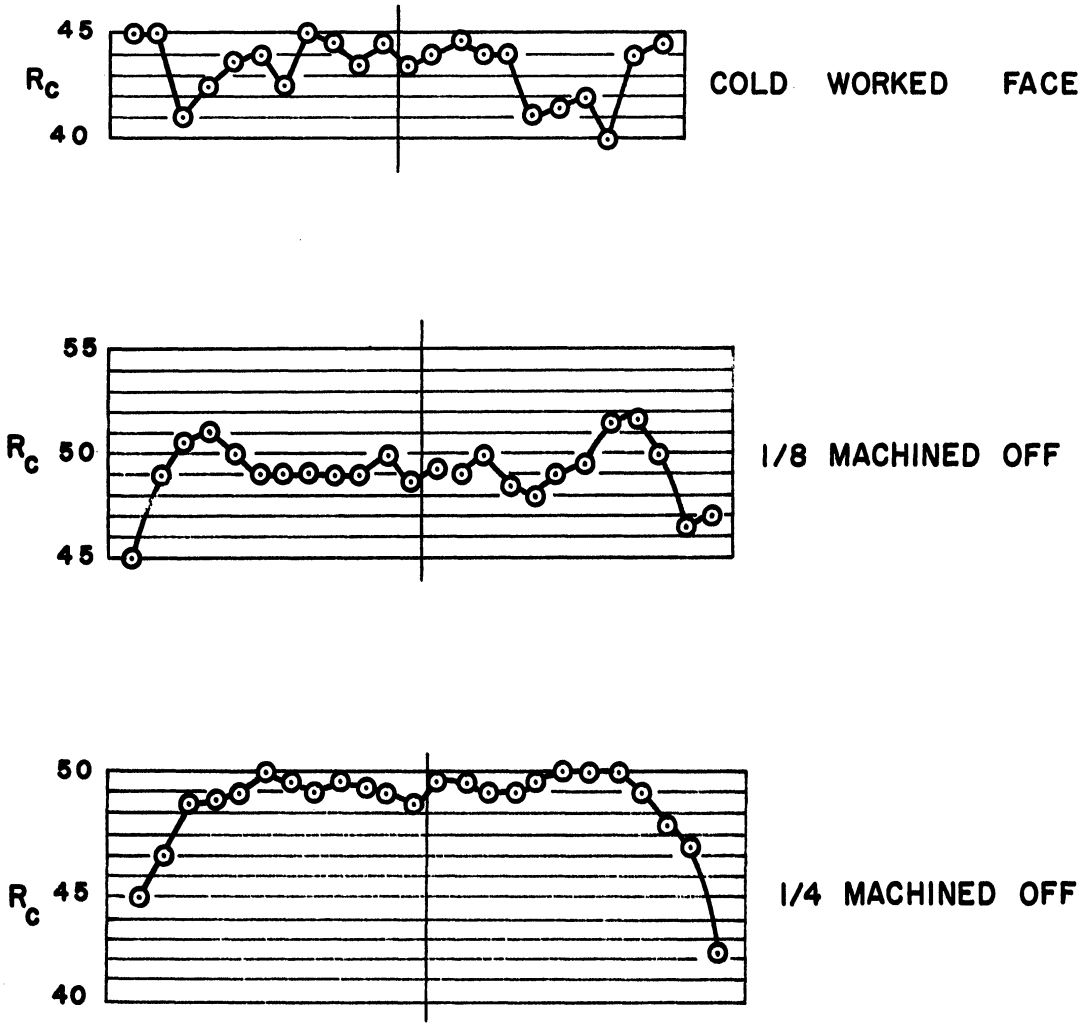

Figure V-90. Hardness Traverse Along the Diameter of a Cold Worked High Strength Steel Cylinder.

traverses across the diameter of a high strength alloy deformed by compression from an annealed state. The traverses are for different depths from one end of the block. The periodicity of the hardness values is obvious. Since the strength of a given material is directly related to its hardness, it is obvious that the deformation has not been uniform although barrelling was kept to a minimum by proper lubrication.

(c) Time Dependence. Although all the tests were carried out at very low speeds - about 0.050 inch per minute head speed - the strain rate was not uniform since the deforming lengths were not the same. The effect of strain rate, therefore, was small but not absent. Also, 1100-0 aluminum alloy is known to creep while sustaining a load. The effect of creep was, however, very small compared to the large strains to which the material was subjected and hence it was ignored.

CHAPTER VI

CONCLUSIONS

From the previous analysis of the data obtained in this investigation the following conclusions can be made concerning the strain hardening characteristics of annealed, hot rolled commercially pure aluminum. These same conclusions, for the most part should be applicable to any single phase solid solution of a metal having a cubic latice structure. The conclusions are divided into four groups as below:

A. General Properties Determined by Processing History

1. In the annealed state such a material is approximately isotropic in strength properties, but not necessarily in strains.
2. The material is orthotropic and one of the axes of orthotropy being the axial direction.

B. Expected Results and Conclusions of Previous Investigations Confirmed

1. Stress-strain relations for all states of prestrain and direction of testing can be expressed by an exponential type relation, $\sigma = \sigma_o \epsilon^m$, over certain ranges of strain.
2. The value of the constant σ_o increases with increasing prestrain for any given kind of testing in a given direction.
3. The exponent m decreases with increasing prestrain.

4. Ductility in all the directions is a maximum at the annealed state of the material and decreases with increasing prestrain, both tensile and compressive.
5. Ductility in the transverse direction is lower than that in the axial direction.

C. Conclusions in Variance with Current Concepts

1. Strains produced by loading consecutively in two directions are not additive. For large strains the concept of "effective strain" seems to be questionable.
2. Flow stress for testing in the opposite sense to that of the prestrain is always lower than that in the same sense and direction as the prestrain; the difference is about 5 to 20%. The Bauschinger effect, defined as reduction of flow stress on reversal of the sense of loading, is present for all prestrain states.
3. When stressed along the axial direction, the resultant strain hardening affects the flow properties in all the directions essentially the same way. In other words, the strain hardening is primarily isotropic, with a small kinematic component of 1 to 1-1/2 ksi superimposed on it. This is in contradiction to the kinematic hardening theory which does not seem to be valid for large prestrains as occurs in the present investigation.

D. Further Observations and Conclusions

1. The range of strain over which the exponential type of relation is valid increases with increasing pre-strain.

2. The direction of smaller transverse strain appears to have higher flow stress properties than the direction of larger transverse strain. In fact, it is found that the transverse yield strength in the direction of the smaller prestrain is up to 5% higher than the longitudinal yield strength in the direction and sense of the prestrain. This is rather different from what one would expect since the strains obtained in the two transverse directions are different in sense from that in the direction of loading.

3. When tested in axial compression after axial tensile prestrain, the stress-strain curves appear to converge to that of the annealed material for subsequent strains greater than 0.25. In other words, the effect of previous prestrain is removed after a certain reversed strain in this case.

4. (a) When tested in compression in a transverse direction after an axial compressive prestrain of about 0.4 the material shows a yield point phenomenon similar to that of annealed low carbon steels. The stress-strain curve reaches a maximum of stress, and then a slight strain softening is noticed.

(b) The amount of strain softening increases with increasing prestrain, being a fraction of a ksi at about $\epsilon = 0.4$ and about 1 ksi or about 4% for $\epsilon = 2.0$.

5. The Bauschinger effect is present not only in the direction of prestrain, but also in the transverse directions. During prestraining, if the transverse strain in a certain direction is, say, tensile, then the flow stress in tension in that direction is higher than that in compression. Similarly for compressive strains.

6. The greatest amount of directionality in flow stress is found at small plastic strains where the elastic and plastic strains are of comparable magnitude.

APPENDIX A

RELATIONSHIP BETWEEN POISSON'S RATIOS

According to Hill's theory for anisotropic flow, plastic strain increments for multiaxial loading are given by Equation (III-1). When the principal directions of stresses coincide with the axes of orthotropy, the coefficients L, M and N do not appear in the equations, since τ's and γ's are all identically zero.

For uniaxial loading in the X direction,

$$(d\epsilon_x) = (d\lambda)(H + G)\,\sigma_x$$

$$(d\epsilon_y) = -(d\lambda)\,H\,\sigma_x$$

and

$$(d\epsilon_z) = -(d\lambda)\,G\,\sigma_x$$

Therefore

$$\mu_{yx} = \frac{(d\epsilon_y)}{(d\epsilon_x)} = \frac{-H}{(H + G)}$$

$$\mu_{zx} = \frac{(d\epsilon_z)}{(d\epsilon_x)} = \frac{-G}{(H + G)}$$

where $\mu_{\alpha\beta}$ is the plastic Poisson's ratio in the α direction for loading in the β direction. Similarly, it can be shown that,

$$\mu_{xy} = \frac{-H}{(F + H)}$$

$$\mu_{zy} = \frac{-F}{(F + H)}$$

$$\mu_{xz} = \frac{-G}{(G + F)}$$

and $$\mu_{yz} = \frac{-F}{(G + F)}$$

Hence, we have

$$\frac{\mu_{xy}\mu_{yz}\mu_{zx}}{\mu_{yx}\mu_{zy}\mu_{xz}} = \frac{\frac{-H}{(F + H)} \times \frac{-F}{(G + F)} \times \frac{-G}{(H + G)}}{\frac{-H}{(H + G)} \times \frac{-F}{(F + H)} \times \frac{-G}{(G + F)}} = 1$$

APPENDIX B

CONSTRUCTION OF YIELD SURFACE

It is assumed, and to a close approximation it is true, that the yield criterion for metals is independent of superimposed hydrostatic stress of arbitrary magnitude. A consequence of this postulate is that the yield surface is a cylinder of infinite length, its generator being equally inclined to the axes of stress space. Hence, a plane equally inclined to the axes will be normal to the generator of the yield surface and the yield surface is completely defined by the trace of the yield surface on such a plane. Such a plane passing through the origin of the co-ordinate axes is known as the π plane. The projection of the three stress axes on the π plane make 120° with each other as shown in Figure A-1. It can be readily shown that the projection of a point in stress space with co-ordinates $\sigma_{\alpha\alpha}$, $\sigma_{\beta\beta}$ and $\sigma_{\gamma\gamma}$ is given by

$$x = \frac{\sigma_{\alpha\alpha} - \sigma_{\gamma\gamma}}{\sqrt{2}} \quad ; \quad y = \frac{2\sigma_{\beta\beta} - \sigma_{\gamma\gamma} - \sigma_{\alpha\alpha}}{\sqrt{6}}$$

on the π plane, x and y being two co-ordinates on the π plane as shown in Figure A-1.

In the case of plane strain tests, if $\sigma_{\beta\beta}$ is the applied principal stress in the β direction, then the principal stress in the α direction for zero principal strain in that direction is $-\mu_{\alpha\beta}\sigma_{\beta\beta}$, the third principal stress being zero. $\mu_{\alpha\beta}$ is the plastic Poisson's ratio in the α direction for loading in the β direction.

Knowing the values of $\mu_{\alpha\beta}$ and $\sigma_{\beta\beta}$, the stress point can be shown on the π plane.

In practice it is more convenient to use a geometrical construction as shown in Figure A-2. OB represents $\frac{\sqrt{2}}{\sqrt{3}}\sigma_{\beta\beta}$ and BA is drawn parallel to $\sigma_{\alpha\alpha}$-axis. The point X is such that $\frac{BX}{OB} = -\mu_{\alpha\beta}$. The point X shows the projection of the point representing the stress state for the plane strain test on the π plane.

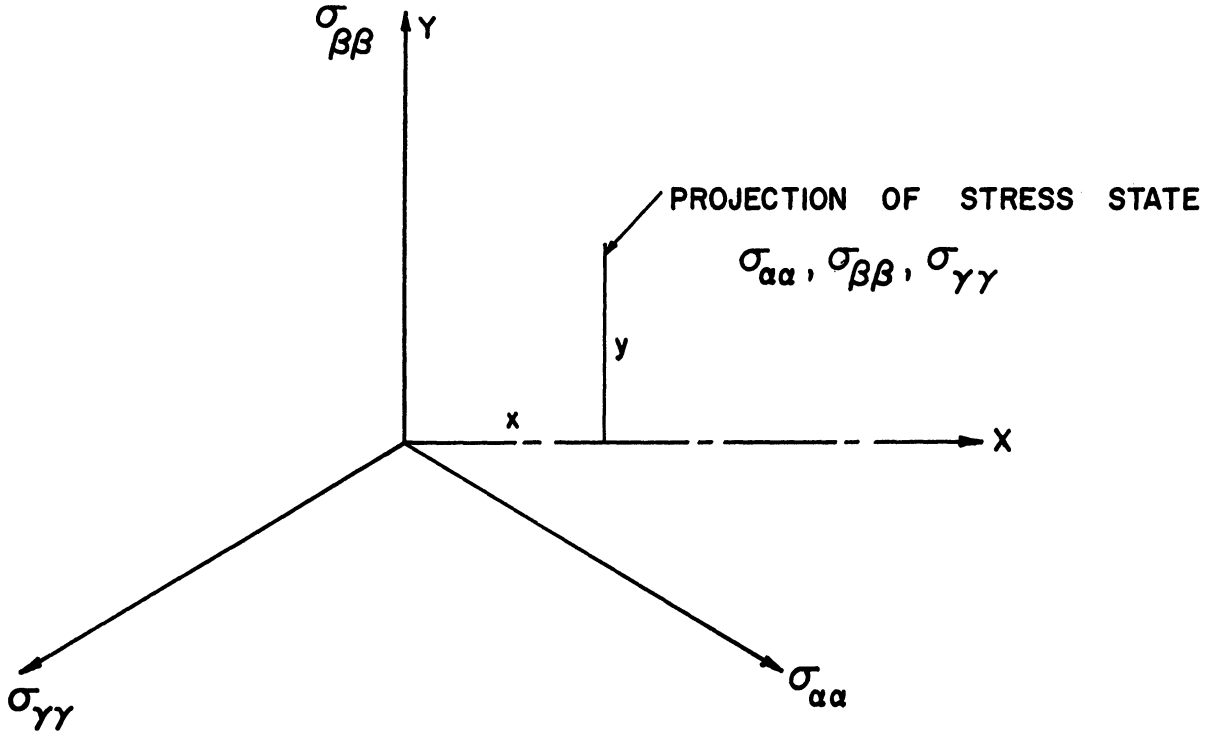

Figure A-1. Co-ordinate Directions on π Plane.

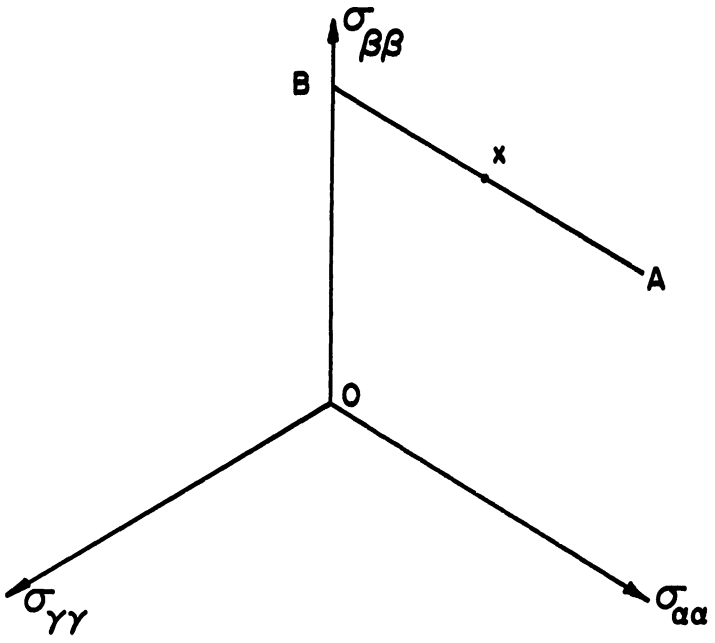

Figure A-2. Construction of Yield Surface.

BIBLIOGRAPHY

1. Haythornthwaite, R. M. "Range of Yield Condition in Ideal Plasticity," Journal of the Engineering Mechanics Division, No. E. M. 6, Proc. Am. Soc. Civil Engineers, 87 (1961) 117-133.

2. Hill, R. "The Mathematical Theory of Plasticity," Oxford Univ. Press, 1960.

3. Taylor, G. I., and Quinney, H. "The Plastic Distortion of Metals," Phil. Trans., Royal Society, (London) 230A (1931) 323-362.

4. Drucker, D. C. "The Significance of the Criterion for Additional Plastic Deformation," Journal of Colloid Science (Rheology Issue) 4, 3 (1949) 299-311.

5. Marin, J., and Wiseman, H. A. B. "Plastic Stress-Strain Relations for Combined Tension and Compression," NACA TN 2737, July 1952.

6. Prager, W. "The Theory of Plasticity, A Survey of Recent Achievements (James Clayton Lecture)," Proceedings, Inst. Mech. Engineers, 169 (1955) 41.

7. Prager, W. "A New Method of Analyzing Stresses and Strains in Work-Hardening Plastic Solids," Journal of Applied Mechanics, 23 (1956) 493-496.

8. Hodge, P. G. Jr. "Piecewise Linear Plasticity," Proc. 9th Inst. Congress of App. Mech., Brussels, Sept. 1956.

9. Hodge, P. G. Jr. "A General Theory of Piecewise Linear Plasticity Based on Maximum Shear," Journal of Mechanics and Physics of Solids, 5 (1957) 242-260.

10. Batdorf, S. B., and Budiansky, B. "A Mathematical Theory of Plasticity Based on the Concept of Slip," NACA TN 1871, April 1949.

11. Batdorf, S. B., and Budiansky, B. "Polyaxial Stress-Strain Relations of a Strain Hardening Metal," Journal of Applied Mechanics, (December 1954) 323-326.

12. Phillips, A. "Combined Tension and Torsion Tests for Aluminum Alloy 2S-0," Journal of App. Mech., 19 (1952) 496-500.

13. Zaitsev, G. P. "A Single Equation for the Plastic Extension of Metals," Fiz. Metal Metallov., 11, 6 (1961) 910-918.

14. Hollomon, J. H., and Lubahn, J. D. "The Flow of Metals at Elevated Temperatures," General Electric Review, Feb.-Apr. 1947.

15. Jackson, L. R. "Work Hardening and Rupture in Metals," Trans. Am. Inst. Mining and Met. Engr., 171 (1947) 622-638.

16. Hollomon, J. H. "Tensile Deformation," Trans. Am. Inst. Mining and Met. Engrs., 161 (1945) 268.

17. Hill, R. "A Theory of the Yielding and Plastic Flow of Anisotropic Metals," Proc. Royal Society (London) 193A (1948) 281-297.

18. Jackson, L. R., Smith, K. F., and Lankford, W. T. Plastic Flow in Anisotropic Sheet Steel, Metals Technology, Tech. Pub. No. 2440 (1948).

19. Dorn, J. E. "Stress-Strain Rate Relations for Anisotropic Plastic Flow," Journal of Applied Physics, 20 (1949) 15-20.

20. van Bueren, H. G. Imperfections in Crystals, North Holland Publishing Company, Amsterdam (1961) 148.

21. Mott, N. F. "A Theory of Work Hardening of Metal Crystals," Philosophical Magazine, 43 (1952) 1151-1178.

22. Washburn, J. "Strain Hardening," Strengthening Mechanisms in Solids, Am. Soc. Metals, (1960) 51-77.

23. Snowden, K. U. "Dislocation Arrangements and Work Hardening in Aluminum Crystals Deformed by Cyclic Strain," Acta Metallurgica, 11, 1963.

24. Swift, H. W. "Plastic Strain in Isotropic Strain Hardening Material," Engineering, 162, p. 381.

25. Sachs, G. "Some Observations on the Forging of Strong Aluminum Alloys," Journal of Institute of Metals, 64 (1939) 261-283.

26. Naghdi, P. M., Essenburg, R., and Koff, W. "An Experimental Study of Initial and Subsequent Yield Surfaces in Plasticity," Journal of Applied Mech., (June 1958) 201-209.

27. Stowell, E. Z., and Pride, R. A. "Poisson's Ratios and Volume Changes for Plastically Orthotropic Material," NACA TN 3736.

28. Klinger, L. J., and Sachs, G. "Dependence of the Stress-Strain Curves of Cold Worked Metals Upon the Testing Direction," Journal of the Aeronautical Sciences, (March 1948) 151-154.

29. Klinger, L. J., and Sachs, G. "Plastic Flow Characteristics of Aluminum-Alloy Plate," Journal of the Aeronautical Sciences, (October 1948) 599-604.

30. Klinger, L. J., and Sachs, G. "Fracturing Characteristics of Aluminum-Alloy Plate," Journal of the Aeronautical Sciences, (December 1948) 731-734.

31. Phillips, A., and Dunkle, H. H. "Directional Properties in Rolled and Annealed Low Carbon Steel," Transactions Am. Soc. Metals, 23 (1935) 398-408.

32. Mehringer, F. J., and McGregor, C. W. "Effects of Cold Rolling on the True Stress-Strain Properties of a Low Carbon Steel," Metals Technology, TP 1849, Sept. 1945.

33. Goss, N. P. "Hot Working, Cold Working and Recrystallization Structure," Trans. Am. Soc. Metals, 24 (1936) 967-1036.

34. Backofen, W. A., Hosford, W. F. Jr., Burke, J. J. "Texture Hardening," Trans. Am. Soc. Metals, 55 (1962) 264-267.

35. Lin, T. H., and Lieb, B. "Rotation of Crystals Under Axial Strain," Journal of Mech. of Phy. of Solids, 10 (1962) 65-72.

36. Whiteley, R. L. "The Importance of Directionality in Drawing Quality Sheet Steel," Trans. Am. Soc. Metals, 52 (1960) 154-169.

37. Hill, R. "A Theory of Yielding and Plastic Flow of Anisotropic Metals," Proc. Royal Society (London), 193, Series A, (1948) 281.

38. Hazlett, T. H., Robinson, A. T., and Dorn, J. E. "An Evaluation of a Theory of Plastic Flow in Anisotropic Sheet Metals," Trans. Am. Soc. Metals, 42 (1950) 1326-1356.

39. Stang, A. H., Greenspan, M., and Newman, S. B. "Poisson's Ratio of Some Structural Alloys for Large Strains," Journal of Research U.S. Nat. Bureau of Standards, RP 1742, 37 (1946) 211-221.

40. Fisher, J. C. "Anisotropic Plastic Flow," Trans. Am. Soc. Mech. Engrs., 71 (1949) 349-356.

41. Naghdi, P. M., Rowley, J. C., and Beadle, C. W. "Experiments Concerning the Yield Surface and the Assumption of Linearity in the Plastic Stress-Strain Relations," Journal of Applied Mech. (1955) 416-420.

42. Ashkenazi, A. K. "On the Problem of Strength Anisotropy of Construction Materials," Soviet Physics, Techical Physics, 4, 3 333-338.

43. Bauschinger, J. "On the Change in Elastic Limit and Strength of Iron and Steel, by Tension and Compression, by Heating and Cooling, and by Repeated Loading," Mitteilungen aus dem Mechanisch-Technischen Laboratorium der K. Polytechnische Schule in München, 2, No. 13, 1886.

44. Schwartzbart, H., Jones, M. H., and Brown, W. F., Jr. "Observations on Bauschinger Effect in Copper and Brass," NACA RM E51D13, June 19, 1951.

45. Sanders, J. L., Jr. "Plastic Stress-Strain Relations Based on Linear Loading Functions," Proc. 2nd U.S. Nat. Congr. of App. Mech. (1954) 455-460.

46. Cunningham, D. M., Thomsen, E. G., and Dorn, J. E. "Plastic Flow of a Magnesium Alloy Under Biaxial Stresses," Proc. Am. Soc. Testing Materials, 47 (1947) 546-553.

47. Marin, J., and Hu, L. W. "Plastic Stress-Strain Relations for Biaxial Tension and Variable Strett Ratios," Proc. Am. Soc. Testing Material, 52 (1952) 1095-1125.

48. Marin, J., and Hu, L. W. "On the Validity of Assumptions Made in Theories of Plastic Flow of Metals," Trans. Am. Soc. Mech. Engrs. 75, (1953) 1181-1190.

49. Hu, L. W., and Marin, J. "Anisotropic Loading Functions for Combined Stresses in the Plastic Range," Journal of Applied Mechanics, (March 1955) 77-85.

50. Hu, L. W. "Studies on Plastic Flow of Anisotropic Metals," Journal of Applied Mechanics, (Sept. 1956) 444-450.

51. Bridgman, P. W. Studies in Large Flow and Fracture, McGraw-Hill Book Co., Inc. 1952.

52. Mehringer, F. J., and MacGregor, C. W. "Effects of Cold-Rolling on the True Stress-Strain Properties of a Low Carbon Steel," Metals Technology, Tec. Pub. 1849, Sept. 1945.

53. Bridgman, P. W. "The Stress Distribution at the Neck of a Tension Specimen," Trans. Am. Soc. Metals, 32 (1944) 553-574.

54. Davidenkov, N. N., and Spiridonova, N. I. "Mechanical Methods of Testing. Analysis of the State of Stresses in the Neck of a Tension Test Specimen," Proc. Am. Soc. Test. Mat., 46 (1946) 1147-1158.

55. Parker, E. R., Davis, H. E., and Flanigan, A. E. "A Study of the Tension Test," Proc. Am. Soc. Testing Mat., 46 (1946) 1159-1174.

56. Ebert, L. J. "Strain Hardening Effects on Plain Carbon and Low Alloy Steels," Doctoral Dissertation, Case Institute of Technology, 1954.

57. Rozalsky, I. "The Effect of Prestraining Under Different Stress States on the Fracture and Flow Properties of 2S-0 Aluminum," Trans. Am. Soc. Metals, 47 (1955) 77-101.

58. Burns, R. S., and Heyer, R. H. "Orientation and Anisotropy in Low Carbon Sheet Steels," Proc. Int. Symp. on the Annealing of Low Carbon Steel, Case Institute of Technology, October 1957.

59. Gerard, G., and Wildhorn, S. "A Study of Poisson's Ratios in the Yield Region," NACA TN 2561, January 1952.

60. Miller, J. A. "Stress-Strain and Elongation Graphs for Aluminum Alloy 75S-T6 Sheet," NACA TN 2085, April 1950.

61. Mehan, R. L. "Effect of Combined Stress on Yield and Fracture Behavior of Zircaloy-2," Am. Soc. Mech. Engrs. Paper No. 60-WA-96.

62. Rittenhouse, P. L., and Picklesimer, M. L. "Metallurgy of Zircaloy-2, Part I. The Effects of Fabrication Variables on the Anisotropy of Mechanical Properties," ORNL-2944 (U.S.A.E.C.)

63. Rittenhouse, P. L., and Picklesimer, M. L. "Metallurgy of Zircaloy-2, Part II. The Effects of Fabrication Variables on the Preferred Orientation and Anistropy of Strain Behavior," ORNL-2948 (U.S.A.E.C.).

64. Mott, N. F. "A Theory of Workhardening of Metal Crystals," Philosophical Magazine, Ser. 7, 43 (1952) 1151-1178.

65. Wilsdorf, H. G. F., and Schmitz, J. "The Observation and Introduction of Dislocation Tangles in the Easy Glide Range of Aluminum," Journal of Applied Physics, 33, 5 (1962) 1750-1754.

66. Tomlinson, H. M. "An Electropolishing Technique for the Preparation of Metal Specimens for Transmission Electron Microscopy," Philosophical Magazine, Ser. 8, 3 (1958) 867-871.

67. Segall, R. L., and Partridge, P. G. "Dislocation Arrangements in Aluminum Deformed in Tension or by Fatigue," Philosophical Magazine, Ser. 8, 4 (1959) 912-919.

68. Zener, C., and Hollomon, J. H. "Effect of Strain Rate Upon Plastic Flow of Steel," Journal of Applied Physics, 15 (1944) 22-32.

69. Siebel, E. "Berichte der Fachausschüse des Vereins deutscher Eisenhütenleute," Werkstoffausschuss, Ber. 71, 1925.

70. Kula, E. B., and Larson, F. R. "Ductility Relationships in Tensile Testing," WAL TR No. 111/25, Watertown Arsenal Laboratories, Watertown, Mass., October 1957.

71. Nunes, J. "Flow-Stress-Strain Relationships in Tension Tests of Steel," Materials Research and Standards, Am. Soc. Test. Mat. (Sept. 1963) 719-722.

72. Alexander, J. A. "The Effect of Coulomb Friction in the Plain Strain Compression of a Plastic-Rigid Material," Journal of Mech. and Phy. of Solids, 3 (1955) 233-245.

73. Datsko, J. Unpublished Data, The University of Michigan, Ann Arbor, Michigan.